Division of Pharmaceutical Chemistry and Technology
Faculty of Pharmacy
University of Helsinki
Finland

Ion mobility based separation techniques for the direct analysis of gaseous and solid samples and fundamental studies of gas phase reactions

Riikka-Marjaana Räsänen

ACADEMIC DISSERTATION

To be presented, with the permission of the Faculty of Pharmacy of the University of Helsinki, for public examination in lecture hall 107, Latokartanonkaari 7, Viikki B-building, on December 15th 2017, at 12 o'clock noon.

Helsinki 2017

Supervisors
Docent Tiina J. Kauppila
Division of Pharmaceutical Chemistry and Technology
Faculty of Pharmacy
University of Helsinki

Professor Gary A. Eiceman
Department of Chemistry and Biochemistry
New Mexico State University

Co-supervisor
Professor Tapio Kotiaho
Division of Pharmaceutical Chemistry and Technology
Faculty of Pharmacy
University of Helsinki
and
Department of Chemistry
Faculty of Science
University of Helsinki

Reviewers
Docent Elina Kalenius
Department of Chemistry
Faculty of Mathematics and Science
University of Jyväskylä

Docent Mikko Sipilä
Department of Physics
Faculty of Science
University of Helsinki

Opponent
Francisco Fernández-Lima
Department of Chemistry and Biochemistry
Florida International University

ISBN 978-951-51-3896-5 (pbk.)
ISBN 978-951-51-3897-2 (PDF)
http://ethesis.helsinki.fi/

Unigrafia
Helsinki 2017

Preface

The work described in this thesis was carried out in the Laboratory of Applied Environmental Chemistry, University of Kuopio (Mikkeli 2007); Department of Structural Engineering and Building Technology, Aalto University (Espoo, 2009); Department of Chemistry and Biochemistry, New Mexico State University (Las Cruces, USA, 2010); School of Chemistry and Biochemistry, Georgia Institute of Technology (Atlanta, USA, 2013); and Division of Pharmaceutical Chemistry and Technology, University of Helsinki (Helsinki 2012-2014). The funding was provided by the European Union, City of Mikkeli, Environics Oy, Ministry of Education of Finland, and Academy of Finland. CHEMSEM graduate school is also acknowledged for financial support.

First I would like to thank my supervisor Docent Tiina Kauppila for giving me the opportunity to finish my thesis in the Division of Pharmaceutical Chemistry and Technology. Your support and guidance helped me to reach the finish line. Thank you also to co-supervisor Professor Tapio Kotiaho for helpful comments and questions during the writing process. I am also grateful to my supervisor Professor Gary Eiceman from the New Mexico State University, Las Cruces, USA, for welcoming me twice to his laboratory for a research visit and for teaching me so much about ion mobility.

I acknowledge and deeply respect Emeritus Professor John Stone from Queens University, Kingston, Canada for help with data processing and interpretation, as well as in the writing process. You always had time to reflect the chemistry behind the experiments and the results.

I am also grateful to Professor Facundo Fernández from the Georgia Institute of Technology for the opportunity to work in his laboratory and Osmo Anttalainen from Environics, who always had time to write me a thorough answer to my questions.

I would like to acknowledge all the co-authors for their contribution to the work, and all the co-workers in Mikkeli, Espoo, Helsinki, Las Cruces, and Atlanta for interesting discussions related to research, science, and life. Additionally, Docent Elina Kalenius (University of Jyväskylä) and Docent Mikko Sipilä (University of Helsinki) are acknowledged for the reviewing and commenting this manuscript.

Above all, I am the most grateful to my family. Thank you mom and dad. Your daycare help and support during the last couple of years has been, and still is, essential and priceless. Antti, thank you for being you. You stayed calm and patient and tolerated my bursts of despair during this tournament. There are no words to describe the gratitude that I have for you. Finally, I want to give huge hug for my two precious daughters. Being with you two makes me realize what really is important, you are the treasures of my life.

Vantaa, December 2017

Riikka-Marjaana Räsänen

Abstract

This thesis describes the applicability of different types of IMS instruments in the direct measurements of gaseous and solid samples and in fundamental studies of gas-phase ion chemistry. A handheld chemical detector containing an aspiration ion mobility spectrometry (AIMS) was applied in the monitoring of gas phase explosive triacetone triperoxide (TATP) from air flow. The instrument-normalized detection threshold (20 pA) was exceeded already with the lowest sample concentration of 0.3 mg m^{-3}. The response time of the instrument was less than five seconds. AIMS was also used to monitor chemical changes in the headspaces of the chambers containing microbe contaminated and sterile particle board samples in humid conditions. It was possible to separate the distinct chemical profiles of the chambers with sterile and microbe-contaminated specimen by principal component analysis. Overall, AIMS was found to be an adequate technique in dynamic screening of TATP and in monitoring of the changes in the microbe metabolism.

Ambient ionization techniques, direct analysis in real time (DART) and desorption atmospheric pressure photoionization (DAPPI), were combined with travelling wave ion mobility-mass spectrometry. In the surface analysis of almond, pharmaceuticals, vitamin tablets and dried blood spot sample, the ion mobility separation reduced the chemical noise in the mass spectra and increased the signal-to-noise ratio. In the comparative studies of DAPPI and DART ionization, the limits of detection were between 30−290 and 330−8200 fmol for DAPPI and DART, respectively, for the tested compounds bisphenol A, benzo[a]pyrene, ranitidine, cortisol, and α-tocopherol.

Finally, the reactions of phenol and fluorinated phenols with Cl^- in ambient pressure were investigated by drift tube ion mobility-mass spectrometry. For the least fluorinated phenols (phenol, 2-fluorophenol and 2,4-difluorophenol) with the lowest gas-phase acidities, the Cl^- adducts $[M+Cl]^-$ and $[2M+Cl]^-$ were the major products in both low and high sample concentration. For the highly fluorinated phenols (2,3,6-trifluorophenol and pentafluorophenol), $[M-H]^-$ and $[2M-H]^-$ were the main products in high sample concentration. In low concentration $[M-H]^-$ and $[M+Cl]^-$ were the main products. In case of pentafluorophenol (PFP), in high temperature conditions the dimer was $[2PFP-H]^-$ instead of $[2PFP+Cl]^-$.

In conclusion, IMS has many advantages and application possibilities. It allows the rapid detection and continuous monitoring of volatiles directly from ambient air. IMS can also be used as a pre-separation technique in ambient mass spectrometry, without increasing the total analysis time remarkably. In IMS, it is also possible to study gas phase reactions in ambient conditions. Some of the IMS applications presented in this thesis could be developed further to be a permanent part of routine monitoring, analysis, and research work. For example, in the fundamental studies of phenols, the possibility to use updated versions of the instruments could improve the accuracy of the experiments. In addition, broader studies with several experimental conditions, would increase the possibility to develop the method further, especially in the monitoring of TATP, and building material and microbe emissions from the gas phase with AIMS.

Contents

List of original publications

This thesis is based on the following publications:

I Riikka-Marjaana Räsänen, Marjaana Nousiainen, Kaleva Peräkorpi, Mika Sillanpää, Lauri Polari, Osmo Anttalainen, Mikko Utriainen. (2008). Determination of gas phase triacetone triperoxide with aspiration ion mobility spectrometry and gas chromatography-mass spectrometry. *Analytica Chimica Acta,* 623:59-65.

II Riikka-Marjaana Räsänen, Markus Håkansson, Martti Viljanen. (2010). Differentiation of air samples with and without microbial volatile organic compounds by aspiration ion mobility spectrometry and semiconductor sensors. *Building and Environment,* 45:2184-2191.

III Riikka-Marjaana Räsänen, Prabha Dwivedi, Facundo M. Fernández, Tiina J. Kauppila. (2014). Desorption atmospheric pressure photoionization and direct analysis in real time coupled with travelling wave ion mobility-mass spectrometry. *Rapid Communications in Mass Spectrometry,* 28:2325-2336.

IV Riikka-Marjaana Räsänen, Peter Fowler, Maneeshin Rajapakse, Tiina Kauppila, Gary Eiceman, John Stone. The reaction of Cl^- with fluorophenols as a function of fluorine number: an ion mobility-mass spectrometry, atmospheric pressure photoionization mass spectrometry and theoretical study. (Submitted).

The publications are referred to in the text by their roman numerals.

Author's contribution to the publications included in this thesis:

I Ion mobility data was collected by the author with some contributions from Lauri Polari. Mass spectrometry data was collected by the author. Author had the main responsibility for writing the manuscript.

II Ion mobility and mass spectrometry data was collected by the author. Author had the main responsibility for writing the manuscript.

III The ion mobility and mass spectrometry data was collected by the author with some contributions from Prabha Dwivedi. Author had the main responsibility for writing the manuscript.

IV Author had the shared responsibility of the experimental work and data processing and the shared responsibility for writing the manuscript.

Abbreviations and symbols

AIMS	Aspiration ion mobility spectrometry
APCI-RI	Atmospheric pressure chemical ionization with radioactive ion source
API	Atmospheric pressure ionization
APPI	Atmospheric pressure photoionization
ATD	Automatic thermal desorption
B[a]P	Benzo(a)pyrene
BPA	Bisphenol A
CCS	Collision cross-section
CD-APCI	Corona discharge-atmospheric pressure chemical ionization
CID	Collision-induced dissociation
CV	Compensation voltage
CWA	Chemical warfare agent
DAPPI	Desorption atmospheric pressure photoionization
DART	Direct analysis in real time
DC	Direct current
DESI	Desorption electrospray ionization
DFP	2,4-Difluorophenol
DFT	Density functional theory
DMS	Differential mobility spectrometry
DT-IMS	Drift tube ion mobility spectrometry
E	Electric field
EA	Electron affinity
E_{COM}	Centre of mass collision energy
ESI	Electrospray ionization
FAIMS	Field asymmetric ion mobility spectrometry
FE	Field effect transistor (in Publication II)
FET	Field effect transistor (in Publication I)
FP	2-Fluorophenol
GC	Gas chromatography
GC-IM-MS	Gas chromatography-ion mobility-mass spectrometry
IE	Ionization energy
IM	Ion mobility
IMS	Ion mobility spectrometry
IM-MS	Ion mobility-mass spectrometry
K	Mobility coefficient
K_0	Reduced mobility
LC	Liquid chromatography
LOD	Limit of detection
MOS	Metal oxide semiconductor
MS	Mass spectrometry
MVOC	Microbial volatile organic compound
m/z	Mass-to-charge ratio

N	Number density of the neutral gas molecules
P	Phenol
PA	Proton affinity
PAH	Polycyclic aromatic hydrocarbon
PCA	Principal component analysis
PFP	Pentafluorophenol
R	Resistance during a chemical exposure
R_0	Resistance during the background air exposure
RF	Radio frequency
RH	Relative humidity
RIP	Reactant ion peak
S/N	Signal-to-noise ratio
SV	Separation voltage
TATP	Triacetone triperoxide
TD-GC-MS	Thermal desorption-gas chromatography-mass spectrometry
T_{eff}	Effective temperature
TFP	2,3,6-Trifluorophenol
TVOC	Total volatile organic compound
TWIMS	Travelling wave ion mobility spectrometry
V	Response of sampled air as voltages
V_0	Response of background air as voltages
VOC	Volatile organic compound
VUV	Vacuum ultraviolet
$\Delta_{acid}G°$	Gas phase acidity
µAPPI	Micro atmospheric pressure photoionization
Ω	Collision cross-section

1 Introduction

In the field of analytical chemistry there is a continuous need for fast, sensitive, and accurate analysis techniques in both laboratory and field conditions. One attractive separation and detection technique is ion mobility spectrometry (IMS), the roots of which date back to the late 19th century. Principally, in IMS the analytes are ionized in the ion source and guided to the separation region, where they travel to the detector under an influence of an electric field.[1-3] The ions are separated according to their different mobilities within the field and the ion separation is dependent on the shape, size, mass, and charge of the ions. The instruments can be operated in ambient or near ambient conditions so that large vacuum pumps and power sources are not necessary. The sensitivity of IMS is high and the separation is fast, even less than a second for a sample, compared to chromatographic separation techniques which typically require several minutes.

Since the late 20th century, research and development work around the ion mobility in the gas phase and IMS instrumentation has generated a selection of new type of IMS instruments. The instruments vary e.g. on the size, *in situ* usability, sample introduction system, and especially on the way that the electric field is applied in the ion separation region.[3-7] Here the abbreviation IMS is used generally for all the different IMS techniques. Different abbreviations are used when specific techniques are discussed.

The variety of instrumentations has made it possible to apply IMS to a wide application area.[8-12] The use of radioactive ion sources has allowed, for example, the development of portable IMS devices for fast analysis of harmful substances.[6,13-16] This is due to the fact that radioactive ion sources do not require external power sources to operate, still eliciting stable and continuous ion production,[3] although, several other ion sources have been applied with IMS as well. Portable IMS has been used in fast monitoring of e.g. chemical warfare agents (CWA)[14,17-20] and explosives.[13,18,21,22]

Analyte identification with both handheld IMS devices and standalone instruments is limited, however.[3,23,24] To increase the reliability of the IMS analysis, IMS has been hyphenated with mass spectrometry (MS). In MS, compounds are vaporized, ionized, and gaseous ions are separated according to their mass-to-charge ratio (m/z) in vacuum conditions. When IMS is hyphenated with MS, the identification and quantification of the analytes separated in IMS is improved. On the other hand, the ion mobility (IM) separation brings an extra dimension to the MS analysis. The combination of IMS and MS will result in a powerful multidimensional separation and analysis technique that has higher peak capacity than MS or IMS alone.[23-25]

In ambient MS, analytes are desorbed, ionized, and guided to the MS directly from the authentic sample without pre-handling or pre-separation.[26-29] However, in ambient techniques sampling is done in an open air environment where may be background impurities that disturb the measurements and bring uncertainty to the analysis. Nevertheless, ambient MS methods have been used e.g. for fast analysis of drugs of abuse,[30-34] pharmaceuticals,[27,35] and lipids.[36] It is also an effective tool in acquiring preliminary data from a large number of samples.[37,38] Hyphenation of IMS with ambient MS is one possibility to reduce the effect of background impurities and to increase the reliability of ambient MS analysis.[39-42]

IMS can be operated in ambient pressure and therefore it allows the fundamental studies of gas phase ions under ambient conditions. For example, IMS can be used to monitor the dissociation reactions of the ions. The ions generated in ambient pressure travel in the drift region of IMS instrument from the ion source to the detector. The reactions can be observed as intensity changes in the IM spectra. IMS has been used in the studies of the dissociation[43-45] and kinetics of decomposition reactions of gas phase ions.[46-50] IMS has also been applied in the study of effective temperatures of gas phase ions.[43-45,50-52]

This thesis focuses on the applicability of a different type of IM-based separation techniques. In Publication I, aspiration IMS (AIMS) was applied in the direct detection of gaseous explosive triacetone triperoxide (TATP). TATP is used in improvised explosives by terrorists and therefore its direct and fast detection is essential in public places like airports. Comparative studies were made with gas chromatography-mass spectrometry (GC-MS). AIMS was also applied to the detection of building material emissions and microbial-originated volatile organic compounds (MVOCs) (II) directly from the headspace of building material samples. The goal was to study the applicability of AIMS in the monitoring of the changes in the chemical compositions of the emissions from the microbe-contaminated and sterile-building-material specimen in damp conditions. The comparative studies were made with thermal desorption-gas chromatography-mass spectrometry (TD-GC-MS). Travelling wave ion mobility-mass spectrometry (TWIM-MS) was hyphenated with ambient MS for the direct analysis of solid samples (III). The objective was to improve the spectrum interpretability and to increase the signal-to-noise ratio (S/N), while retaining the speed provided by the ambient MS. In Publication IV the aim was to study the products of the reactions of phenol (P) and fluorinated phenols with Cl^-, and the effect of the gas phase acidities ($\Delta_{acid}G°$) of the phenols with different number of F substituents to the reaction products. The reaction products were studied comprehensively with IMS, MS, and theoretical calculations.

1.1 Ion mobility spectrometry techniques

In IMS the analytes are vaporized and ionized and gas phase ions are separated in ambient or near ambient pressure.[3,7] An electric field is applied in the instrument and it will have an effect on the motion of the gas phase ions. Ions with diverse shape, size, and charge will move in the field with different velocities, and ideally can be totally separated. With IMS it is also possible to separate isomers and isobars, because the separation process is dependent on the shape and size of the ions and not just the mass. The possibility to study collision cross-section (CCS) with IMS has increased the interest to apply IMS in the studies of biological samples.[53-56] The principles of the IMS techniques used in this work are described below.

1.1.1 Linear drift tube ion mobility spectrometry

A conventional linear drift tube ion mobility spectrometry (DT-IMS) consists of an ion source, an ion shutter, a drift tube, and a detector (Figure 1).[3,7] The ions are formed in the

ion source and reaction region of the drift tube, and they are passed through the ion shutter as short pulses to the separation area of the drift tube. At the end of the separation area there is an aperture grid and a detector, which in a standalone instrument is typically a Faraday plate. The length of the drift tube may vary and is generally about 5−20 cm. In addition, the instrument contains a power source to apply voltages to the drift tube to form the electric field from the ion source end to the detector end. DT-IMS operates under a low electric field ($E < 1000$ V cm^{-1}, approximately) and atmospheric or reduced pressure. A drift gas flow is applied into the drift tube from the detector end and vented out the ion source end of the drift tube. Drift gas helps to keep the neutral molecules out of the drift region and it has an effect on the ion separation through collisions with the ions.

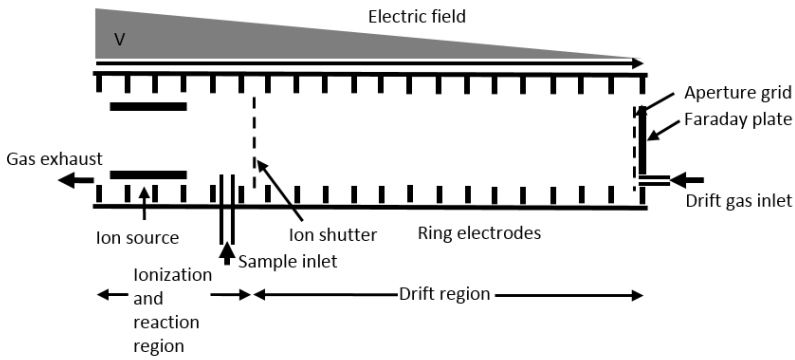

Figure 1. Schematic of a DT-IMS instrument.

In the separation region, the ions will travel in swarms from the ion shutter to the detector under the influence of an electric field (E). The ion swarms are separated depending on the mass, charge, and shape of the ions. The drift time (t) of the ion swarm from the shutter to the detector is measured. The drift time and the drift length (L) can be used to calculate the velocity (v) and the mobility (K) of the ions (Equation 1).

(1) $$K = \frac{L}{tE} = \frac{v}{E}$$

Typically, the DT-IMS mobility spectrum presents a reactant ion peak (RIP) and ionized analyte peaks. An example is shown in Figure 2, where 2,4-difluorophenol (DFP) negative mode IM spectrum is presented with three different concentrations. The spectrum shows the RIP and DFP monomer and dimer peaks. Only the RIP, which in this case was Cl^-, is present in the IM spectrum, when there is no sample present in the instrument (Figure 2 dotted line). When the analyte is introduced into the system (Figure 2 solid line), the ionized analyte monomer appears and the RIP intensity decreases, because the ionization of the analyte consumes the charge of the RIP. With high concentration (Figure 2 dashed line), the analyte dimer appears and both monomer and RIP intensities decrease and RIP may disappear totally.

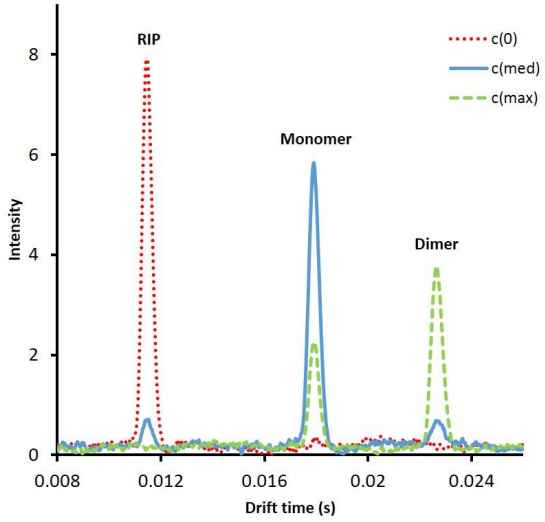

Figure 2. Negative mode DT-IMS mobility spectrum for three different DFP concentrations: c(0), c(med), and c(max) corresponding concentrations zero, medium, and high, respectively. The drift tube temperature was 98 °C, E = 250 V cm^{-1}, and the RIP was Cl^-.

K is described with Equation 2,[3,57] where q is the electronic charge, μ is the reduced mass of the ion and the neutral gas molecule in the gas bath, k is the Boltzmann constant, α is a correction factor, and Ω is the temperature dependent CCS of the ion-neutral pair. T_{eff} is the effective temperature, which is the sum of the total energy of the ion and the energy received from the electric field. In DT-IMS the contribution of the low electric field on ion heating is negligible and therefore in DT-IMS T_{eff} is considered to be the temperature of the surrounding gas bath.

(2) $$K = \frac{3}{16}\frac{q}{N}\left(\frac{2\pi}{\mu k T_{eff}}\right)^{1/2}\left(\frac{1+\alpha}{\Omega(T_{eff})}\right)$$

K can be normalized to normal temperature and pressure (Equation 3) to determine the 'reduced mobility' (K_0). K_0 is used to compare the mobility data measured in different experimental conditions, e.g. temperature, pressure, and drift tube.[13,21,58-61]

(3) $$K_0 = K\left(\frac{273}{T}\right)\left(\frac{P}{760}\right)$$

In low electric-field conditions, the ratio E/N is low (N is the number density of the neutral gas molecules in the instrument). In this situation, the ions in the drift tube are thermalized, because the collisions with the surrounding neutral gas molecules will diminish the energy that the ions obtain from the electric field. Therefore, until recent publications,[62,63] it was determined that in low field conditions and given pressure, the K

is independent of the electric field strength. However, Hauck *et al.* (2016) have recently shown that K_0 is actually dependent on the electric field strength in low electric field conditions, and it decreases as a function of (E/N) at field strengths below 4 Townsend (1 Townsend = $1*10^{-17}$ V cm^2).[62,63] The reason for the dependency was concluded to be the increment in the ion-neutral CCS caused by increased long-range ion-neutral interaction potential of the amplified electric field.

Equation 2 shows that CCS and μ have a major effect on the value of K. Therefore, the separation of ions in DT-IMS is dependent on the mass and shape of the ion, and the surrounding gas atmosphere. Equation 2 also shows that temperature is an important parameter. Since DT-IMS is typically used under ambient conditions, water is present in the ion source, and it has an important role in the ionization reactions. The ions are clustered and hydrated in low temperature conditions.[64] When temperature is increased, the ion clusters are less hydrated, and they will move faster within the drift tube. When temperature is increased enough, the ions may dissociate. Declustering and dissociation will show in the IM spectrum as changes in the ion peak positions towards shorter drift times. Also new peaks may appear as a result of ion dissociation. When the ion dissociation happens in the drift region, it can be visually observed as baseline elevation in the IM spectrum (Figure 3). This phenomenon has been used in fundamental studies of gas phase ion dissociation reactions with dual shutter DT-IMS instruments.[46-50] Typically, DT-IMS contains one ion shutter between the ion source / reaction region and the separation region. In the dual shutter DT-IMS, a second shutter is applied to divide the drift region to two sections. With two shutters, it is possible to select the desired ion swarm to pass to the second drift region, where the dissociation of the selected ion can be studied.

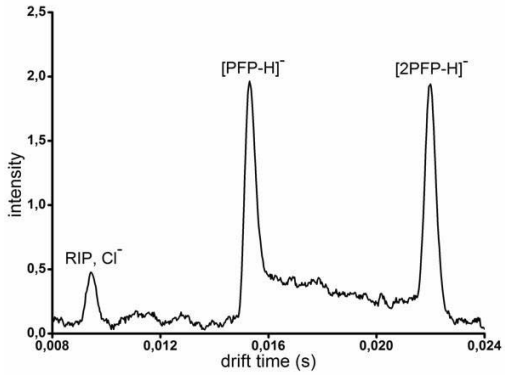

Figure 3. Separation of pentafluorophenol (PFP) deprotonated monomer ([PFP−H]$^-$) and dimer ([2PFP−H]$^-$) in DT-IMS with Cl$^-$ as the reactant ion. The baseline elevation between the monomer and the dimer shows the dissociation of the dimer ion to monomer. The drift tube temperature was 142 °C and E 250 V cm^{-1}.

1.1.2 Differential mobility spectrometry

In low electric field conditions in DT-IMS, the heating of the ions caused by the electric field is negligible compared to the thermal energy of the system. Instead, in high electric field conditions (typically E = 10−30 kV cm^{-1}) and given pressure, the high field will accelerate the ions and increase the number of collisions between the ions and the neutral molecules in the gas atmosphere.[3,4,65-67] The ions will experience heating caused by the electric field. The IM becomes strongly dependent on the electric field strength. This dependency has been used to develop an ion separation technique based on the high frequency asymmetric wave form (radio frequency, RF) field,[3,4,65,66,68,69] where the low and high portions of the electric field changes repeatedly. The technique is called differential mobility spectrometry (DMS) or field asymmetric ion mobility spectrometry (FAIMS).[3,65,66,70] The difference between DMS and FAIMS is mainly on the shape of the electrodes in the analyser. In FAIMS, the electrodes are cylindrical and in DMS planar.

Typically, DMS consists of two parallel plate electrodes, a detector, an amplifier, a power source, an ion source, and electronics for instrument control.[71,72] The dimensions of the DMS electrodes are approximately: length = 1.5 - 2 cm, width = 0.5 cm, and gap = 0.5 mm between the electrodes. Compared to DT-IMS, there are no ion shutters, which are fragile and may be difficult to build. The analytes are sucked into the instrument with the transport gas flow and ionized.

The principle of ion travel in DMS is presented in Figure 4. High frequency (typically 1 MHz) asymmetric waveform, so called separation voltage (SV), is applied to the other plate electrode.[3,65,70] The other electrode is held in ground potential. SV forms an electric field called separation field between the electrodes. The asymmetric form of the SV causes the low field (ca. 1 kV cm^{-1}) and the high field (E ≈ 10−30 kV cm^{-1}) phases to change over short time periods. When the gas phase ions travel with the transport gas flow between the electrodes, the high and low field changes of the separation field make the ions oscillate. The ions will travel towards the other plate electrode, and finally collide towards it. An ion can pass through the separation field to the detector by applying so called compensation voltage (CV) to the electrodes. This causes a small electric field superimposed with the separation field. It will offset the ion drift and allow the ion to stay between the plate electrodes and reach the detector. Other ions will collide towards the electrodes of the analyser and will be neutralized. The DMS mobility spectrum of an ion mixture can be measured by scanning the CV in a range of SV. This way, optimal separation conditions for the target analyte can be determined.

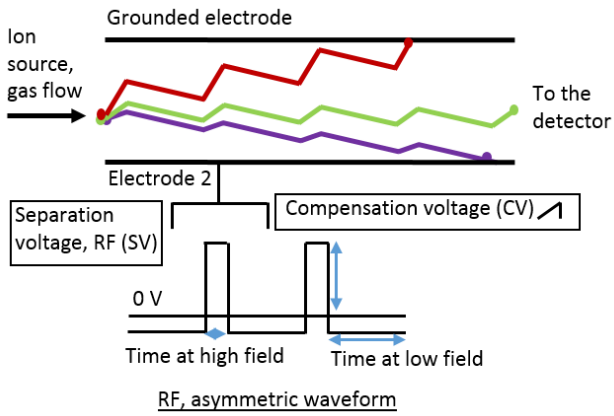

Figure 4. Schematic of the ion travel principle in DMS and the asymmetric waveform.

Since DMS is operated in ambient conditions, the ion swarms contain hydrated ion clusters in the low field part of the applied SV. When the electric field increases to the high field portion of the waveform duty cycle, the ions gain energy from the high field, and the ions de-cluster. If the gained field energy is high enough, the ions may dissociate. Ion heating by field energy has been used to study dissociation reactions of gas phase ions.[50-52,73] For example, together with dual shutter DT-IMS studies, T_{eff} has been determined e.g. for dimethyl methylphosphonate[51] and a series of 2-ketones.[50]

1.1.3 Aspiration ion mobility spectrometry

In AIMS, the ambient air is continuously pumped into the analyser, where ionized compounds are detected by electrodes.[3,6,14] As an example of a typical AIMS analyser, ChemPro100i, a handheld air monitoring instrument is described. AIMS is constructed of two parallel plates, which both contain eight pairs of collecting electrodes (Figure 5).[6] The electrodes collecting positive ions (channels 1-8) are placed on one plate and the electrodes collecting negative ions (channels 9-16) on another. An electric field is applied between the plates perpendicular to them. The compounds in the monitored gas flow are ionized through a series of ionization reactions initiated by radioactive ^{241}Am,[6,74,75] or for example ^{63}Ni ion source.[14] The formed ion clusters are guided into the analyser, where the electric field disturbs the travel of the ions. Under the influence of the electric field, the ions with high mobility will move rapidly between the electrode plates and hit the first electrodes in the analyser (Figure 5 a). The ions with low mobility will move slowly between the plates and travel longer with the gas flow. The low mobility ions will hit the farthest electrodes in the analyser.

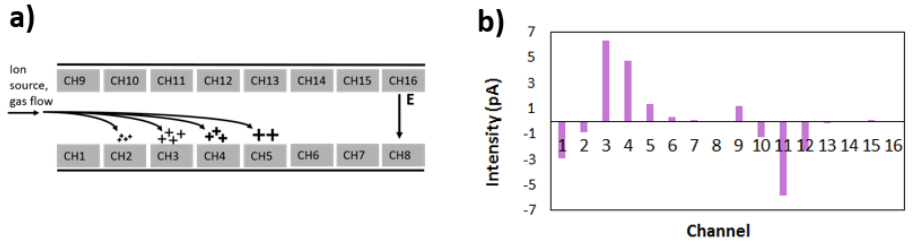

Figure 5. a) Schematic of the separation principal of positive ions in AIMS and b) an example of the AIMS intensity pattern response (sniff sampling of dry particle board).

When the ions hit the electrodes they will cause a current change, which is measured. The result is an intensity pattern, also called a chemical profile. An example of the AIMS response of a sniff-test of dry particle board is presented in Figure 5 (b). AIMS is based on ion counting technology.[3] The higher the amount of ions hitting the electrode, the higher is the measured signal intensity. On the positive polarity channels (channels 1-8) the current increment[6] indicates that the ion concentration has increased. The current decrement indicates a decline in the concentration. On the negative polarity channels (channels 9-16) it is the opposite. The polarity of the electric field can be changed in short time intervals. Therefore both positive and negative ions can be monitored simultaneously.

Even though the AIMS resolution is low and the capability to identify compounds is limited, AIMS has been applied especially on the detection of high proton affinity (PA) compounds like CWAs.[14,15] Likewise, AIMS has been used to detect pesticides[75,76] and volatile organic compounds (VOC),[77] and to monitor fish freshness[78] and gaseous fermentation products.[74,79]

In ChemPro100i, after the AIMS, there are six sensors, which enhance the detection performance of the instrument. One is a field effect transistor (FE / FET) sensor, which operates in the diode-coupled mode. Chemical reactions on the surface of catalytic metal and in the interface of catalytic metal and SiO_2 insulator result an effective dipole layer at the metal-insulator interface, inducing a measurable potential drop. The metal-insulator interface is selective only for hydrogen atoms. In the FE / FET sensor, the response is measured as voltage difference (ΔV) between the sampled air (V) and the background air (V_0). Five sensors are metal oxide semiconductor sensors (MOS). Three of the MOS sensors are micro hot-plate type sensors (MOS1, MOS2, and MOS3), and two are ceramic gas sensors (SC1 / SCell1 and SC2 / SCCell2). The material of MOS1, MOS2, and SC1 / SCCell1 sensors is WO_3, and of MOS3 and SC2 / SCCell2 sensors SnO_2. The semiconductor sensors measure the resistance change, when ions hit the sensors and the resistance decreases when the ion concentration increases. The semiconductor sensor responses are monitored as the change in ratio (R/R_0) of the sensor resistance during a chemical exposure (R) and the sensor resistance during the background air exposure (R_0). More detailed description of the ChemPro100i and the detection principle of the device are described by Utriainen *et al.*[6]

1.1.4 Travelling wave ion mobility spectrometry

Travelling wave ion mobility spectrometry (TWIMS) is the newest widely applied IMS technique. Compared to DT-IMS, DMS, and AIMS, which are operated at ambient pressure (DT-IMS also in reduced pressure), TWIMS is operated at reduced pressure. The drift chamber in TWIMS consists of a series of ring electrodes.[5,55,80-82] RF voltage with an opposite phase is applied on adjacent rings. Direct current (DC) is superimposed to the RF of the ring electrodes. The DC potential pulses are applied repeatedly during short time intervals, and potential pulses are rolled over the series of electrodes. This provides a kind of moving electric field, 'a travelling wave', in the drift region. The ions introduced into the drift chamber are driven through the chamber under the force of a potential difference. The phenomenon related to the ion separation and travel through the drift chamber is complex.[80] However, in principal the ions with high mobility stay in front of or on the top of the potential pulse longer, and the ions with low mobility are forced behind the wave. The ion separation takes place according to the differences in the relative mobilities of the ions. The main parameters affecting the ion separation are the wave speed through the drift chamber and the DC potential (wave height).

TWIMS has been integrated into one instrument complex with time of flight mass spectrometry, and was commercialized about a decade ago.[81,82] TWIM-MS is also utilized with liquid chromatography (LC) and this combination of instruments has increased the application of IMS in the analysis of biological samples, because like DT-IMS, it enables the study of CCS[83] and e.g. protein folding. TWIM-MS has been used for example in proteomics,[54,55,82,84,85] the study of carbohydrates,[86,87] and in conformation studies of isomeric carotenoids.[88]

1.2 Ionization techniques

In IMS, the separation of analytes takes place in the gas phase and under an electric field. Therefore, the analytes need to be vaporized and ionized before they enter the drift region of the instrument. The ionization techniques used in this research are described below.

1.2.1 Atmospheric pressure chemical ionization with radioactive ion source

Atmospheric pressure chemical ionization with radioactive ion source (APCI-RI) is a traditional ionization technique in IMS.[1] In APCI-RI, the most used radioactive isotope is ^{63}Ni that emits beta-particles.[3,89] These high energy primary electrons start the ionization reactions by colliding with ambient gas molecules, typically nitrogen (Table 1, Reaction 1).[3] A series of reactions (Table 1, Reactions 2-6) lead to the formation of protonated water clusters.[90] These function as the positive reactant ions and ionize the analytes (A) through proton transfer reactions (Table 1, Reaction 7). When reactant ions and analyte molecules collide, an energetic intermediate adduct ion or transition state $[(H_2O)_n+A+H]^{+*}$ is formed (Table 1, Reaction 7). This requires collision with a third body (Z) for stabilization, and to form the protonated product ion cluster, or it may dissociate back to reactant ions.

Table 1. Positive ion formation in radioactive atmospheric pressure chemical ionization. A = analyte, Z = neutral molecule in the gas phase.[a]

Reaction	#
$N_2 + e^- \rightarrow N_2^+ + e^-(primary) + e^-(secondary)$	1
$N_2^+ + 2N_2 \rightarrow N_4^+ + N_2$	2
$N_4^+ + H_2O \rightarrow 2N_2 + H_2O^+$	3
$H_2O^+ + H_2O \rightarrow H_3O^+ + OH$	4
$H_3O^+ + H_2O + N_2 \rightleftarrows [(H_2O)_2 + H]^+ + N_2$	5
$[(H_2O)_2 + H]^+ + H_2O + N_2 \rightleftarrows [(H_2O)_3 + H]^+ + N_2$	6
$[(H_2O)_n + H]^+ + A \rightleftarrows [(H_2O)_n + A + H]^{+*} + Z \rightleftarrows [(H_2O)_{n-1} + A + H]^+ + H_2O + Z$	7

[a] Reactions from references [3,90]

Besides protonated water clusters, other positive reactant ions, like hydrated ammonium ions $[(H_2O)_n+NH_4]^+$, can be observed in the IM spectrum. When these ions are present as impurities, originating for example from the drift gas or the instrument, they can also function as unwanted reactant ions, change the expected ion chemistry, and lead to false interpretation of the IM spectrum.

The formation of protonated analyte clusters is mainly dependent on the energy between the analyte and the water clusters. The formed product ions can be estimated by studying the PAs of the molecules that participate in the ionization reaction. Protonation of the analyte is possible if the PA of the analyte is higher than that of the reactant ion (e.g. protonated water clusters). Therefore, APCI-RI is poorly suited to low polarity compounds with low PAs such as alkanes.

Dopants can be used to manipulate the reactant ion chemistry.[91-93] For example, a dopant with a PA higher than that of water, but lower than that of the analyte, can be used to form reactant ions. This will limit the ionization of interfering compounds and their observation in the mobility spectrum. Chemicals used as dopants in IMS are e.g. acetone, ammonia and dimethyl sulfoxide,[93] which carry PAs of 812, 853, and 884 kJ mol^{-1}, respectively.[94]

In negative APCI-RI, the reactant ions are formed in reactions between thermalized electrons and surrounding gas molecules with positive electron affinity (EA) (Table 2, Reaction 1).[3,89] In clean air, the thermalized electrons can ionize oxygen (EA 0.45 eV) forming superoxide ions $O_2^{-\cdot}$ and hydrated superoxide ions $[(H_2O)_n+O_2]^{-\cdot}$. These reactions (Table 2, Reactions 1-3) need a third body (Z) collisions for the stabilization of the formed excited ions.[95] Negative analyte ions are typically detected as adducts, deprotonated molecules, or negative molecular ions. $[(H_2O)_n+O_2]^{-\cdot}$ can form an adduct with the analyte (A) (Table 2, Reaction 4), but the excited ion $[(H_2O)_n+A+O_2]^{-*}$ needs a third body (Z) collision to form a stable adduct $[(H_2O)_{n-1}+A+O_2]^-$. The formation of deprotonated molecules depends on the $\Delta_{acid}G°$ of the compound. Compounds with higher $\Delta_{acid}G°$ than the $\Delta_{acid}G°$ of the reactant ion can form deprotonated molecules (Table 2, Reaction 5). Negative molecular ions are formed as a result of a charge exchange if the EA (analyte) > EA (reactant ion) (Table, 2 Reaction 6). Ionization of analytes by electron capture (Table 2, Reaction 7) is possible, if the analyte EA > 0.

Table 2. Negative ion formation in radioactive atmospheric pressure chemical ionization. Z = a neutral molecule (e.g. H_2O or O_2) in the gas phase that is needed for the stabilization of the product ion, A = analyte.[a]

Reaction	#
$O_2 + e^- + Z \longrightarrow O_2^- + Z$	1
$H_2O + O_2^- + Z \rightleftarrows [H_2O + O_2]^- + Z$	2
$nH_2O + [H_2O + O_2]^- + Z \rightleftarrows [(H_2O)_n + O_2]^- + Z$	3
$[(H_2O)_n + O_2]^- + A + Z \rightleftarrows [(H_2O)_n + A + O_2]^{-*} + Z \rightleftarrows [(H_2O)_{n-1} + A + O_2]^- + H_2O + Z$	4
$[(H_2O)_n + O_2]^- + A + Z \rightleftarrows [(H_2O)_n + A + O_2]^{-*} + Z \rightleftarrows [(H_2O)_n + A - H]^- + HO_2 + Z$	5
$[(H_2O)_n + O_2]^- + A + Z \rightleftarrows [(H_2O)_n + A + O_2]^{-*} \rightleftarrows [(H_2O)_n + A]^- + O_2 + Z$	6
$A + e^- + Z \longrightarrow A^- + Z$	7
$CCl_4 + e^- + Z \rightarrow CCl_4^{-*} + Z \rightarrow Cl^- + CCl_3 + Z$	8
$Cl^- + nH_2O + Z \rightarrow [(H_2O)_n + Cl]^- + Z$	9
$[(H_2O)_n + Cl]^- + A + Z \rightleftarrows [(H_2O)_n + A + Cl]^{-*} + Z \rightleftarrows [(H_2O)_n + A - H]^- + HCl + Z$	10

[a] Reactions from references [3,95,96]

Similar to positive ion APCI-RI, negative reactant ions can also be formed from impurities in the ambient air. Typical impurities that disturb the negative ion IM spectra have EAs above oxygen. These include, for example, nitrogen dioxide (EA 2.73 eV) and halogenated compounds like $CHCl_3$ (EA 0.62 eV).[94]

Sometimes negative reactant ions can be modified with a suitable chemical. An often-used negative reactant ion is Cl^-, e.g. for the analysis of explosives.[21,96-99] Cl^- can be produced from CCl_4 (EA 0.80 eV) through a dissociative electron capture reaction with the thermal electrons (Table 2, Reaction 8), and form hydrated chloride reactant ions (Table 2, Reaction 9). As with higher $\Delta_{acid}G°$ than the $\Delta_{acid}G°$ of the reactant ion can form deprotonated molecules (Table 2, Reaction 5). When Cl^- is used as the reactant ion, it can ionize the analyte for example through proton transfer reaction (Table 2, Reaction 10), if the $\Delta_{acid}G°$ of the analyte is higher than $\Delta_{acid}G°$ of Cl^-.

Other radioactive ion source alternatives for ^{63}Ni are Tritium[100] and ^{241}Am,[6,74,75] which emit beta and alpha particles, respectively. Alpha particles initiate the ionization reaction by forming primary reactant ions from ambient air, but the reaction pathway to analyte ions is not fully understood.

One reason for the utilization of radioactive ion sources is the development of fast, easy-to-use, and portable *in situ* devices in fast analysis of harmful compounds. APCI-RI requires no maintenance or power to operate, it is inexpensive, and the formation of ions is stable and continuous. However, the use of radioactive materials requires permits and annual follow-up of the laboratory practices and possible leakage of radioactive material. The correct disposal of used drift tubes and ion sources is also controlled.[3] IMS with APCI-RI has been used for the analysis of explosives,[13,18,21] drugs,[101,102] and CWAs.[14,15,18,20,103]

1.2.2 Atmospheric pressure photoionization

Atmospheric pressure photoionization (APPI) is a broadly used ionization technique in liquid chromatography-mass spectrometry.[104-110] It is also applied with IMS.[111-118] In APPI, the ionization of an analyte is possible through charge exchange, which depends on the ionization energy (IE) of the compound instead of the PA. Therefore APPI is a suitable ionization method for neutral and non-polar compounds with low PAs, and it has been used, for example, in the analysis of steroids,[108,119,120] and polycyclic aromatic hydrocarbons (PAH).[104,121]

In APPI the ionization (Table 3) is initiated by 10.0 eV photons (minor portion 10.6 eV) emitted from a vacuum ultraviolet (VUV) lamp.[109,122] An analyte (A) with IE below 10 eV can absorb the photon and eject an electron and form a molecular ion $A^{+\bullet}$ (Table 3, Reaction 1).[109,122] Common LC solvents (methanol, water, acetonitrile) have an IE above 10 eV[94] and therefore will not be ionized by the photons. Typically, a dopant (D) with an IE below 10 eV is used in APPI to enhance the ionization efficiency,[109,123-125] because direct ionization of the analyte is inefficient.[109,122] The dopant can absorb the photon energy and form molecular ions ($D^{+\bullet}$, Table 3, Reaction 1). $D^{+\bullet}$ can react with the analyte through charge exchange if the IE of the analyte is lower than the IE of the dopant (Table 3, Reaction 2).

Table 3. Ionization reactions in atmospheric pressure photoionization. A = analyte, D = dopant, S = solvent and M = e.g. analyte, solvent or oxygen.[a]

Reaction	Notes	#
$h\nu + A \text{ or } D \rightarrow A^{+\cdot} \text{ or } D^{+\cdot} + e^-$	IE(A or D) < $h\nu$	1
$D^{+\cdot} + A \rightarrow D + A^{+\cdot}$	IE(A) < IE(D)	2
$D^{+\cdot} + A \text{ or } S \rightarrow [D-H]^{\cdot} + [A \text{ or } S + H]^+$	PA(A or S) > PA[D−H]$^\bullet$	3
$D^{+\cdot} + D \rightarrow [D-H]^{\cdot} + [D+H]^+$	PA(D) > PA[D−H]$^\bullet$	4
$[D \text{ or } S + H]^+ + A \rightarrow D \text{ or } S + [A+H]^+$	PA(A) > PA(D or S)	5
$e^- + M \rightarrow M^{-\cdot}$	EA(M) > 0	6
$M^{-\cdot} + A \rightarrow M + A^{-\cdot}$	EA(A) > EA(M)	7
$M^{-\cdot} + A \rightarrow [M+H]^{\cdot} + [A-H]^-$	$\Delta_{acid}G°$(A) < $\Delta_{acid}G°$[M+H]$^\bullet$	8

[a] Reactions from references [109,110,122-128]

Proton transfer between the analyte and $D^{+\bullet}$ is possible, if the PA of the analyte is higher than PA of the dopant (Table 3, Reaction 3).[109,122,124] If the dopant has high PA, the molecular ions of the dopant are not observed in the spectrum.[124] For example, the PA of acetone is 812 kJ mol^{-1},[94] and in the spectrum acetone is observed as a protonated molecule $[D+H]^+$ ion. This is due to a rapid self-protonation of acetone (Table 3, Reaction 4).[126] $[D+H]^+$ of acetone can further ionize the analytes with a proton transfer reaction, in case the PA of the analyte is above the PA of acetone (Table 3, Reaction 5).

The dopant molecular ions can also ionize the solvent molecules (S) through proton transfer, if the solvent PA is higher than the PA of the deprotonated $D^{+\bullet}$ (Table 3, Reaction 3).[109,110,122] Consequently, protonated solvent molecules can ionize the analyte through proton transfer (Table 3, Reaction 5),[110,122] if the PA of the analyte is higher than the PA of the solvent. If several solvents are present at the same time, the ionization processes will

become more complicated.[122,124] Moisture also strongly affects the ionization process, as it is always present under atmospheric pressure ionization conditions. Water and solvent clusters have been suggested to take part in the ionization reactions.[129]

In negative ion APPI, the ionization starts, when the electrons ejected by the dopant molecules (Table 3, Reaction 1),[109,122] or released from metal surface of the ion source,[130] are captured by analyte, solvent, or oxygen molecules (M, Table 3, Reaction 6).[127,128] This is possible for species with positive EA.[127,128] The formed negative molecular ions can react further with other species by charge exchange (Table 3, Reaction 7) or proton transfer (Table 3, Reaction 8). These reactions depend mainly on the EAs and the $\Delta_{acid}G°$s of the reactive species. Since oxygen is always present in atmospheric pressure ion sources, and it has a high EA (0.45 eV),[94] it is likely to take part in the ionization process.[127] Accordingly, superoxide ions formed by electron capture can ionize analyte molecules through charge exchange or proton transfer (Table 3, Reactions 7 and 8, respectively).[127]

1.2.3 Desorption atmospheric pressure photoionization

Desorption atmospheric pressure photoionization (DAPPI)[27] belongs to a group of ambient ionization techniques also called 'direct open air surface sampling techniques'.[26] In ambient ionization, the analytes are desorbed and ionized directly from the sample surface. The gas phase ions are guided to the MS for the analysis without pre-separation of the compounds. Using DAPPI, a VUV-lamp is placed directly above the sample, solvent delivery, and MS inlet (Figure 6). The solid sample is exposed to a hot solvent jet, which thermally desorbs compounds from the sample surface.[27,131] Ionization of the analytes is initiated by 10.0 eV photons (minor portion 10.6 eV) emitted by the VUV-lamp. The ionization reactions in DAPPI are similar to the reactions in APPI (Table 3).[131] In DAPPI, the hot solvent jet is used as the dopant.

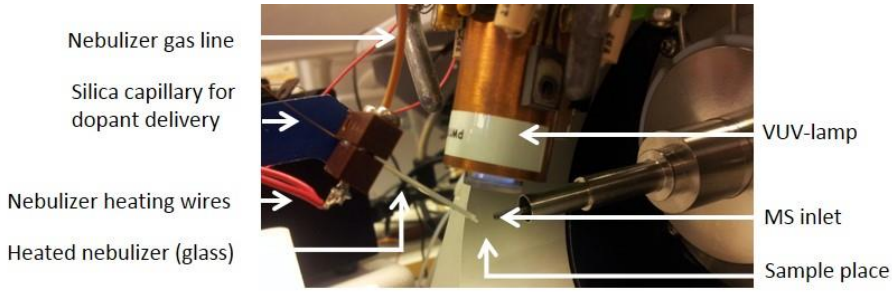

Figure 6. Photo of DAPPI setup.

Like APPI, DAPPI is well suited for the ionization of low polar and neutral compounds. DAPPI has been applied to the detection of e.g. drugs of abuse,[30,31,132,133] PAH compounds,[134] explosives,[135] plant combustion material,[136] lipids[36,137] and nonpolar vitamins.[36]

1.2.4 Direct analysis in real time

Like DAPPI, direct analysis in real time (DART) is an ambient ionization technique.[29,138] In DART, the samples are analysed directly without pre-handling in ambient conditions. A schematic picture of the DART ion source is presented in Figure 7. In DART, a heated reagent gas flow, typically He, is directed between two electrodes. Excited state species He^* are created from the reagent gas in glow discharge between two electrodes. The reagent gas flows out from the ion source. The sample is placed between the ion source exit and the MS inlet capillary, where it is exposed to the outflowing hot reagent gas. The analytes are thermally desorbed from the sample surface and ionized by gas phase ionization reactions. The formed ions are guided into the MS.[29] The ionization process in positive ion DART is described below.

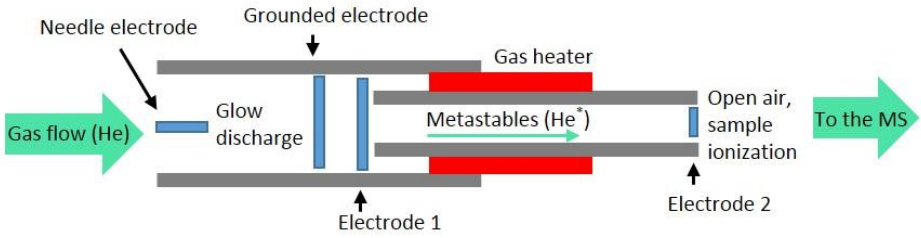

Figure 7. Schematic of DART ion source.

It is suggested that the ionization reactions in DART start with direct Penning ionization between He^* and neutral gas phase molecules (M, e.g. water, solvent or oxygen) forming $M^{+\bullet}$ (Table 4, Reaction 1).[29,138,139] This will happen if the IE of M is lower than the internal energy of He^*. He forms excited state species (2^3S state) with internal energy of 19.8 eV. These species will efficiently ionize water with IE of 12.62 eV. Water is found with high abundance in ambient conditions and the reaction between He^* and water produces protonated water clusters $[(H_2O)_n+H]^+$ (Table 4, Reaction 2).[138,139] Instead of direct Penning ionization, the ionization of the analytes is likely to happen via proton transfer reactions between protonated water clusters and the analytes (A) (Table 4, Reaction 3). The protonated water clusters can also ionize solvent (S) molecules through proton transfer (Table 4, Reaction 3).

Table 4. Positive ion ionization reactions in direct analysis in real time. He = reagent gas, He^* = gas metastable, M = (e.g. water, solvent or oxygen), A = analyte, and S = solvent.

Reaction	Note	#
$He^* + M \rightarrow He + M^{+\cdot} + e^-$	IE(M) < 19.8 eV	1
$He^* + (H_2O)_n \rightarrow He + [(H_2O)_{n-1} + H]^+ + OH^-$	IE(H_2O) = 12.62 eV	2
$[(H_2O)_n + H]^+ + A\ or\ S \rightarrow (H_2O)_n + [A\ or\ S + H]^+$	PA(A or S) > PA($H_2O)_n$	3
$S^{+\cdot} + S_n or\ A \rightarrow [S - H]^{\cdot} + [S_n or\ A + H]^+$	PA(S or A) > PA([S−H]$^{\bullet}$)	4
$[S_n + H]^+ + A \rightarrow S_n + [A + H]^+$	PA(A) > PA(S_n)	5
$S^{+\cdot} or\ O_2^{+\cdot} + A \rightarrow S\ or\ O_2 + A^{+\cdot}$	IE(A) < IE(S or O_2)	6

[a] Reactions from references [29,138,139]

The ionized molecule in Reaction 1 (Table 4, Reaction 1) may also be a solvent (S).[139] The formed $S^{+\bullet}$ can undergo proton transfer reactions with other solvent molecules and form protonated solvent clusters $[S_n+H]^+$ (Table 4, Reaction 4). These can ionize the analyte via proton transfer reactions forming protonated analyte molecules (Table 4, Reaction 5). $S^{+\bullet}$ may also ionize the analyte through charge exchange or proton transfer reactions (Table 4 reactions 6 and 4 respectively). Under certain low humidity conditions, atmospheric oxygen (IE 12.07 eV) can be ionized through Penning ionization (Table 4, Reaction 1) to form molecular ions of oxygen,[138] which can ionize the analytes through charge exchange (Table 4, Reaction 6) if the IE of the analyte is lower than the IE of the oxygen molecule.

DART, as well as DAPPI, is a suitable ionization method for small molecules (maximum MW ~ 1000 Da), because the desorption process is thermal and dependent on the vapor pressure of the compounds. DART has been applied to the analysis of e.g. drugs of abuse,[34,140,141] CWAs,[142] explosives,[143] and mycotoxins.[144,145]

1.2.5 Other ionization techniques used with ion mobility spectrometry

Another ionization technique applied in IMS is corona discharge-atmospheric pressure chemical ionization (CD-APCI). In CD-APCI, the ionization takes place under atmospheric pressure. The ionization mechanism in CD-APCI is similar to that of APCI-RI. Both APCI-RI and CD-APCI are suitable for low molecular weight compounds (< 1000 Da).

Electrospray ionization (ESI) is an atmospheric pressure ionization technique used especially in MS.[146] In ESI, a sample solution flows through a stainless-steel needle. High voltage is applied to the needle and an electric field is formed between the needle and the counter electrode, e.g. at the MS inlet. Due to the electric field, the sample flow, and an assisting nebulizer gas, a spray of charged sample droplets is formed out of the electrospray needle. The spray has the shape of a cone and charged sample droplets are released from the tip of the cone. Droplets will move towards the counter electrode at the MS inlet. Charged analyte molecules are formed, when the solvent evaporates and surface tension of the droplets cannot preserve the charge. The droplets break down repeatedly to smaller charged droplets, on the way to the MS inlet, until charged analyte molecules are left.[147,148] ESI is suitable for compounds with polar or semi-polar nature and for high molecular weight compounds like many biological analytes.

The most applied ambient MS technique with IMS is desorption electrospray ionization (DESI).[28] In DESI a solid sample is sprayed with a jet of charged solvent, which can be compared to ESI spray. The analytes are rapidly dissolved and carried away from the sample surface by the continuous solvent flow and formed secondary droplets are directed to the MS.[149,150] Ionization mechanism reminds ESI mechanism,[146-148] but the gas phase ion molecule reactions have been suggested as well.[151] The nature of the spray makes the DESI suitable for polar and semi-polar compounds. Also, DESI is suitable for higher molecular weight compounds than DART and DAPPI, because desorption of the analytes from the sample surface is not a thermal process.

1.3 Applications of ion mobility spectrometry

IMS has been widely used as a standalone instrument, but the coupling with chromatographic techniques and MS has increased the application possibilities of IMS.[2,3,18,24,54,70,89,152] The chromatographic separation and MS detection allows the qualitative and quantitative analysis of complicated samples with more reliability than can be achieved with IMS alone. In addition, the IM separation brings an extra dimension to the analysis, which results in higher peak capacity than the individual analysis techniques alone.[23-25]

Traditionally IMS has been utilized in the analysis of explosives,[13,18,21,98,153] illicit drugs,[101,102,154] CWAs,[14,15,19,20,155] VOCs and other volatiles,[1,16,69,74,79,156] and pharmaceuticals.[9,10,157] Through instrument development, the capability of IMS to separate isomers[11,12,115,158,159] and determine the CCS of a compound[160-163] has improved, consequently drawing increased interest in IMS. Ion mobility-mass spectrometry (IM-MS) instruments have been applied to the analysis of metabolites,[25,164,165] carbohydrates,[12,86] lipids,[59,166] proteins,[53-56,82,85,167-169] and lately also to the mass spectrometric imaging of surfaces e.g. animal tissue.[170-172]

Some examples of IMS applications related to this research are listed in Tables 5-8. TATP (Publication I) has been studied with standalone IMS instruments,[22,173-180] and gas chromatography-ion mobility spectrometry[181] and IM-MS (Table 5).[22,173,177,178,180,182] The studies, where MVOCs emitted from microorganisms in damp building materials (Publication II) have been monitored by IMS, are few. In these studies, MVOCs have been analysed mainly with DT-IMS (Table 6).[183-187] There have been a larger number of studies related to building material emissions or indoor air quality monitoring by IMS (Table 6).[71,156,188-196]

Table 5. Applications of ion mobility spectrometry in the analysis of triacetone triperoxide.

Instrument	Sample / compound	Notes	Ref
DAPP-IMS[a]	Triacetone triperoxide in different matrices	Thermal desorption of solid sample, dopant acetone, limits of detection on ng level	[176]
DT-IMS,[b] DT-IM-MS[c]	Dried sample solution of Triacetone triperoxide and other explosives	Thermal desorption, ^{63}Ni ionization, gas phase ion chemistry study	[178]
ITMS,[d] ITMS-MS[e]	Dried sample solution of triacetone triperoxide and other explosives	Thermal desorption, ^{63}Ni ionization, gas phase ion chemistry study	[177]
PSPME-IMS[f]	Headspace sampling of triacetone triperoxide	Thermal desorption, ^{63}Ni ionization, ng level detection	[174]
DT-IMS,[b] IM-MS[c]	Triacetone triperoxide vapor from solid sample	^{63}Ni ionization, ammonia dopant, triacetone triperoxide was detected as ammonia adduct	[22]
GC-IMS[g]	Triacetone triperoxide, different matrices	Thermal desorption, ^{63}Ni ionization, gas chromatography separation reduced false positives	[181]
DT-IMS[b]	Triacetone triperoxide and other explosives in hair sample	Direct sampling of hair, swabbing of hair and solvent extract from hair	[179]
DT-IMS,[b] DT-IM-MS[c]	Triacetone triperoxide both pure sample and diluted in toluene	Toluene changed the ion mobility spectrum peak positions and increased intensity	[173]

[a] Dopant-assisted positive photoionization-ion mobility spectrometry, [b] drift tube ion mobility spectrometry, [c] drift tube ion mobility spectrometry-mass spectrometry, [d] ion trap mobility spectrometry, [e] ion trap mobility spectrometry-mass spectrometry, [f] planar solid-phase microextraction-ion mobility spectrometry, [g] gas chromatography-ion mobility spectrometry.

Table 6. Applications of ion mobility spectrometry in the analysis of microbial volatile organic compounds, building material emissions, and indoor air quality.

Instrument	Sample / compound	Notes	Ref
Microbial volatile organic compounds applications			
DT-IMS[a]	Pine sapwood specimens inoculated with microbe spores in emission chamber, produced microbial volatile organic compounds	Tritium ion source, headspace sampling, inoculated and non-inoculated samples were separated during cultivation time according to microbial volatile organic compounds production	[187]
DT-IMS[a]	14 microbial volatile organic compounds and their mixtures, field sampling in indoors	Tritium ion source, microbial volatile organic compound limits of detection 3–96 μg m^{-3}, field sampling suggested mould growth	[185]
DT-IMS[a]	Pesticide standards and indoor and outdoor air samples	Thermal desorption, ^{63}Ni ionization, limits of detection 8 – 600 pg	[189]
Building material emissions and indoor air quality			
AIMS[b]	62 chemicals emitting from in indoor environments	^{241}Am ionization, sniff testing	[188]
DT-IMS[a]	Pharmaceutical standards, indoor air samples on Teflon membrane	Thermal desorption, ^{63}Ni ionization	[195]
MCC-UV-IMS[c]	Emission measurements of various compounds from surfaces indoors	UV ionization, sampling of volatiles with emission cell, limits of detection in ppb range	[194]
DMS[d]	Continuous monitoring of volatile organic compounds in indoors and outdoors	Photoionization, target compounds with low ionization energies like benzene, toluene and xylene were detected successfully	[71]
DT-IMS[a]	Monitoring laboratory air with planned and unplanned exposures of volatile chemicals	^{63}Ni ionization; water, acetone and dimethyl sulfoxide reagent gases	[156]

[a] Drift tube ion mobility spectrometry, [b] aspiration ion mobility spectrometry, [c] multi capillary column-ultraviolet ionization-ion mobility spectrometry, [d] differential mobility spectrometry

Ambient ionization techniques for direct sampling of compounds of interest have been coupled with both standalone IMS[197-203] and hyphenated IM-MS instruments.[39-42,170-172,204-213] Altogether, the most applied ambient ionization technique has been DESI[39-42,172,203,204,207,208,212] and the most applied IMS instrument TWIMS.[39-41,170,171,204-206,208,209,211-214] Ambient ionization coupled with IM-MS has been applied to the analysis of CWAs,[204] pharmaceuticals,[40-42,203,210] drugs of abuse,[206] proteins,[39,208] and to the surface imaging of synthetic[214] or biological tissue samples.[170-172,207,211] In ambient ionization IM-MS applications, the advantage of fast IM separation has been the increase in the peak capacity, decrease in the chemical noise in the mass spectrum, the increment in the S/N, and the separation of isomers. Some examples of applications of ambient ionization coupled with IMS or IM-MS are presented in Table 7.

Table 7. Applications of ambient ionization ion mobility spectrometry and ion mobility-mass spectrometry.

Instrument	Sample / compound	Notes	Ref
LAESI-TWIM-MS[a]	Synthetic fibers and polymers	Surface imaging, finish layer characterization and compound identification was achieved	[214]
DESI- / LMJSSP-FAIMS-MS[b]	Metabolites, lipids, and proteins on biological tissue	Surface imaging, ion mobility separation increased the signal-to-noise ratio and enabled the detection of unseen compounds	[207]
LAESI-TWIM-MS[a]	Plant and animal tissues	Surface imaging, ion mobility separation enabled the separation of isobaric compounds and enhanced spectral quality	[170]
PS-FAIMS-MS[c]	Isomers of opiates	Field asymmetric ion mobility spectrometry was capable to separate structural isomers	[210]
DART-DT-IMS[d]	Toxic chemicals	Transmission mode direct analysis in real time enhanced the sensitivity compared to glass rod sampling of a chemical	[200]
DESI-TWIM-MS[e]	Chemical warfare agents in vials and spiked forensic media	Solid phase microextraction sampling of chemical warfare agents in vial headspaces, unique ion mobility spectra for each compound, fast analysis	[204]
DESI-DMS-MS[f]	Pharmaceutical tablets, standard, mixture of isobaric compounds	Ion mobility separation reduced the chemical noise and increased the signal-to-noise ratio, isobaric compounds were baseline separated in differential mobility spectrometry	[42]
DESI-TWIM-MS[e]	Proteins (tryptically digested)	Isobaric peptides were differentiated, ion mobility separation clarified the mass spectra	[208]
DESI-TWIM-MS[e]	Pharmaceutical drug formulation	Ion mobility separation enhanced the spectral quality and increased the selectivity for the compounds of interest	[40]

[a] Laser ablation electrospray ionization-travelling wave ion mobility-mass spectrometry, [b] desorption electrospray ionization- / liquid microjunction surface sampling probe-field asymmetric ion mobility spectrometry-mass spectrometry, [c] paper spray ionization-field asymmetric ion mobility spectrometry-mass spectrometry, [d] direct analysis in real time-drift tube ion mobility spectrometry, [e] desorption electrospray ionization-travelling wave ion mobility-mass spectrometry, [f] desorption electrospray ionization-differential mobility spectrometry-mass spectrometry

One advantage of several IMS instruments is their ability to operate under ambient conditions. This allows the study of gas-phase ion chemistry under atmospheric pressure by IMS. Some examples of studies related to this topic are also listed in Table 8.

Table 8. Applications of ion mobility spectrometry in fundamental research.

Instrument	Sample / compound	Notes	Ref
dual-shutter DT-IMS[a]	Nitrate explosives	^{63}Ni ionization, experimental and theoretical study of the kinetics of thermal decomposition of nitrate explosive Cl^- adducts	[47]
dual-shutter DT-IMS[a]	Nitroglycerin	^{63}Ni ionization, experimental and theoretical study of the kinetics of thermal decomposition of nitroglycerin Cl^- adduct	[49]
DMS,[b] GC-DMS,[c] DMS-MS[j]	Series of carboxylic acid esters	^{63}Ni ionization, the dissociation of proton-bound dimers of esters by electric field heating was studied	[52]
dual-shutter DT-IMS[a], DMS,[b] DMS-MS[d]	Series of 2-ketones from acetone to nonanone	^{63}Ni ionization, the Arrhenius parameters of dissociation of proton-bound dimers of 2-ketones and T_{eff} of the dimers were determined	[50]
DMS,[b] DMS-MS[d]	Dimethyl methylphosphonate vapor	^{63}Ni ionization, the effective temperature of dimethyl methylphosphonate proton-bound dimer dissociation was determined	[51]
dual shutter DT-IMS[a]	1,4-dimethylpyridine and methylphosphonate vapor	^{63}Ni ionization, proton-bound dimer dissociation enthalpies of 1,4-dimethylpyridine and methylphosphonate were determined.	[46]
DT-IMS,[a] DT-IM-MS[e]	Dinitrocompounds[f]	^{63}Ni ionization, stability studies of the dinitrocompound Cl^- adducts	[215]
DT-IMS[a]	Phenol and fluorophenols	^{63}Ni ionization, stability and dissociation studies of phenol and fluorinated phenol Cl^- adducts	[216]

[a] Drift tube ion mobility spectrometry, [b] differential mobility spectrometry, [c] gas chromatography-differential mobility spectrometry, [d] differential mobility spectrometry-mass spectrometry, [e] drift tube ion mobility-mass spectrometry, [f] 2,3-dimethyl-2,3-dinitrobutane; 1,4-dinitrobutane; 2,3-dimethyl-2,4-dinitropentane

2 Aims of the study

The aims of this research were to study the applicability of ion mobility-based detection techniques in the direct analysis of hazardous compounds from the gas phase, pharmaceuticals and vitamins from solid samples, and in fundamental studies of gas phase ion chemistry.

More specifically the aims of this research were:

- to study the feasibility of aspiration ion mobility spectrometry in the analysis of explosive triacetone triperoxide and microbial originated volatile organic compounds directly from the gas phase without pre-separation (I, II)
- to combine direct surface analysis techniques — desorption atmospheric pressure photoionization and direct analysis in real time — with travelling wave ion mobility-mass spectrometry, and to compare the ionization methods (III)
- to apply desorption atmospheric pressure photoionization and direct analysis in real time without sample pre-handling and compound separation for fast analysis of pharmaceuticals and vitamins directly from authentic solid samples (III)
- to study the applicability of drift tube ion mobility spectrometry, mass spectrometry, and theoretical calculations in fundamental study of the reactions of Cl^- with phenol and fluorinated phenols, in the gas phase (IV).

3 Experimental

The chemicals, gases, samples, instrumentation and experimental procedures used in this research are described here. More detailed descriptions of the experimental component of this research can be found in the original Publications (I-IV).

3.1 Chemicals, gases and samples

The chemicals and gases used in this work are listed in Table 9, and samples in Table 10.

Table 9. Chemicals and gases used in the work. Publ. = Publication.

Chemical (purity)	Manufacturer / supplier	Note	Publ.
Acetone (PA)	Merck (Darmstadt, Germany)	Reagent	I
Acetonitrile (PA)	Merck (Darmstadt, Germany)	Solvent	I
Helium 5.0	AGA, Finland	Carrier gas	I, II
Hydrochloric acid (PA)	Merck (Darmstadt, Germany)	Reagent	I
Hydrogen peroxide (50%, extra pure)	Scharlau Chemie (Barcelona, Spain)	Reagent	I
Synthetic air	AGA (Finland)	Sampling gas	I
Triacetone triperoxide	AccuStandard (New Haven, CT, USA)	Standard in acetonitrile	I
Nitrogen	AGA (Finland)	Used in thermal desorption	II
Tenax TA	Sigma-Aldrich (USA)	Adsorbent	II
Toluene (PA)	Merck (Darmstadt, Germany)	Standard	II
Benzo[a]pyrene (≥95%)	Sigma-Aldrich (St. Louis, MO, USA)	Standard	III
Bisphenol A (≥99%)	Sigma-Aldrich (St. Louis, MO, USA)	Standard	III
Chloroform (≥99.8%)	EMD (Gibbstown, NJ, USA)	Solvent	III
Chloroquine diphosphate salt (≥98%)	Sigma-Aldrich (St. Louis, MO, USA)	Standard	III
Cholecalciferol (≥98%)	Sigma-Aldrich (St. Louis, MO, USA)	Standard	III
Cortisol (≥98%)	Sigma-Aldrich (St. Louis, MO, USA)	Standard	III
Helium 5.0		Reagent gas	III
Methanol (≥99.8+%)	Alfa Aesar (Ward Hill, MA, USA)	Solvent	III
Methanol (≥99.9%)	Sigma-Aldrich (St. Louis, MO, USA)	Solvent	III, IV
Nitrogen	Nitrogen generator	Nebulizer gas	III
Ranitidine hydrochloride (≥99%)	Sigma-Aldrich (St. Louis, MO, USA)	Standard	III
DL-α-Tocopherol (≥99%)	Merck (Darmstadt, Germany)	Standard	III
Toluene (≥99.9%)	Sigma-Aldrich (St. Louis, MO, USA)	Solvent, dopant	III, IV
Purified air	Pure air generator and sieve trap	Drift gas	IV
Carbon tetrachloride (99.9%)	Sigma Aldrich (Milwaukee, WI, USA)	Dopant	IV
Carbon tetrachloride (≥99.8%)	Merck (Darmstadt, Germany)	Dopant	IV

Table 9. continued Chemicals and gases used in the work. Publ. = Publication.

Chemical (purity)	Manufacturer / supplier	Note	Publ.
2,4-Difluorophenol (99%)	Sigma-Aldrich (St. Louis, MO, USA)	Sample	IV
2-Fluorophenol (98%)	Sigma-Aldrich (St. Louis, MO, USA)	Sample	IV
Nitrogen	Airgas Inc. (Radnor, PA, USA)	Carrier gas	IV
Nitrogen	Nitrogen generator	Nebulizer and collision gas	IV
Pentafluorophenol (≥99%)	Sigma-Aldrich (St. Louis, MO, USA)	Sample	IV
Phenol (99%)	Sigma-Aldrich (St. Louis, MO, USA)	Sample	IV
2,3,6-Trifluorophenol (98%)	Sigma-Aldrich (St. Louis, MO, USA)	Sample	IV

Table 10. Samples used in the work. Publ. = Publication

Sample	Supplier / source	Note	Publ.
Triacetone triperoxide, purity 93.8 wt-%	Synthesized by Finnish Defence Forces Technical Research Centre (Lakiala, Finland)	Analysed as such	I
Sterile and microbe contaminated particle board	Local manufacturer	Sample	II
Almonds	Local supermarket	Analysed as such	III
Dried blood spots on Whatman filter paper, 10 µL of human blood spiked with chloroquine (3 µM)	Dr. Michael D. Green (Center for Disease Control and Prevention (CDC), Atlanta, USA)	Analysed as such	III
Levonorgestrel tablets, fake and genuine	Paul N. Newton (Centre for Tropical Medicine, Churchill Hospital, University of Oxford, UK) and Dr. David Jenkins (FHI 360, USA)	Analysed as such	III
Multivitamin tablets (One A Day)	Local supermarket, (Bayer Healthcare LLC, Morristown, NJ, USA)	Analysed as such	III

3.2 Instrumentation and programs

Table 11 describes the instruments used in the research. Some instruments and experimental procedures are described in more detail below.

Table 11. Instruments and programs used in the research. Publ = Publication.

Instrument/program	Manufacturer	Note	Publ.
ChemPro100i, a hand held chemical detector	Environics Inc. (Mikkeli, Finland)	Instrument is described in section 1.1.3 and its application is described below	I, II
Gas chromatography column HP-5	Agilent Technologies (Wilmington, DE, USA)	Used for triacetone triperoxide quantification	I
Gas chromatography (6890)-mass spectrometry (5975)	Agilent Technologies (Wilmington, DE, USA)	Used for triacetone triperoxide quantification	I
LogInspector	Environics Inc. (Mikkeli, Finland)	Software for ChemPro100i data processing	I, II
Automatic Thermal Desorption ATD 400 autosampler – Autosystem XL Arnel gas chromatograph – TurboMass mass spectrometer	PerkinElmer (Waltham, MA, USA)	Used to analyse volatiles from air samples collected to tubes filled with Tenax Ta adsorbent	II
SIMCA-P 10.0	Umetrics (Umeå, Sweden)	Program used for principal component analysis	II
Gas chromatography column PE-5MS	PerkinElmer (Waltham, MA, USA)	Quantification of volatiles	II
µAPPI,[a] direct infusion system	Home-built	Described below, used to optimization of TWIM-MS[b] conditions	III
DAPPI[c] ambient ion source	Home-built	Used with TWIM-MS[b] Synapt G2	III
DART[d] SVP ambient ion source	IonSense Inc. (Saugus, MA, USA)	Used with TWIM-MS[b] Synapt G2	III
DART SVP IonSense	IonSense Inc. (Saugus, MA, USA)	Software to control the DART[d] ion source	III
DriftScope version 2.1	Waters Corp. (Milford, MA, USA)	Software for data processing of TWIM-MS[b] data	III
MassLynx version 4.1	Waters Corp. (Milford, MA, USA)	Software for data collection and processing of TWIM-MS[b] data	III
Power supply, DC, PSM-3004	G W Instek	Used to heat the microchip nebulizer	III
Teflon substrate	VINK Finland (Kerava, Finland)	DAPPI[c] sampling plate	III
Synapt G2 HDMS	Waters Corp. (Manchester, UK)	Used with both DAPPI[c] and DART[d] in mass spectrometry and TWIM-MS[b] modes	III

Table 11. continued Instruments and programs used in the research. Publ = Publication.

Instrument/program	Manufacturer	Note	Publ.
VAPUR gas-ion separator tube (GIST)	IonSense Inc. (Saugus, MA, USA)	Interface used Synapt G2 HDMS and DAPPI[c] and DART[d], described below	III
2C diaphragm pump	Vacuubrand (Wertheim, Germany)	Pump used in VAPUR	III
Vacuum ultraviolet rf krypton discharge lamp, PKR 100	Heraeus Noblelight (Cambridge, UK)	Used in atmospheric pressure photoionization ion source	III, IV
Linear IMS_1.0 software	National Instrument Corporation (Austin, TX, USA)	Ion mobility spectrometry operation	IV
Analyst 1.5	AB Sciex (Concord, ON, Canada)	Mass spectrometry data collection	IV
Analyst 1.6	AB Sciex (Concord, ON, Canada)	Mass spectrometry data processing	IV
µAPPI,[a] direct infusion system	Home-built	Sample and dopant nebulization, described below	IV
Gas chromatography	Hewlett-Packard (5890)	Used in GC-IM-MS[e]	IV
Gas chromatography column DB-5	J&W Scientific Inc., Folsom, CA, USA	Used in GC-IM-MS[e]	IV
GC-IM-MS[e]	House made (NMSU, Las Cruces, NM, USA)	Described below	IV
Gaussian 03W program	Gaussian Inc. (Wallingford, CT, USA)	Used with B3LYP functional with 6-311G+(dp) basis set	IV
Shimadzu-2010 LCMS mass spectrometer	Shimadzu Corporation (Kyoto, Japan)	Used in GC-IM-MS[e]	IV
PE Sciex API 365 mass spectrometer	AB Sciex (Concord, ON, Canada)	Used in collision induced dissociation studies of fluorophenols	IV
2010 MS LCMSsolution programs	Shimadzu Corporation (Kyoto, Japan)	For mass spectrometer operation in GC-IM-MS[e]	IV
Power supply, ISO-TECH 603	Thurlby-Thanders Instruments Ltd. (Huntingdon, England)	Used to heat the microchip heated nebulizer	IV

[a] Micro atmospheric pressure photoionization, [b] travelling wave ion mobility-mass spectrometry, [c] desorption atmospheric pressure photoionization, [d] direct analysis in real time, [e] gas chromatography-ion mobility-mass spectrometry

A handheld chemical detector ChemPro100i (I, II)

In Publications I and II, a handheld chemical detector was used to detect peroxide-based explosive TATP (I), MVOCs and VOCs (II). The instrument contained an ^{241}Am ion source, AIMS, and a series of six sensors.[6] The instrument is described in paragraph 1.1.3 'Aspiration ion mobility spectrometry'.

In Publication I, TATP was sampled from the controlled air flow of purified air with AIMS. To determine the concentration of TATP in the air flow, it was collected from the air to acetonitrile traps in two gas washing bottles in a series. The TATP concentration in the acetonitrile traps was analysed by GC-MS.

In Publication II, air samples were collected from test chambers with sterile and microbe-contaminated samples during the incubation of the microbes. The sampling was done from the head space of the chambers through sterile and filtered lines on incubation days 2, 4, 7, 11, 14, 17, and 22. The sampling was first done with ChemPro100i to monitor AIMS and sensor responses for the substances in the chamber head space. Comparative measurements were performed by transferring the head space samples to tubes that contained Tenax TA adsorbent. After the Tenax TA sampling, the ChemPro100i responses were collected again. Tenax TA sample tubes were analysed by TD-GC-MS. The detected compounds were quantified as toluene equivalents.

µAPPI direct infusion system (III, IV)

In micro atmospheric pressure photoionization (µAPPI) direct infusion system (Figure 8), solvent (with sample) is delivered to the MS as a heated jet by a microchip-heated nebulizer with the help of the nebulizer gas. The solvent jet and the APPI lamp are typically placed in front of the MS so that the signal intensity is maximized. The sample flow, nebulizer gas flow, and the chip temperature can be adjusted. The manufacturing of the microchip[217] and the chip holder[134] has been described elsewhere as well as the µAPPI system combined with MS.[218] In Publication III, µAPPI was used to optimize the TWIM-MS parameters for DAPPI and DART experiments. In Publication IV, µAPPI was used to deliver phenol and fluorophenols in separate solutions to the MS (Figure 8) for the Cl^- and fluorophenol experiments.

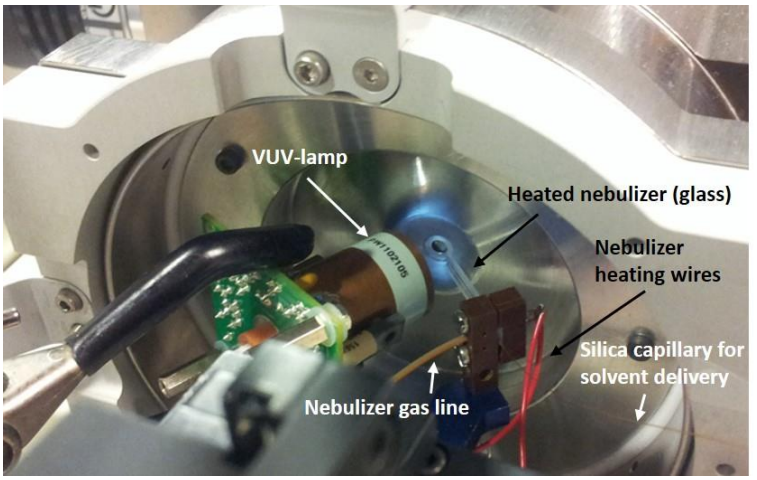

Figure 8. µAPPI setup in front of MS inlet.

Vapur interface to Synapt G2 (III)

In Publication III, DAPPI and DART ion sources were combined with TWIM-MS (Synapt G2 HDMS). The Z-Spray ion source of the Synapt G2 HDMS was fitted with the Vapour gas-ion separator tube interface (IonSense)[219] which enabled the use of both DAPPI and DART ion sources (Figure 9).

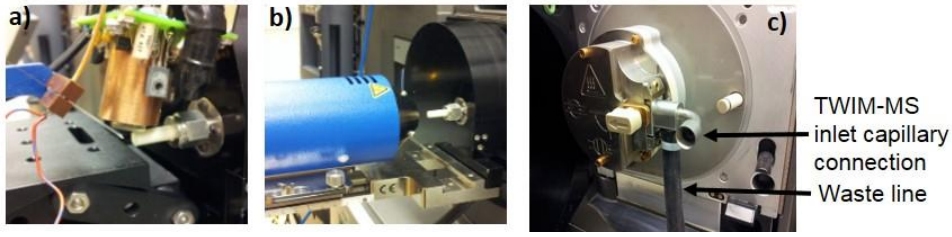

Figure 9. Photo of ion source connections for Synapt G2: a) DAPPI and b) DART in front of the modified Z-Spray ion source and c) opened modified Z-Spray ion source.

Gas chromatography-ion mobility-mass spectrometry (IV)

The DT-IMS used in gas chromatography-ion mobility-mass spectrometry (GC-IM-MS) studies of fluorophenols in Publication IV was built in-house. The instrument was built from a series of stainless steel ring electrodes with Teflon insulators. ^{63}Ni was used to create ions. The drift region of the instrument was 9.7 cm long and it was separated from the ion source/reaction region with an ion shutter. The instrument was heated with a rope heater. The samples were prepared in methanol and delivered to IMS using a gas chromatograph (GC). A capillary column was connected to the ion source/reaction region via a heated transfer line. The same transfer line was used to deliver CCl_4. Purified air was used as the drift gas, and it was connected to the drift tube from the detector end flange and vented from the ion source end flange. The instrument was hyphenated with MS from the Faraday detector hole in the ion source end with heated stainless-steel tubing and a Swagelok union (Swagelok company, Solon, OH, USA). A more detailed description of the instrument is given elsewhere.[47]

4 Results

The main results of the research are summarized in this section. More thorough presentations of the results are provided in the original Publications (I-IV).

4.1 Direct detection of gaseous analytes by aspiration ion mobility spectrometry (I, II)

It is challenging to detect for example hazardous chemicals, explosives and drugs of abuse rapidly, and reliably under field conditions. For these purposes, portable easy-to-use IMS devices with an APCI-RI ion source have been developed as chemical detectors, because e.g. many CWAs are volatile organophosphorus compounds, which have high PA and are therefore easily ionized with APCI-RI. Also, many explosives are detectable in negative ion mode quite selectively as adduct ions.

In Publications I and II, two different applications to monitor analytes directly from the gas phase with a portable AIMS chemical detector are described. The instrument was applied to the detection of explosive TATP (I) and monitoring of MVOCs and building material emissions (II).

4.1.1 Monitoring of gas-phase triacetone triperoxide (I)

Home-made organic peroxide explosives are commonly used by terrorists. One example is the ring formed peroxide TATP ($C_9H_{18}O_6$). The peroxide bonds give the compound its explosive and unstable nature, and because it is quite easy to synthesize also in primitive laboratory conditions, it has been used in so called 'improvised explosives' by terrorists. The detection of TATP directly from the gas phase is tempting, because TATP is relatively volatile (vapour pressure at 25 °C is ≈ 7 Pa) compared to typical nitrogen-containing explosives (e.g. vapour pressure of trinitrotoluene is ≈ $5*10^{-4}$ Pa).[220] In this research, synthesized TATP was produced to carrier gas flow and monitored with a hand held chemical detector ChemPro100i (I). The instrument consists of an AIMS (named IMCell) (see Figure 5), a group of six sensors and an APCI-RI ion source. To determine the experimental TATP concentrations in the gas flow, TATP was collected to two acetonitrile traps and analysed by GC-MS. IMCell and sensor responses were collected also by sniff-testing the TATP headspace in the opened container containing TATP sample.

Three different unknown concentrations of gaseous TATP were generated from solid TATP. The GC-MS results proved that the air flow from the gas generator contained mainly TATP. Each gas chromatogram showed one peak, for which the mass spectra showed characteristic ions of TATP at *m/z* 43, 59, 75, 101, and 117, which were most likely $[C_2H_3O]^+$, $[C_3H_7O]^+$, $[C_3H_7O_2]^+$, $[C_3H_6O_4]^+$, $[C_3H_6O_5]^+$, respectively. These ions are known to be fragmentation products of TATP.[94,221,222] TATP fragmented extensively, and the $M^{+\bullet}$ of TATP at *m/z* 222 was detected only with the highest TATP concentration. However, fragmentation is in good agreement with other studies, which have shown that due to the

peroxide structure, TATP decomposes easily in laser photoionization[222] and in electron ionization MS.[223]

TATP concentrations in the acetonitrile traps were determined by GC-MS, and these results were used to calculate the TATP concentrations in the gas phase. The obtained TATP concentrations in the gas phase, the corresponding measured IMCell sums (sum of the IMCell channel responses) and the TATP sniff-test IMCell sum responses are presented in Table 12. TATP was detected by IMCell in both positive and negative channels and the response time was less than five seconds. The instrument normalized detection threshold (20 pA) was reached already with the lowest TATP gas phase concentration of 0.3 mg m^{-3} = 0.03 ppm, corresponding to the IMCell sum response of 23.4 pA.

Table 12. Triacetone triperoxide concentrations in the gas phase and IMCell sum values.

Gas phase concentration (mg m^{-3})	IMCell sum (pA)
0.3	23.4
7.7	94.9
26.0	154.3
sniff test, concentration not determined	44.5

Figure 10 presents the IMCell response for TATP gas phase concentration of 26.0 mg m^{-3} and the sniff-test. The intensities of the IMCell channels (more about the channels in chapter 1.1.3. 'Aspiration ion mobility spectrometry') varied according to the TATP concentration, but the intensity pattern was the same in all concentrations. The pattern was the same also with the sniff-tests, which implies that the responses were due to TATP. In all the gaseous TATP concentrations, and the sniff-test, the most intense signal was detected on IMCell channel 4. In addition, the intensity was higher in positive channels than in negative channels (Figure 10). This implies that TATP produced more positive ions than negative ions in the gas phase, probably during ionization.

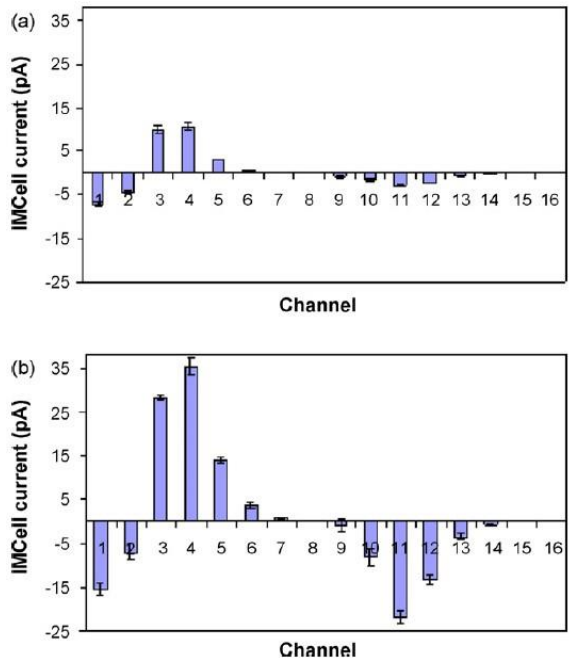

Figure 10. IMCell responses of TATP, mean values of four repetitions and standard error of means: (a) sniff-test, IMCell sum 44.5 pA, relative humidity 40 %; (b) TATP concentration in gas flow 26.0 mg m^{-3}, IMCell sum 154.3 pA, relative humidity 2.5 %. 1-8 are positive channels and 9-16 are negative channels.

Figure 10 shows that the IMCell response was more abundant in TATP gas phase concentration 26.0 mg m^{-3} (b) than in the sniff-tests (a). The sniff-test results usually resemble the maximum gas phase concentration of a sample, and therefore the TATP sniff-tests should have resulted in higher IMCell responses. The reason for the lower signal in the sniff-tests compared to the gas generator experiments could be the different humidity conditions in the experiments. In the gas generator experiments, the relative humidity (RH) was 2.5 %. In the sniff-tests the data was collected under ambient conditions and 40 % RH. Under high humidity conditions, as here in the sniff-tests, the reactant ions are strongly hydrated, and less product ions are formed compared to the low humidity conditions, where the reactant ions are less hydrated, and the reaction equilibrium favours the product ion formation.[3]

Sensor results supported the IMCell results. Figure 11 represents the relative resistance changes of different semiconductor sensors as a function of TATP concentration. The FET sensor failed to respond to TATP, and therefore the FET sensor intensities are not shown. When the semiconductor sensors were exposed for TATP, the relative resistances (R/R_0) of the sensors decreased. This showed a clear response for TATP in every measured concentration. The only exception was the MOS2 sensor, for which the relative resistance increased over one when the TATP concentration was 0.3 mg m^{-3}. This is most likely due to the low R_0 value and the low sample concentration. SCCell2 and MOS3 sensors became saturated after the lowest measured concentration. This means that these sensors are not

capable of discriminating between the different TATP concentrations. SCCell1, MOS1, and MOS2 sensors showed a dynamic range up to 8 mg m^{-3}.

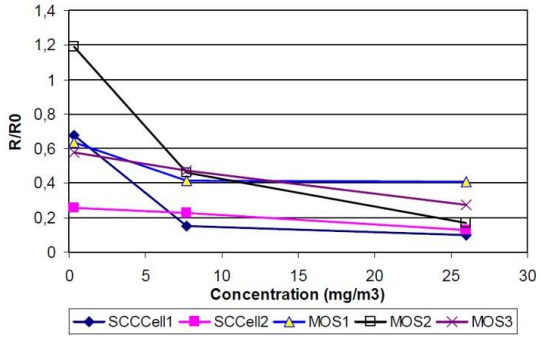

Figure 11. The relative resistance changes (mean values of three measurements and standard error of means) of semiconductor sensors as a function of TATP concentration.

The calculated theoretical TATP concentration in the saturated headspace of a closed container is approximately 627 mg m^{-3} = 69 ppm. This is clearly higher concentration than the concentrations measured and detected in this study from the gas flow under very low RH conditions. Additionally, TATP was detectable in sniff tests from the TATP headspace, which suggests that the sensitivity of the used AIMS is high enough for the detection of TATP, at least directly from the headspace of a container containing solid TATP. To confirm the feasibility, thorough experiments under different humidity conditions and concentrations should be performed. The effect of the possible interfering compounds (for example acetone and other solvents) on the detection should be studied as well.

4.1.2 Monitoring of volatiles in the headspace of building materials (II)

Many building materials work as a substrate for microbe reproduction especially in the high humidity conditions and metabolic action of the microbes produces a variety of MVOCs. These as well as building material emissions were monitored with ChemPro100i hand held chemical detector containing an AIMS (named IMCell) and a group of six sensors (II). The measurements were done from the headspace of a chamber (M) containing particle board samples contaminated by microbes. Another chamber (S) with particle board samples was held in sterile conditions and used as a reference. Both chambers M and S were held in high humidity conditions. AIMS and sensor data was collected from the headspaces of the chambers on days 2, 4, 7, 11, 14, 17, and 22 when the incubation of the microbes proceeded. At the same time, gaseous samples were collected to sample tubes with Tenax TA adsorbent and analysed by TD-GC-MS. The VOCs in the emission chambers were identified and quantified as toluene equivalents. The TD-GC-MS results were compared with those obtained with a ChemPro100i. Data was analysed by hand and by principal component analysis.

4.1.2.1 *Aspiration ion mobility spectrometry and semiconductor sensor measurements*

The air monitoring of both chambers S and M gave a strong response in the IMCell for both positive and negative ions in all the measurements. Figure 12 represents the IMCell results obtained on the 17th incubation day from both chambers S (Figure 12 a) and M (Figure 12 b). On the 17th incubation day microbe growth was not visible in chamber S, but could be visually detected on the surface of the building materials in chamber M. Figure 12 shows that the IMCell responses for chamber M are slightly different than for chamber S on both positive and negative channels. On positive IMCell channels in chamber S measurements, the highest signal was recorded on channel 3 (32.1 pA). The highest signal in chamber M was measured on channel 4 (37.0 pA). These differences were most likely caused by the microbe growth and volatiles originating from microbe metabolism in chamber M.

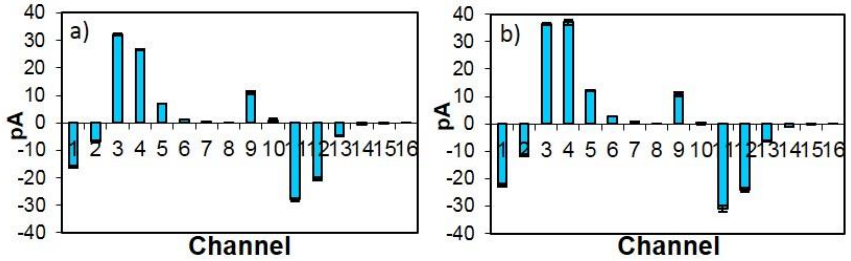

Figure 12. IMCell responses (mean values and standard error of means of six repetitions of the sixth measurement time) for chambers a) S and b) M. 1-8 are positive channels and 9-16 are negative channels.

The differences in the sensor responses between chamber S and M measurements on the 17th incubation day are evident (Figure 13). The relative resistance of all the MOS sensors decreased during the sampling from the headspace of both chambers S and M. The decrement was higher for chamber M (Figure 13 b) than for chamber S (Figure 13 a) measurements. This indicates higher VOC concentration in the chamber M headspace than in chamber S. The only exception is the MOS1 sensor, for which the resistance was lower in chamber S than in chamber M measurements. The reason for this could be that during the incubation, the concentrations of some compounds for which the MOS1 sensor is specific decreased because of microbe growth in chamber M. The ΔV of FE sensor was higher in chamber M than in chamber S measurements. FE sensor is sensitive for hydrogen only and the higher FE sensor response may indicate microbe activity since mould has been reported to produce e.g. ammonia.[224]

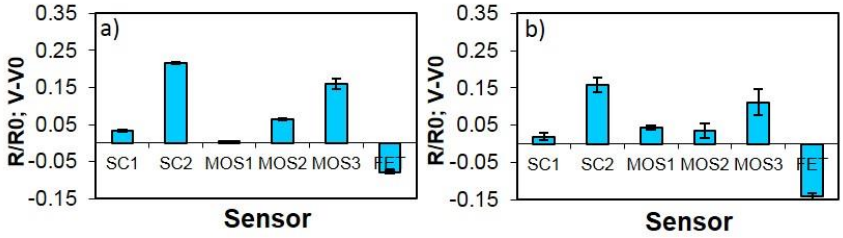

Figure 13. Sensor responses (mean values and standard error of means of six repetitions of the sixth measurement time) for a) chambers S and b) M atmospheres. Semiconductor sensor responses were detected as relative resistance changes and FET sensor responses as voltage difference.

The large data set of response changes of IMCell and sensors are difficult to compare and nothing can be said about the identities of the compounds affecting to the responses. Therefore, all the ChemPro100i data was analysed with multivariate data analysis technique called principal component analysis (PCA) to determine whether it would be possible to distinguish the chemical profiles of the test chambers M and S. In PCA a large data table with many observations and variables, is simplified without losing important information, by calculating new variables called *principal components* as linear combinations from the original data set.[225] The observations in PCA calculations were the seven samplings from both chambers S and M during the experiment. The observations were named S1-S7 for chamber S and M1-M7 for chamber M. The results are presented as score and loadings plots. Score plots show which observations separate from each other and loadings plot show which variables are causing the separation.

The PCA variables were the responses of the IMCell channels 1, 2, 4-8, and 10-16. Channels 3 and 9 were excluded from the model, because they had no influence on the results. The score plot of PCA (Figure 14 a) shows that the chemical profiles of chambers S and M were distinguished as the incubation proceeded. Data from measurements S1, S2, M1 and M2 grouped together and could not be separated. The reason is that these experiments were done after two days (measurements S1 and M1) and four days (measurements S2 and M2) of incubation, when the microbe growth was just starting and the volatiles in the headspace of chambers S and M were similar at the beginning of the incubation. As the incubation proceeded, the chemical profiles of the measurements M3-M7 and S3-S7 separated from the chemical profiles of the measurements S1, S2, M1, and M2. The chemical profiles of the measurements M3-M7 and S3-S7 were different from each other. The reason for these separations is most probably caused by the microbe growth and the MVOC production in chamber M. The loadings plot (Figure 14 b) shows that the separation of the data collected from chambers S and M after the fourth day of incubation was mostly caused by the responses on IMCell channels 1, 2, 4-7, and 10. The data from channels 1, 2, and 10 correlated positively with the measurements S3-S7, which are from measuring times when the incubation had already proceeded. The responses on IMCell channels 4-7 correlated with chamber M measurements M3-M7.

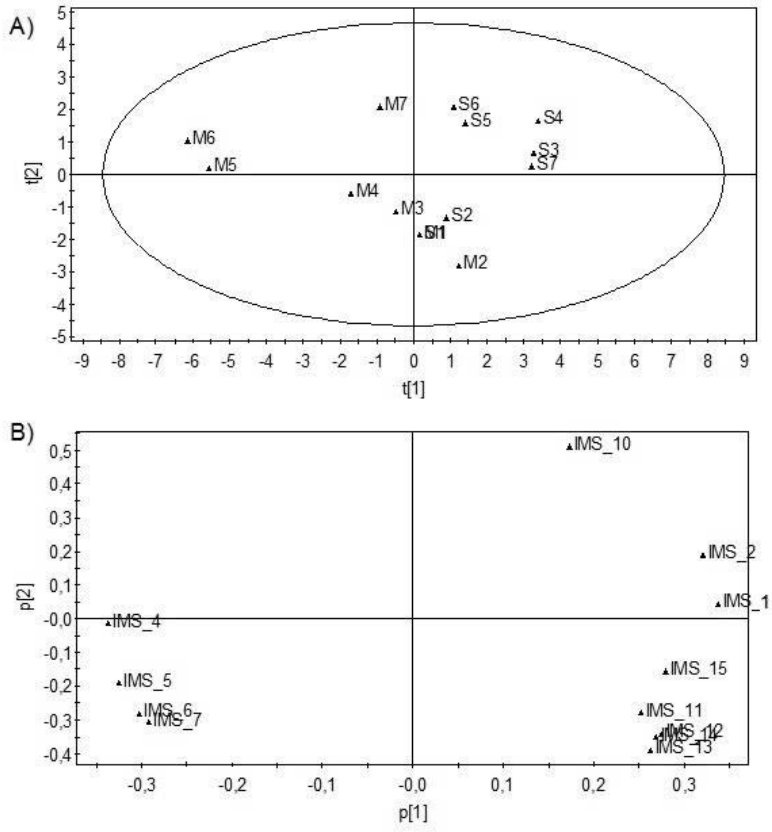

Figure 14. a) PCA score plot and b) loading plot of the IMCell responses of the seven sampling times from chambers M and S. The chambers are marked in the score plot a) as M1-M7 and S1-S7. IMCell channels 1-16 are marked with IMS_1 – IMS_16 in the loadings plot b).

In the second PCA, only the sensor responses were used as variables. Separation between the chemical profiles of chambers S and M was achieved after the microbe growth had started. Separation of measurements S2-S7 from the measurements M1-M7 was achieved when the variables corresponding to SC2 and FE sensors were removed from the model. The loadings plot showed that the chamber M observations M1-M7 correlated with the MOS1 sensor, and the MOS2, MOS3, and SC1 sensors correlated with the observations of chambers S2-S7. This suggests that the concentration drop of the compounds affecting the MOS1 sensor response in chamber M resulted in separation of the chemical profiles of chambers M and S.

Finally, PCA was performed for both IMCell and sensor data together. The responses of the IMCell channels 1, 2, 4-8, and 10-16 and the responses of MOS1, MOS2, MOS3, and SC1 sensors were used as PCA variables. The score plot and the loadings plot are presented in Figure 15. The results show that the chemical profiles of chamber S and M headspaces are different after two sampling times. The data of measurements S1, S2, M1, and M2 are

grouped together on the upper right hand corner of the score plot (Figure 15 a). The data of measurements S3-S7 are separated on the lower right-hand corner and M3-M7 spread on the left side of the score plot. The loadings plot shows that the responses of IMCell channels 1, 2, 4-7, and 10, as well as the MOS1 sensor, have the strongest influence on the separation of the chambers S and M chemical profile data (Figure 15 b). This was already observed in the PCA analysis of IMCell and sensor data.

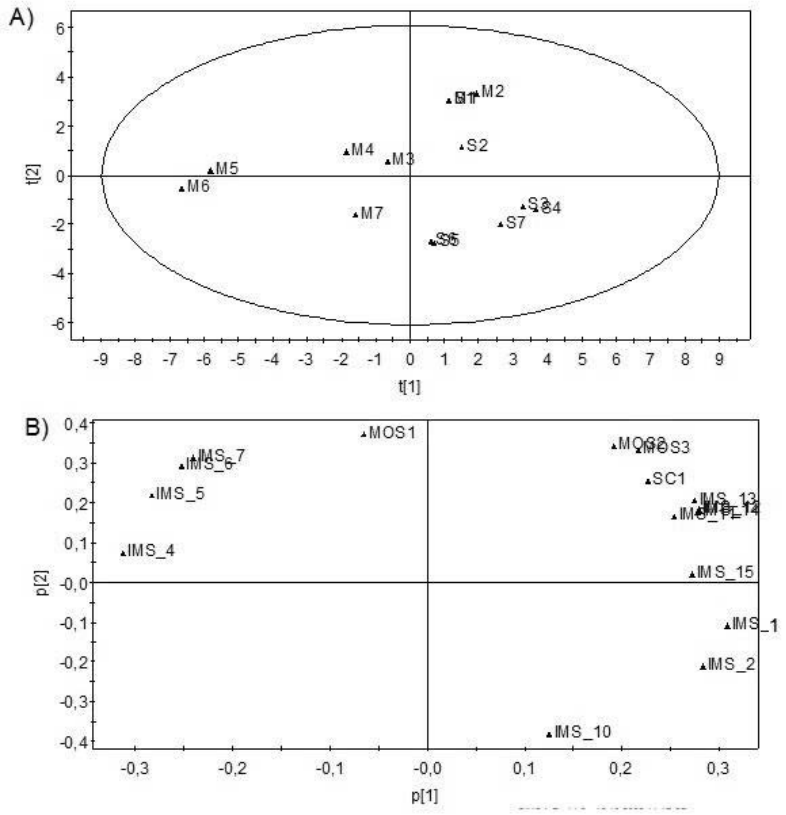

Figure 15. a) PCA score plot and b) loadings plot of the IMCell and sensor responses of the seven sampling times from chambers M and S. The chambers are marked in the score plot a) as M1-M7 and S1-S7. The IMCell channels 1-16 are marked with IMS_1 – IMS_16 and sensors with their abbreviations in the loadings plot b).

4.1.2.2 TD-GC-MS measurements and comparison with AIMS results

The headspace of chambers S and M were sampled to tubes containing Tenax TA adsorbent on incubation days 2, 4, 7, 11, 14, 17 and 22. The samples were analysed by TD-GC-MS to identify the possible MVOCs in chamber M. TD-GC-MS results were compared with IMCell result. Sampling on second and 17th incubation days was used to identify the MVOCs. However, damp particle board emits the same compounds that the microbes produce in their metabolic action. Therefore, the separation and identification of MVOCs from the background VOCs is difficult.

First, TD-GC-MS data from both chambers S and M were equalized and compared. After studying the chromatogram peak intensity changes, the following three cases were considered for the data obtained from chamber M. In case (1) the compound peak intensity increased, which could be caused by material emissions, microbial metabolic action, or both. In case (2), the peak intensity decreased, which was assumed to originate from the normal metabolic function of the microbes or the decrease in the material emission. In case (3) a new peak that was not present in chamber S, appeared. The new peaks were assumed to originate from microbe growth and metabolism and can reasonably be categorized as MVOCs.

The TD-GC-MS results showed that new compounds were produced to the headspace of both chambers S and M when the particle board samples got damp. Three new compounds were found from chamber M that were not present in chamber S. These can be definitively identified as MVOCs, comprising the compounds 2-pentanone,[226] propyl acetate, and 4-methyl-2-hexanone.[224] Altogether 46 other MVOCs were identified from chamber M by comparing the peak intensity changes in the chromatograms of the headspace samples from chambers S and M (Table 13). However, these compounds were also emitted by the particle board samples and were present in chamber S also. MVOC concentrations were determined as toluene equivalents. Table 13 shows the maximum concentrations of the MVOCs during the incubation. α-Pinene had the highest concentration at 886.4 μg m^{-3} of all the detected MVOCs, whilst 2-Pentanone, was identified as a new compound in chamber M and presented the second highest concentration at 582.3 μg m^{-3}. Other compounds reaching a concentration of over 200 μg m^{-3} were 3-carene and D-limonene. These, as well as α-pinene, were identified as MVOCs, but they are also found from many natural sources like pine trees. This explains their high concentration in the chambers containing particle board specimen.

Table 13. Identified microbial volatile organic compounds in chamber M and their maximum concentrations. In the parenthesis is the incubation day when the maximum concentration was achieved. Comp. No = compound number, Conc. = concentration.

Comp. No	Compound	Conc. [µg m^{-3}]	Comp. No	Compound	Conc. [µg m^{-3}]
1	2-Butanone	16.8 (4)	26	2-Pentylfuran	150.1 (17)
2	2-Pentanone[a]	582.3 (17)	27	3-Carene	442.9 (17)
3	Propyl acetate[a]	9 (17)	28	Isoterpinolene	6.5 (11)
4	4-Methyl-2-pentanone	10 (14)	29	*m*-Cymene	5.2 (22)
5	2-Methyl-3-pentanone	9.9 (17)	30	*o*-Cymene	171.9 (17)
6	Toluene	61.4 (4)	31	D-Limonene	249.2 (17)
7	1-Pentanol	53.4 (11)	32	γ-Terpinene	6.3 (22)
8	2-Heptanone	36.8 (14)	33	Acetophenone	4.9 (7)
9	Octane	186.6 (2)	34	*p*-Cymenene	14.4 (17)
10	Butyl acetate	10.5 (7)	35	2-Carene	6.2 (17)
11	2-Methylpyrazine	1.9 (22)	36	*o*-Cymenene	62.1 (17)
12	Cyclohexanone	3.1 (22)	37	2-Nonanone	4.1 (11)
13	4-Methyl-2-hexanone[a]	5.4 (22)	38	Fenchyl alcohol	11.9 (17)
14	5-Methyl-2-hexanone	1.7 (4)	39	L-Camphor	44.1 (22)
15	1-Hexanol	12.9 (11, 14)	40	Borneol	11.2 (14)
16	Tricyclene	14.6 (14)	41	Isopinocamphone	6.9 (22)
17	α-Phellandrene	9.2 (14)	42	4-Carene	13 (17)
18	Hexanoic acid methyl ester	1.7 (14)	43	D-Verbenone	17 (17)
19	α-Pinene	886.4 (17)	44	L-Bornyl acetate	6.1 (11)
20	Camphene	92.4 (17)	45	Verbenone	7.9 (17)
21	1,2,3,4,5,8-Hexahydronaphthalene	63.7 (17)	46	α-Copaene	4.1 (17, 22)
22	*p*-Cymene	35.8 (17)	47	Eremophilene	3.4 (22)
23	β-Phellandrene	2.2 (22)	48	γ-Cadinene	0.8 (22)
24	β-Pinene	103 (17)	49	α-Muurolene	16.4 (4)
25	1-Octen-3-ol	3.4 (14)			

[a] New compound detected and definitively identified as microbial volatile organic compound in the contaminated chamber.

Total volatile organic compound (TVOC) concentration was determined from the concentrations of all the identified VOCs in the headspaces of both chambers S and M. TVOC concentrations were compared to IMCell sum results to determine the corresponding IMCell response. TVOC concentration varied from 836.9 to 3797.4 µg m^{-3} during the incubation. IMCell sum varied between 105 and 154 pA, which is clearly over the normalized detection threshold of IMCell (20 pA). The TVOC concentration change and the corresponding IMCell sum change of chamber M headspace during the incubation is presented in Figure 16 (a). The concentration changes of MVOCs 2-pentanone, 4-methyl-2-hexanone, and propyl acetate in chamber M are presented in Figure 16 (b). As can be seen the IMCell sum and the corresponding TVOC concentration trends resemble each other. The concentrations of the MVOCs 2-pentanone, propyl acetate, and 4-methyl-2-hexanone also follow the same trend, where the compound concentrations increase during the incubation. The concentration of 2-pentanone increased rapidly after the 11th incubation day, achieving a maximum concentration on the 17th incubation day. Propyl acetate also reached the maximum concentration on the 17th incubation day, and 4-Methyl-2-hexanone

on the 22nd day. Altogether 11 out of 49 compounds reached the maximum concentration on the 22nd incubation day and 20 out of 49 reached the maximum concentration on the 17th incubation day.

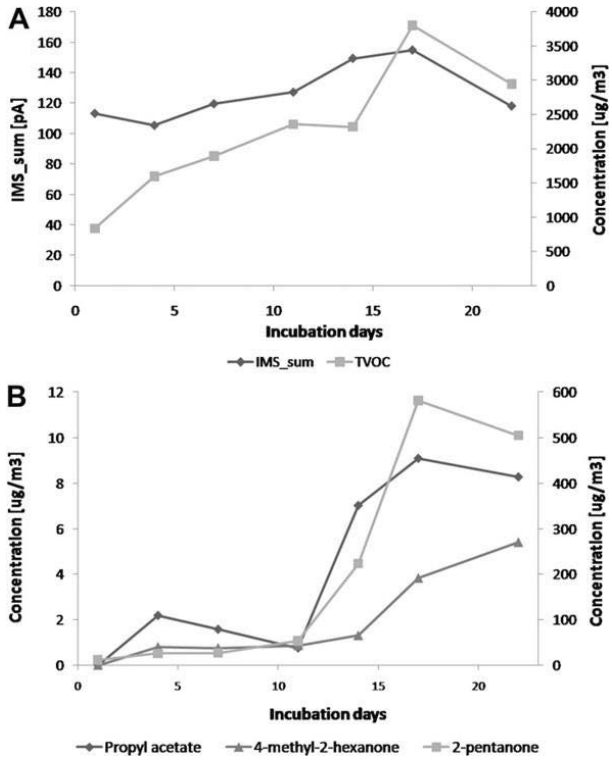

Figure 16. a) IMCell sum response (left vertical axis) and TVOC concentration (right vertical axis) as a function of incubation days and b) propyl acetate and 4-methyl-2-hexanone (left vertical axis) and 2-pentanone (right vertical axis) as a function of incubation days.

The TD-GC-MS data was also analysed with PCA. The score plot and the loadings plot are presented in Figures 17 (a) and 17 (b), respectively. The PCA observations were the seven samplings from both chambers S and M headspaces. The intensities of 49 chromatogram peaks that were identified as MVOCs were chosen as the variables. These included the MVOCs found in chamber M, but not in chamber S. The variables are marked in the loadings plot as their compound number presented in Table 13. The score plot shows how the measurements M4-M7 data separated from the rest of the measurements to the right-hand side of the plot (Figure 17 a). The separation is most likely due to microbial metabolic action, which caused changes in the compound concentrations in the chamber M headspace. The M1-M3 data grouped together with the S1-S7 data. A small discrimination between the first S1 and M1 measurements and the M2, M3, and S2-S7 measurements can be seen.

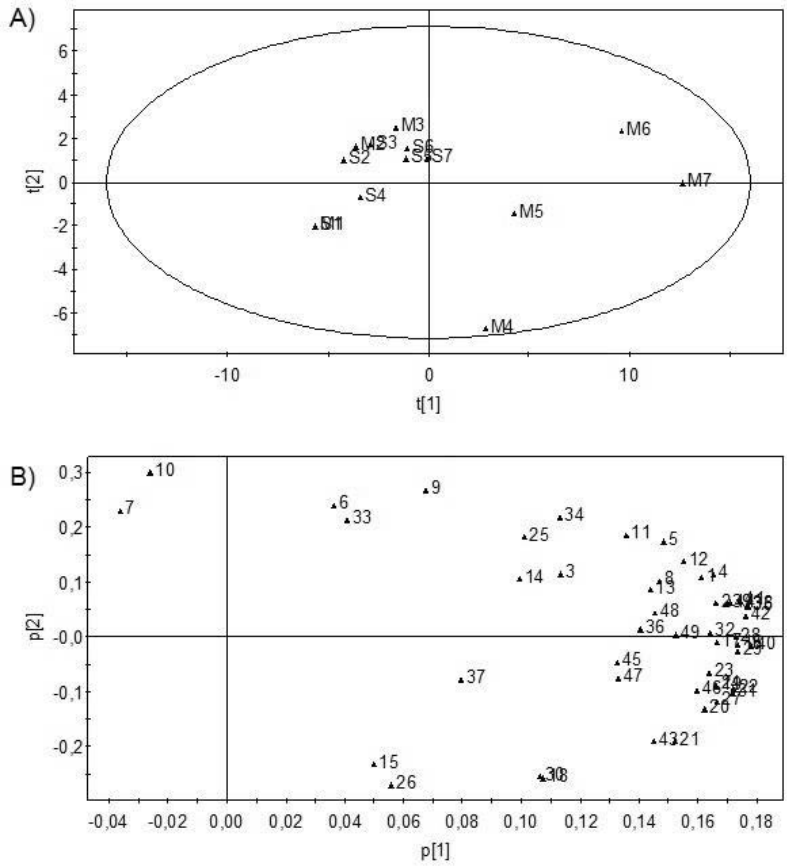

Figure 17. a) PCA score plot and b) loadings plot of seven TD-GC-MS measurements from chambers M (M1-M7) and S (S1-S7). The variables in the loadings plot b) are the detected compounds marked with their compound numbers as in Table 13.

The loadings plot in Figure 17 (b) shows how compounds 7 and 10 (1-pentanol and butyl acetate, respectively) correlate with the measurements M1-M3 and S1-S7. In both cases there is no microbe growth or the metabolic action of the microbes is still low. The rest of the compounds were affected more strongly by the separation of the chemical profiles of the chambers S and M headspaces during the incubation. This is expected, since the variables were the detected MVOCs and there were differences between the chemical profiles of chamber M and S headspaces. It can be concluded that starting from the fourth sampling on the 11th incubation day, the changes in the compounds and their concentrations in the headspace of chamber M resulted in differentiation of the chemical profiles of chambers S and M.

4.2 Direct detection of analytes from solid samples (III)

Ambient MS is a tool for fast screening of analytes directly from surfaces. However, background impurities and other interfering agents may complicate the spectra and therefore fast separation techniques are often needed before MS detection. In Publication III, ambient ionization techniques DAPPI and DART were coupled with TWIM-MS in desorption atmospheric pressure photoionization- and direct analysis in real time-travelling wave ion mobility-mass spectrometry (DAPPI- and DART-TWIM-MS respectively). The IM separation was applied as a pre-separation technique before the MS detection to reduce the chemical noise in the mass spectra. A comparative study of DAPPI and DART ionization techniques was also performed.

4.2.1 Comparison of DART and DAPPI ionization techniques

Comparison of DAPPI and DART ionization techniques was performed by desorption atmospheric pressure photoionization-mass spectrometry (DAPPI-MS) and direct analysis in real time-mass spectrometry (DART-MS) with five selected compounds, which included both polar and non-polar compounds with a capability to desorb thermally. Compounds were: bisphenol A (BPA), benzo[a]pyrene (B[a]P), cortisol, ranitidine, and α-tocopherol. The sampling of standard solutions of selected compounds was done from sample plates covered with Teflon film (DAPPI) or from glass rods injected with sample (DART). The sample volume was 1 µL for both DAPPI and DART. The studied analyte concentrations were 1, 10, and 100 µM. The detected base peaks and the estimated limits of detection (LOD) for each analyte are presented in Table 14. The estimated LODs were extrapolated from the lowest experimentally detected concentration for the base peak of each compound.

Table 14. The ions observed with desorption atmospheric photoionization (DAPPI) and direct analysis in real time (DART), the estimated limits of detection (LOD), the relative standard deviation (RSD %, n = 3) and DART:DAPPI LOD ratio.

Compounds	Base peak (*m/z*)		Estimated LOD [fmol] and RSD (%)		LOD ratio
	DAPPI	DART	DAPPI	DART	DART:DAPPI
Bisphenol A	$[M-CH_3]^{+\bullet}$ (213)	$[M-CH_3]^{+\bullet}$ (213)	90 (8)	8200 (26)	91
Benzo[a]pyrene	$M^{+\bullet}$ (252)	$[M+H]^+$ (253)	30 (9)	330 (11)	11
Ranitidine	$[M-C_8H_{12}ON]^+$ (176)	$[M-C_8H_{12}ON]^+$ (176)	290 (33)	2500 (11)	9
Cortisol	$[M-COCH_2OH]^{+\bullet}$ (303)	$[M-COCH_2OH]^{+\bullet}$ (303)	150 (14)	920 (37)	6
α-Tocopherol	$M^{+\bullet}$ (430)	$[M-H]^+$ (429)	190 (28)	3200 (19)	17

The most intense peaks with both DAPPI and DART for BPA, cortisol, and ranitidine were the same. For BPA, the main ion was at *m/z* 213 ($[M-CH_3]^{+\bullet}$),[227] for ranitidine at *m/z* 176 (fragment type $[M-C_8H_{12}ON]^+$),[228] and for cortisol at *m/z* 303 (which is probably the cleavage of from $M^{+\bullet}$).[229] For cortisol and ranitidine, the second-most abundant peak was the $[M+H]^+$ ion with both DAPPI and DART. Cortisol and ranitidine showed several fragment ions with both techniques. The masses of the ions and the intensity ratios were similar. With DAPPI, B[a]P was ionized through charge exchange and detected as $M^{+\bullet}$ ion

at *m/z* 252. With DART, the main peak of B[a]P was the $[M+H]^+$ ion at *m/z* 253, in addition, the $M^{+\bullet}$ ion of B[a]P, with an intensity of approximately 15 % of the intensity of $[M+H]^+$, was detected. The $M^{+\bullet}$ was thought to have generated through Penning ionization by the He metastables. With both techniques, small amounts of oxidation products were observed with B[a]P. With DAPPI, α-tocopherol was detected as an abundant $M^{+\bullet}$ ion at *m/z* 430, and as a $[M-H]^+$ ion at *m/z* 429. With DART, the main peak of α-tocopherol was the $[M-H]^+$ ion at *m/z* 429. α-Tocopherol oxidation products were also detected with both techniques.

DAPPI and DART could both ionize all the selected compounds. The LODs were between 30−290 and 330−8200 fmol for DAPPI and DART, respectively (Table 14). The LOD ratio of DART and DAPPI shows clearly, that from 6 to 91 times higher sample concentration was needed with DART than with DAPPI to reach the LODs of the analytes.

4.2.2 Direct surface analysis using DAPPI- and DART-TWIM-MS

DAPPI and DART were both applied to the direct surface analysis of authentic solid samples. IM separation was utilized as a pre-separation technique before MS to enhance the selectivity of the analysis.

4.2.2.1 The analysis of dried chloroquine-spiked blood spots

The feasibilities of DAPPI- and DART-MS in the rapid and direct analysis of chloroquine from dried blood spots on filter paper were investigated here. With both methods, chloroquine was detected as the $[M+H]^+$ ion at *m/z* 320. (Figure 18 a and b). With DAPPI, also a typical $[M-C_4H_{11}N]^+$ fragment of chloroquine at *m/z* 247 was observed. DAPPI showed eight times higher $[M+H]^+$ ion intensity and 14 times higher S/N for chloroquine than DART. In order to clean up the DART mass spectrum from interfering agents and to improve the S/N, TWIM separation was applied with DART-MS. The advantage of this extra dimension is shown in Figures 18 (c-f). Figures 18 (c) and 18 (d) present the total IM spectrum (= an IM spectrum with all the detected ions) of all the ions produced by DART from the dried blood spot sample, and the combined mass spectrum from the total IM data, respectively. The chloroquine ion at *m/z* 320 is not clearly observed in the combined mass spectrum in Figure 18 (d). However, Figure 18 (e) shows the single IM spectrum, which is an extracted IM spectrum of a specific ion, of the ion at *m/z* 320 with a peak at drift time 3.9 ms. The mass spectrum of this peak in Figure 18 (f) clearly shows higher relative abundance and better S/N for the chloroquine $[M+H]^+$ ion at *m/z* 320 compared to Figure 18 (b).

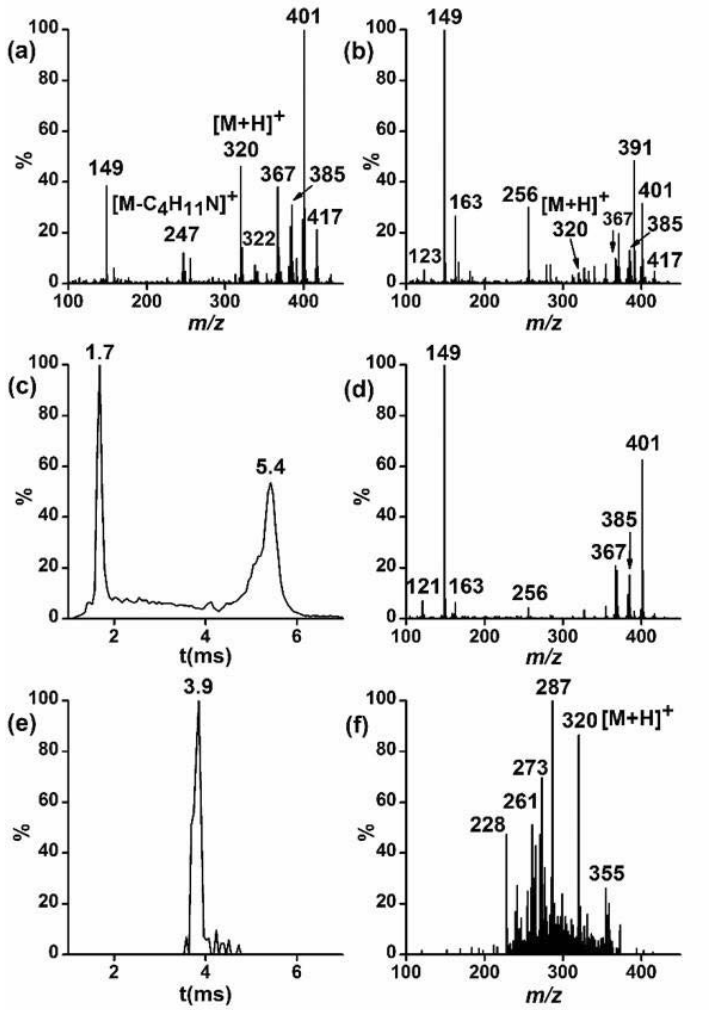

Figure 18. a) DAPPI-MS, b) DART-MS, and c-f) DART-TWIM-MS analysis of a dried blood spot spiked with chloroquine (detected as the $[M+H]^+$ ion at *m/z* 320). c) DART-TWIM-MS total IM spectrum of the dried blood spot, d) combined mass spectrum from the total IM data in c), e) single IM spectrum of $[M+H]^+$ ion of chloroquine at *m/z* 320, f) combined mass spectrum from the IM data in e). The ion at *m/*z 149 is background.

4.2.2.2 Analysis of almond surface by DART- and DAPPI-TWIM-MS

TWIM separation was applied with rapid ambient MS techniques DAPPI and DART in the analysis of α-tocopherol from the almond surface. Figure 19 (a) and 19 (b) show the total IM spectrum, and the combined mass spectrum from the total IM data of all the ions produced, respectively, in almond surface experiments by positive mode DAPPI. Figures 19 (c) and 19 (d) show the corresponding data for DART. α-Tocopherol was detected as $M^{+\bullet}$ at *m/*z 430 with both techniques. With DART, the intensity of $[M-H]^+$ at *m/z* 429 was

approximately 75 % of the main peak intensity and the typical fragment of α-tocopherol at *m/z* 165 was observed as well. As described previously, a higher α-tocopherol intensity was achieved with DAPPI than with DART. This was also observed in the almond surface analysis with clearly higher abundance of $M^{+\bullet}$ ion at *m/z* 430 achieved with DAPPI than with DART. Similarly, oxidation products of α-tocopherol were observed with both techniques.

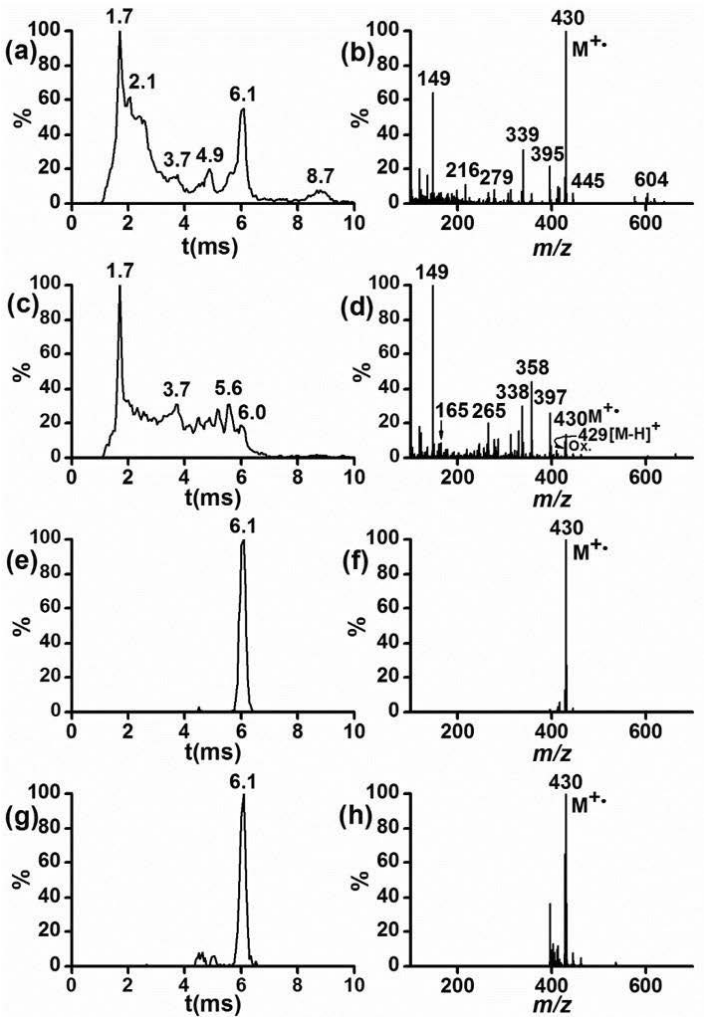

Figure 19. DAPPI- and DART-TWIM-MS of almond surface: a) DAPPI-TWIM-MS total IM spectrum, b) combined mass spectrum from the total IM data in a), c) DART-TWIM-MS total IM spectrum, d) combined mass spectrum from the total IM data in c) (Ox. corresponds to oxidation products at *m/z* 445, 447 and 462), e) single DAPPI-IM spectrum of $M^{+\bullet}$ ion of α-tocopherol at *m/z* 430, f) combined mass spectrum from the IM data in e), g) single DART-IM spectrum of the $M^{+\bullet}$ ion of α-tocopherol at *m/z* 430, h) combined mass spectrum from the IM data in g).

Figures 19 (e) and (f) show the single IM spectrum of the $M^{+\bullet}$ ion at *m/z* 430 and the combined mass spectrum of the single IM data, respectively, obtained with DAPPI. Figures 19 (g) and (h) show the corresponding data for DART. With both techniques α-tocopherol $M^{+\bullet}$ ion at *m/z* 430 was observed in drift time 6.1 ms. The IM separation reduced the chemical noise in the mass spectra and the improvement was notable especially with DART. For DART, the S/N was for α-tocopherol $M^{+\bullet}$ ion 27 times higher in the mobility-filtered spectral data than in mass spectrum acquired with MS alone (Figures 19 d and 19 h).

4.2.2.3 DAPPI-TWIM-MS of vitamin products and pharmaceuticals

Ambient MS analysis is an effective tool for the rapid screening of active ingredients in pharmaceutical formulations.[26,29,230] However, sample matrices can be complex and compounds can interfere with the ionization or the identification of the chemicals of interest. Utilization of IM separation before MS with ambient techniques has proven to reduce the chemical noise in the mass spectrum and to increase the S/N of compounds of interest. Here, the applicability of TWIMS as a fast gas-phase separation technique with DAPPI-MS was studied more in the analysis of authentic multivitamin and pharmaceutical tablets.

First a scratched multivitamin tablet surface was analysed by DAPPI-TWIM-MS. Six out of thirteen vitamins, and caffeine, were detected in the product. Figures 20 (a) and 20 (b) show the total IM spectrum and the combined mass spectrum from the total IM data, respectively, obtained with DAPPI. The combined mass spectrum (Figure 20 b) shows several high intensity peaks which include: nicotinamide (vitamin B_3) $[M+H]^+$ ion at *m/z* 123; pyridoxine (vitamin B_6) $[M+H]^+$ ion and dehydration products at *m/z* 170, 152, and 134 respectively; caffeine $[M+H]^+$ ion at *m/z* 195; and α-tocopherol (vitamin E) $M^{+\bullet}$ ion at *m/z* 430. α-Tocopherol oxidation product and α-tocopheryl acetate at *m/z* 446 and 472, respectively, are also observed.

Three other vitamins with low intensities were also observed. The single ion IM spectra of biotin, thiamine, and cholecalciferol are presented in Figures 20 (c), 20 (e), and 20 (g), respectively. The corresponding combined mass spectra are presented in Figures 20 (d), 20 (f), and 20 (h). Biotin (vitamin B_7) was detected as $[M+H]^+$ ion at *m/z* 245, thiamine (vitamin B_1) as M^+ at *m/z* 265, and cholecalciferol (vitamin D_3) as $M^{+\bullet}$ at *m/z* 384. It can be seen, that the S/N of each of these ions has significantly increased: for example, cholecalciferol S/N was seven times higher when IM separation was used compared to the case when the mass spectrometric analysis was performed alone. The cholecalciferol $M^{+\bullet}$ mass spectrum is shown in Figure 20 (h) in the insert showing an enlargement from the mass range of *m/z* 370−400. The α-tocopherol concentration was 1500 times higher in the vitamin product than the cholecalciferol concentration, which explains why the intensity of the cholecalciferol peak is low compared to α-tocopherol.

Detected compounds desorbed thermally and were detectable on positive ion mode, but some vitamins reported in the vitamin product were not detected under the experimental conditions of the current study. Reason for this may be for example the acidity (ascorbic acid, folic acid), photodegrability (retinol, β-carotene) or high molecular weight (cyanocobalamin) of the compound. Negative mode MS and/or solvent modification could probably facilitate the detection of these compounds.

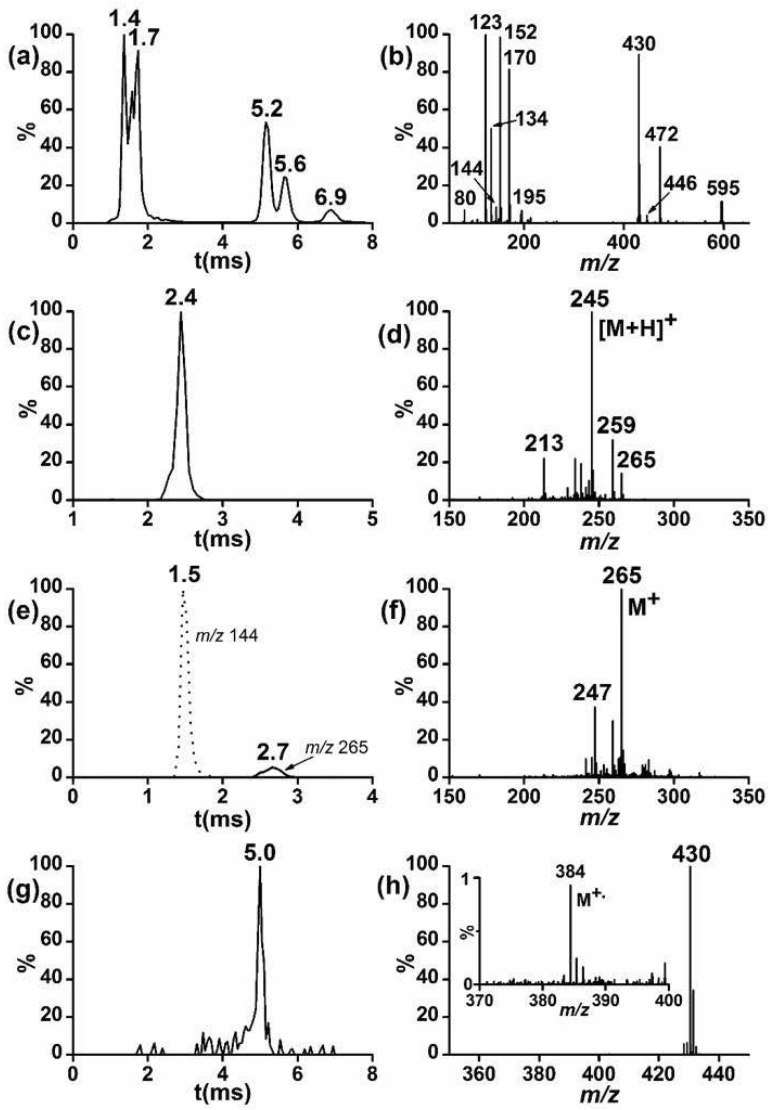

Figure 20. DAPPI-TWIM-MS analysis of the scratched surface of a multivitamin tablet: a) total IM spectrum; b) combined mass spectrum from the total IM data, where the ion at *m/z* 123 is $[M+H]^+$ of nicotinamide, 170 is $[M+H]^+$ of pyridoxine, 195 is $[M+H]^+$ of caffeine, 430 is $M^{+\bullet}$ of α-tocopherol, and 472 is $[M+H]^+$ of α-tocopheryl acetate; c) single IM spectrum for biotin $[M+H]^+$ at *m/z* 245; d) combined mass spectrum from the IM data in c); e) single IM spectrum for the thiamine $M^{+\bullet}$ ion at *m/z* 265 (and for thiamine fragment ion at *m/z* 144 with dashed line); f) combined mass spectrum from the IM data in e); g) single IM spectrum for the cholecalciferol $M^{+\bullet}$ at *m/z* 384; and h) combined mass spectrum from the IM data in g) (the insert shows an enlargement of the mass spectrum from mass range *m/z* 370−400). The TWIMS wave velocity was 530 m/s and the wave height was 35 V.

DAPPI-TWIM-MS was applied to analysis of genuine emergency contraceptive tablets containing levonorgestrel, and falsified tablets sold as genuine. Figures 21 shows the total IM spectrum (a) and its combined mass spectrum for the genuine tablet (b). Levonorgestrel can be observed with high intensity as $[M+H]^+$ ion at *m/z* 313 (Figure 21 b). Figure 21 (c) shows the IM spectrum of the levonorgestrel $[M+H]^+$ ion with a drift time of 7.9 ms represented by the high intensity peak in the total IM spectrum (Figure 21 a). The mass spectrum corresponding to the single ion IM spectrum in Figure 21 (c) is presented in Figure 21 (d), showing the clear peak of the levonorgestrel $[M+H]^+$ ion at *m/z* 313. The mobility separation removed the whole background from the mass spectrum, allowing the detection of the target compound with increased selectivity.

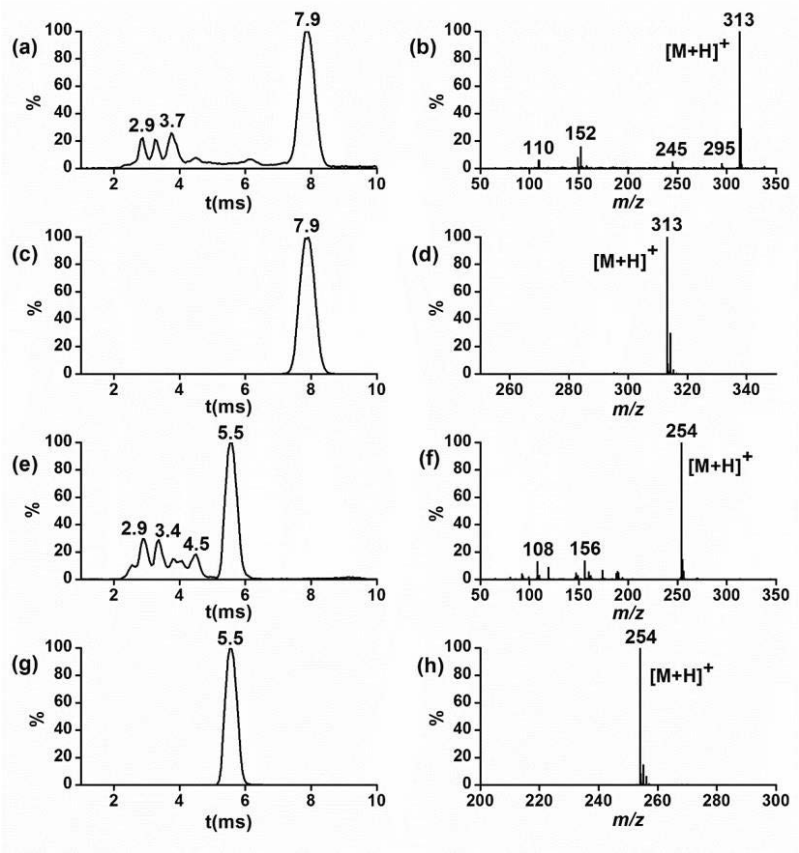

Figure 21. DAPPI-TWIM-MS analysis from the surface of authentic and potentially falsified levonorgestrel tablets: a) total IM spectrum from the authentic tablet; b) combined mass spectrum from the total IM data in a); c) single IM spectrum of the $[M+H]^+$ of levonorgestrel at *m/z* 313 detected from the authentic tablet; d) combined mass spectrum from the IM data in c); e) total IM spectrum from a potentially falsified tablet; f) combined mass spectrum from the total IM data in e); g) single IM spectrum of the $[M+H]^+$ ion of sulfamethoxazole at *m/z* 254 detected from the falsified tablet; h) combined mass spectrum from the IM data in g). The TWIMS wave velocity was 600 m/s and wave height 24 V.

The total IM spectrum and the combined mass spectrum of the total IM spectrum of the falsified tablet are presented in Figure 21 (e) and (f) respectively. No levonorgestrel was found from the unknown tablet by DAPPI-TWIM-MS. Instead, the main ingredient was detected at a drift time 5.5 ms and at *m/z* 254, as shown in the single IM spectrum of the ion at *m/z* 254 and the corresponding mass spectrum in Figures 21 (g) and 21 (h), respectively. The ion at *m/z* 254 was identified as the $[M+H]^+$ ion of the antibiotic sulfamethoxazole with typical fragments at *m/z* 156 and 108. Identification of the active ingredient in the suspect formulation was previously reported by Monge *et al*.[35]

4.3 Experimental and theoretical studies of reactions of phenol and fluorinated phenols with Cl^- in the gas phase (IV)

In Publication IV, a comprehensive experimental and theoretical investigation was pursued to determine the identities and thermochemical details of the phenol, and fluorinated-phenols, reactions with Cl^- and the identities of the dimer ions, especially the PFP dimer. In an earlier DT-IMS study, pentafluorophenol (PFP) dimer was identified as the $[2PFP+Cl]^-$ in experimental temperatures above 150 °C and ambient pressure.[216] This identification was probably not correct. The argument is supported by work related to thermal dissociation of proton-bound dimers[46,51] and Cl^- adducts of nitrate and nitrite esters.[48,49] In Publication IV, GC-IM-MS and collision-induced dissociation (CID) experiments, and theoretical calculations were applied to identify the reaction products of phenol, fluorinated phenols, and Cl^- observed in DT-IMS.

4.3.1 The identification of reaction products by GC-IM-MS

GC-IM-MS experiments were performed to identify the product ions in the reactions of phenol (P), 2,4-difluorophenol, 2,3,6-trifluorophenol (TFP), and PFP with Cl^- in atmospheric pressure. Cl^- reactant ions were formed in dissociative electron capture reaction as presented previously (Table 2, Reaction 6). The separate mass spectra for P, DFP, TFP, and PFP were collected in drift tube temperatures of 70 and 140 °C. The drift field was 250 V cm^{-1}. The formed ions were monitored as a function of sample concentration. Concentrations were not determined exactly, but as monitored intensity changes. When the samples eluted from the GC, the ion intensities were determined across the chromatogram data points of the sample peaks. The GC peak maximum corresponded to the high and the tail to the low sample concentration.

The stable Cl^- adducts $[M+Cl]^-$ in the gas may be produced, when energetic $[M+Cl]^{-*}$ ions are formed in collisions between sample molecules (M) and reactant ions (Cl^-), and stabilized through a collision with ambient molecules (G) (Equation 4). The adduct formation depends on the $\Delta_{acid}G°$ of the molecule. If the molecule is very acidic, a deprotonation reaction (Equation 5) may happen.

$$M + Cl^- \leftrightarrow [M + Cl]^{-*} \xrightarrow{G} MCl^- \quad (4)$$

(5) $$M + Cl^- \leftrightarrow [M + Cl]^{-*} \rightarrow [M - H]^- + HCl$$

In high sample concentration, the adduct formation may lead to formation of a dimer adduct $[2M+Cl]^-$ or the deprotonated dimer $[2M-H]^-$ as shown in Equations 6 and 7 respectively.

(6) $$M + [M + Cl]^- \rightarrow [2M + Cl]^-$$

(7) $$M + [M + Cl]^- \rightarrow [2M - H]^- + HCl$$

In the GC-IM-MS experiments, $[M-H]^-$, $[M+Cl]^-$, $[2M-H]^-$, and $[2M+Cl]^-$ were detected for all the phenols. The relative intensities of the detected ions varied according to the number of F substituents, i.e. the $\Delta_{acid}G°$, and the sample concentration. In addition, in high concentration conditions some trimeric ions were observed with low intensities. $[3M-H]^-$ and $[3M+Cl]^-$ were detected for both P and DFP and $[3M-H]^-$ was detected for TFP.

Figure 22 shows the mass spectra of P and DFP at high and low concentrations at 70 °C. At high concentrations, the main ion for P (Figure 22 a) and DFP (Figure 22 c) was the $[2M+Cl]^-$. The $[M+Cl]^-$ intensity was approximately half for P, and one third for DFP of the $[2M+Cl]^-$ intensity. The $[M-H]^-$ and $[2M-H]^-$ of P and DFP were detected only from the high concentration samples. Their intensities were negligible with both P and DFP, and they may have originated from the dissociation of the $[2M+Cl]^-$ in the IM-MS interface. In low sample concentration, the main ion for both P and DFP was $[M+Cl]^-$ as shown in Figures 22 (b) and 22 (d), respectively. The $[2M+Cl]^-$ intensity was low, and both $[M-H]^-$ and $[2M-H]^-$ were absent for both P and DFP at low sample concentrations.

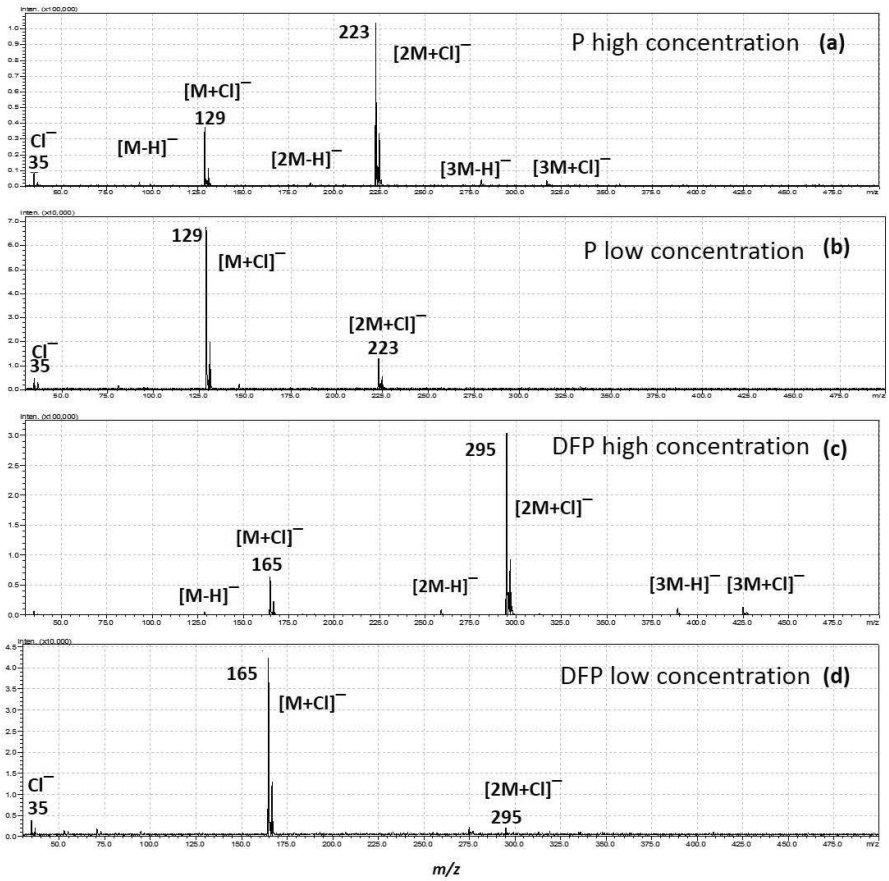

Figure 22. GC-IM-MS mass spectra obtained from the reactions of Cl^- with P at a) high and b) low concentrations and DFP at c) high and d) low concentrations at 70 °C and 1 atm pressure.

Figure 23 shows the mass spectra of TFP and PFP in high and low concentration conditions at 70 °C. At high concentrations, the main ion of TFP (Figure 23 a) and PFP (Figure 23 c) was the deprotonated dimer $[2M-H]^-$. The $[M-H]^-$ intensity was approximately half of the $[2M-H]^-$ intensity for TFP, and one third for PFP. The $[M+Cl]^-$ intensity was negligible for both TFP and PFP. The $[2M+Cl]^-$ intensity was negligible for TFP, and for PFP the $[2M+Cl]^-$ ion was not detected. At low sample concentrations, the main ion of TFP was the $[M+Cl]^-$ (Figure 23 b), and the $[M-H]^-$ intensity was approximately half of the $[M+Cl]^-$ intensity. Both dimers, $[2M+Cl]^-$ and the $[2M-H]^-$, were absent. The main ion of PFP at low concentration (Figure 23 d) was the $[M-H]^-$ and the $[M+Cl]^-$ was present at almost the same intensity as the $[M-H]^-$. For PFP, the $[2M-H]^-$ was also present with minor intensity, but the $[2M+Cl]^-$ was absent.

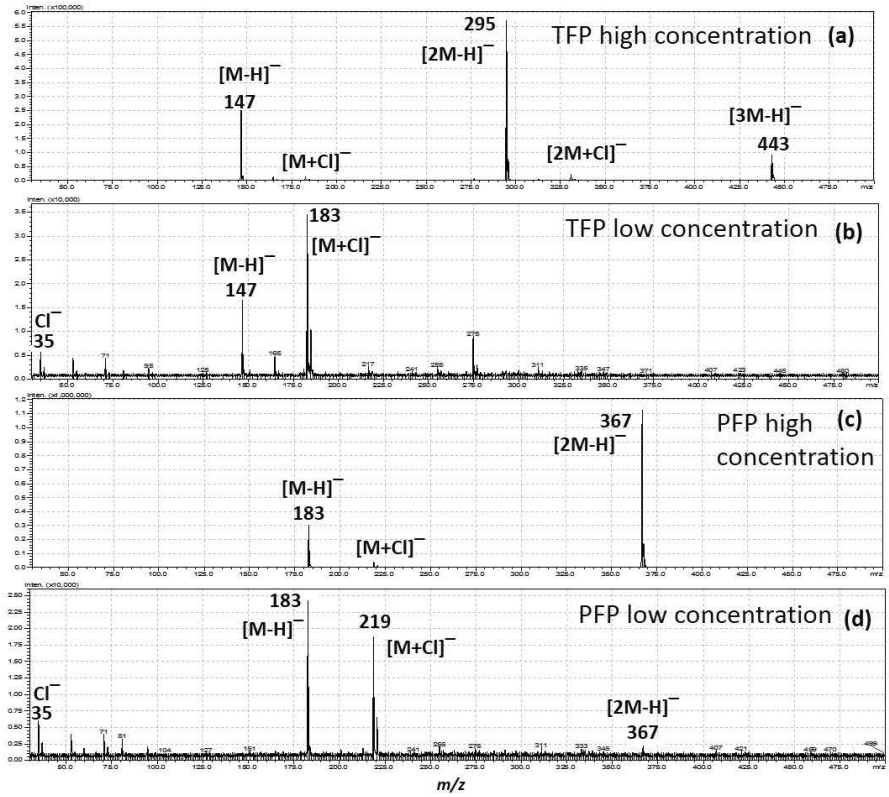

Figure 23. GC-IM-MS mass spectra obtained from the reactions of $Cl^-$and TFP at a) high and b) low concentrations and PFP at high c) and low d) concentrations at 70 °C and 1 atm pressure.

The same main ions for each phenol were observed in drift tubes at 140 °C, as seen at 70 °C but with much lower intensities. For P and DFP, the main ions were $[2M+Cl]^-$ at high and $[M+Cl]^-$ at low concentrations. The $[2M-H]^-$ dominated the TFP and PFP spectra at high concentrations and $[M-H]^-$ at low concentrations. The $[M+Cl]^-$ intensity was much lower at 140 °C compared to 70 °C.

Overall, the number of F substituents impacts the form of the monomer and dimer ions. For phenol and DFP the Cl^- adducts $[M+Cl]^-$ and $[2M+Cl]^-$ were the major products in both low and high sample concentrations and the intensities of the deprotonated species were negligible. For the highly fluorinated phenols TFP and PFP, the deprotonated species $[M-H]^-$ and $[2M-H]^-$ were the main products at high concentrations. At low concentrations, the $[M-H]^-$ and $[M+Cl]^-$ were the main products.

4.3.2 Stabilities of the reaction products of phenols and Cl^-

The stabilities of the product ions in the reactions of phenols and Cl^- were studied with CID experiments (product ion, precursor ion, and neutral loss scans) performed for $[M+Cl]^-$, $[M-H]^-$, $[2M+Cl]^-$, and $[2M-H]^-$ of P, PFP, and 2-fluorophenol (FP) with the used triple quadrupole MS. The collision energy range 5.0–25.0 eV was adjusted from the MS software. The main focus was to investigate the dissociation of $[2M+Cl]^-$ ions. Cl^- ions were produced from CCl_4 by dissociative electron capture, as shown in Table 2, Reaction 8. For this reaction, the electrons were produced by photoionization of toluene dopant (Table 3, Reaction 1).

The precursor ion and neutral loss scans of all the studied phenols showed that the $[2M-H]^-$ was produced from $[2M+Cl]^-$ via loss of HCl (Equation 8). The product ion scan showed that the only product ion of $[2M-H]^-$ was $[M-H]^-$ (Equation 9).

(8) $$[2M + Cl]^- \rightarrow [2M - H]^- + \mathrm{HCl}$$

(9) $$[2M - H]^- \rightarrow [M - H]^- + M$$

The product ion scan of $[PFP+Cl]^-$ gave $[PFP-H]^-$ as the main ion (Equation 10). When the collision energy was increased, a trace of Cl^- could be observed in the mass spectrum with low intensity (Equation 11). Product ion studies showed that for $[P+Cl]^-$ and $[FP+Cl]^-$ Cl^- was the main product ion, and a trace amount of $[M-H]^-$ was observed only in high collision energies.

(10) $$[M + Cl]^- \rightarrow [M - H]^- + HCl$$

(11) $$[M + Cl]^- \rightarrow M + Cl^-$$

Dissociation of $[2M+Cl]^-$ at a range of collision energies was studied in more detail. This was done because of the variety of the possible product ions ($[2M-H]^-$, $[M-H]^-$, $[M+Cl]^-$ and Cl^-), and the uncertainty in the PFP dimer identification in earlier IMS studies.[216] High sample concentrations were needed to obtain sufficiently high $[2M+Cl]^-$ signals. In addition, the collision energy with the used MS instrument was limited to 5.0 eV, which leads to centre of mass collision energies (E_{COM}) of, for example, 0.32 eV and 0.56 eV for $[2PFP+Cl]^-$ and $[P+Cl]^-$, respectively, when nitrogen is used as a collision gas. E_{COM} describes the amount of kinetic energy of the ion that is available for conversion to internal energy. E_{COM} is presented in Equation 12, where in our calculations, the E_{lab} was the used collision energy reported by the MS software, not the actual values measured from the output of the instrument. In Equation 12, m_g is the mass of collision gas molecule, and m_p the mass of the parent ion. The limitation in the lowest available instrumental collision energy, together with low ion intensity, lead to problems in the determination of the product ion intensities in very low collision energies, and made interpretation of the spectra in some cases difficult.

(12) $$E_{COM} = E_{lab} \times \left(\frac{m_g}{m_g+m_p}\right)$$

$[2M+Cl]^-$ product ions as a function of E_{COM} are presented in Figure 24 (a-c) for P, FP, and PFP, respectively. The graphs are fittings of the experimental data points. Figure 24 (c) shows clearly that if the collision energy is extrapolated to zero, the main product ion of $[2PFP+Cl]^-$ dissociation is $[2PFP-H]^-$ (Equation 8). It can also be extrapolated that at approximately 0.25 E_{COM}, the $[PFP+Cl]^-$ and the $[PFP-H]^-$ appeared. In high collision energy conditions, $[PFP-H]^-$ was the only product ion formed from the dissociation of the $[2PFP-H]^-$ and $[PFP+Cl]^-$.

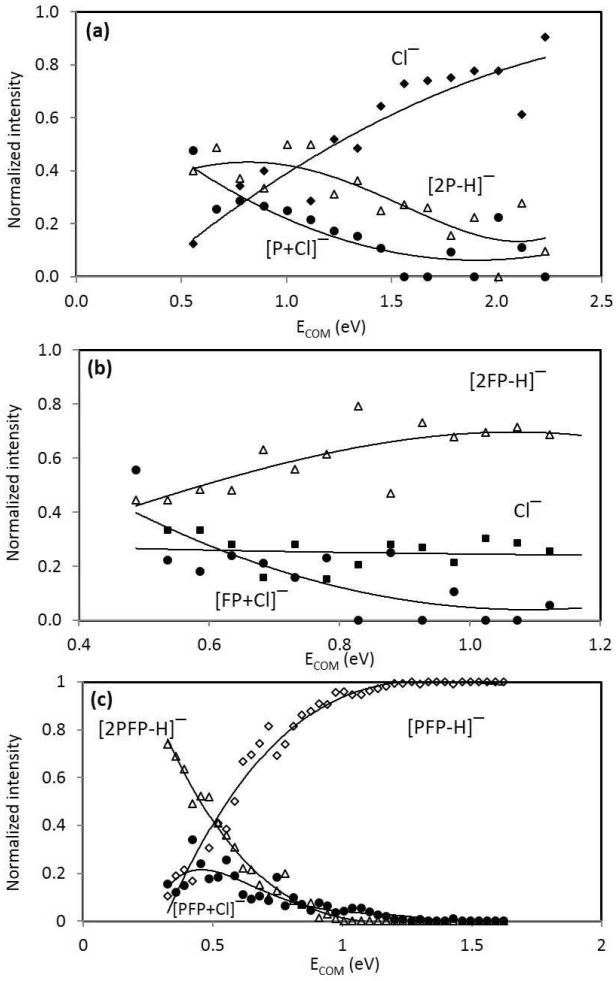

Figure 24. Normalized intensities of the obtained product ions for a) $[2P+Cl]^-$, b) $[2FP+Cl]^-$, and c) $[2PFP+Cl]^-$ in the CID experiments as a function of E_{COM}.

The $[2P+Cl]^-$ dissociation products as a function of E_{COM} are presented in Figure 24 (a). The product ions at low energies are difficult to determine, but extrapolation to zero energy suggests, that the $[P+Cl]^-$ would be the main product ion. When energy is increased, the $[2P-H]^-$ and Cl^- ions appear. The $[2P-H]^-$ and $[P+Cl]^-$ ion intensities dropped to minimum at approximately E_{COM} 2.0. With high collision energies, the main reaction product was clearly Cl^-.

The $[2FP+Cl]^-$ dissociation pattern is the most difficult to interpret (Figure 24 b). Extrapolation of the E_{COM} to zero would suggest that $[FP+Cl]^-$ is the first dissociation product at low collision energies. When the energy is increased, $[2FP-H]^-$ becomes dominant. The Cl^- intensity remains almost constant over the whole energy range. The reason for this is unknown.

4.3.3 Theoretical calculations for explanation of the reaction products

Density functional theory (DFT) calculations of ion structures and the enthalpies of formations were made to assist in the interpretation of the results. The calculations were performed with Gaussian 03W suite of programs.[231] The structures were determined for the phenols P, FP, DFP, TFP, and PFP, and their M, $[M-H]^-$, $[M+Cl]^-$, $[2M-H]^-$, and $[2M+Cl]^-$ ions. The enthalpies were determined for a temperature of 298 K.

4.3.3.1 Ion structures

Figure 25 presents the structures and important bond lengths and angles for P as an example. The computed bond lengths and angles for all the phenols are presented in Tables 15-19. Note that there are two structures for $[2M+Cl]^-$, labeled $[2M+Cl]^-$(A) and $[2M+Cl]^-$(B). In Figure 25 and Tables 17-19 the aromatic rings of the dimer ions $[2M-H]^-$, $[2M+Cl]^-$(A) and $[2M+Cl]^-$(B) are designated a and b, where a denotes the ring with the stronger, i.e. shorter, O─H bond. A short description of the computed structures of M, $[M+Cl]^-$, $[M-H]^-$, $[2M-H]^-$, and $[2M+Cl]^-$ is given here.

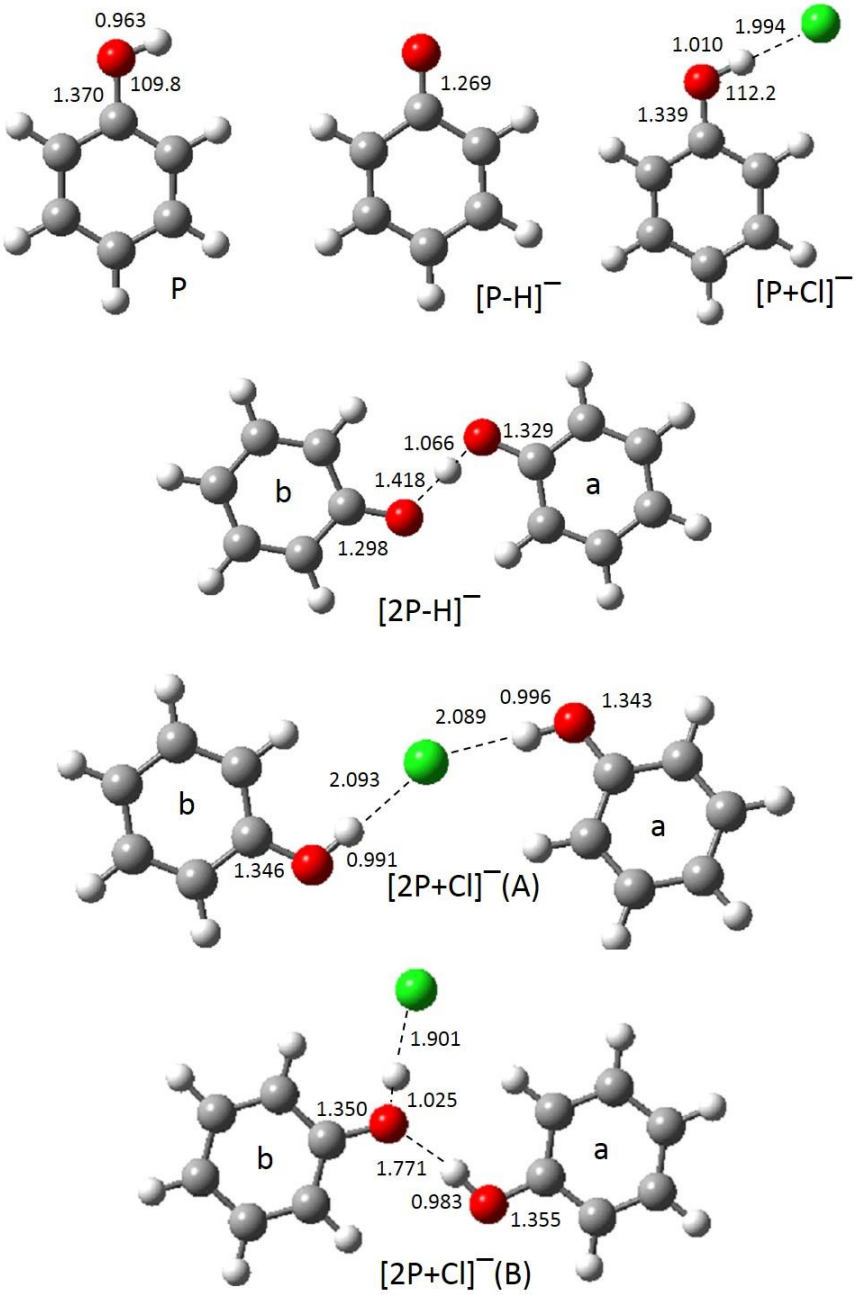

Figure 25. The structures relevant to the reaction between P and Cl^- obtained from the DFT calculations using B3LYP hybrid functional and the 6-311+G(d,p) basis set. Colors are grey = C, white = H, red = O, and green = Cl.

The ground state structures (M) of all the neutral phenols are planar. In the fluorinated phenols, the hydroxyl group is oriented towards the ortho-F. The details of the pertinent bonds and angles are presented in Table 15. The calculated natural bond orbital (NBO) charges in Table 15 show that, except for P, there is little change in the NBO charges with different numbers of fluorine substituents.

Table 15. The selected computed parameters for M and $[M-H]^-$, bond lengths in Å and angles in degrees.

M						$[M-H]^-$	
M	C-O	O-H	> C-O-H	q_O[a]	q_H[a]	C-O	q_O[a]
P	1.370	0.963	109.8	−0.677	0.469	1.269	−0.787
FP	1.362	0.965	109.2	−0.669	0.488	1.264	−0.768
DFP	1.362	0.965	109.3	−0.668	0.488	1.265	−0.774
TFP	1.353	0.966	109.4	−0.648	0.486	1.257	−0.738
PFP	1.352	0.966	109.6	−0.645	0.489	1.236	−0.733

[a] Natural bond orbital (NBO) charges.

All the deprotonated ($[M-H]^-$) phenols are planar and have C−O bond lengths that decrease from 1.269 Å in $[P-H]^-$ to 1.236 Å in $[PFP-H]^-$ as the electron withdrawal by F increases (Table 15).

The attachment of Cl^- at the hydrogen of the hydroxyl group, of each of the phenol to form $[M+Cl]^-$, gave the lowest energy structure. Relevant structural distances and angles are listed in Table 16.

Table 16. Selected computed parameters for $[M+Cl]^-$, bond lengths in Å and angles in degrees.

M	C-O	O-H	H-Cl	< C-O-H	< O-H-Cl	< RO→Cl[a]
P	1.339	1.010	1.994	112.3	180.0	0
FP	1.333	1.014	1.968	111.7	178.8	0
DFP	1.334	1.015	1.961	111.4	177.7	0
TFP	1.318	1.046	1.848	116.6	168.9	35
PFP	1.318	1.057	1.809	115.3	172.2	45

[a] Angle between the ring plane and the O→Cl vector.

The structure of $[2M-H]^-$ of each phenol is a proton-bound dimer of two oxygen-base molecules RO─H···OR. In the structure the O─H and O···H distances differ by approximately 0.3 Å (Table 17). When there are F substituents, the O−H bond distance increases approximately by 0.005 Å from FP to PFP with each additional F substituent. Simultaneously, the longer H···O bond decreases approximately by 0.012 Å from FP to PFP with each additional F substituent. For the maximum hydrogen bond strength, the optimal O─H···O angle would be 180°.[232] This is almost attained with P at 177°, FP at 176°, and DFP at 175°, but for TFP and PFP the angle is at 168°. This difference is reflected in the angle between the planes of the aromatic rings which are 66° for P, 174° for FP, 171° for

DFP, and 68° for both TFP and PFP (Table 17). The reason for the greatly different angles for the phenols with two o-F substituents, TFP and PFP, is the minimization of interactions between F substituents in the two rings.

Table 17. Selected computed parameters for $[2M-H]^-$, bond lengths in Å and angles in degrees.

M	C_a-O_a	C_b-O_b	O_a-H	O_b-H	<(O_a-H-O_b)	<a-b[a]
P	1.329	1.298	1.066	1.418	176.8	166
FP	1.324	1.293	1.064	1.416	175.9	174
DFP	1.326	1.295	1.064	1.415	175.1	171
TFP	1.309	1.284	1.087	1.366	167.5	68
PFP	1.309	1.285	1.089	1.357	168.2	68

[a] Angle between the planes of the a and b aromatic rings.

As illustrated in Figure 25 for P, there are two stable forms of the chloride-bound dimer, $[2M+Cl]^-$(A) and $[2M+Cl]^-$(B). A transition state barrier between the two forms is 26 kJ mol^{-1} and it is approximately the same for each phenol. The aromatic rings of both structures are labelled as a and b. The bond lengths and angles of $[2M+Cl]^-$(A) and $[2M+Cl]^-$(B) for all the phenols are presented in Tables 18 and 19 respectively. $[2M+Cl]^-$(A) has a structure of a chloride-bound homogeneous dimer with two OH···Cl^-···HO hydrogen bonds with almost equal length (see Figure 25 and Table 18). $[2M+Cl]^-$(B) complex is a phenoxide hydrogen-bonded to both phenol and HCl (see Figure 25 and Table 19). As is with $[2M-H]^-$, the number of F substituents has a great effect on the bond lengths and angles between the two aromatic rings in the dimer structure as can be seen from Tables 18 and 19.

Table 18. Selected computed parameters for $[2M+Cl]^-$(A), bond distances in Å, angles in degrees.

M	C_a-O_a	C_b-O_b	O_a-H_a	O_b-H_b	H_a-Cl	H_b-Cl	< (O_a-H_a-Cl)	< (O_b-H_b-Cl)	< (H_a-Cl-H_b)	< a-b[a]
P	1.343	1.346	0.996	0.991	2.089	2.093	178.2	179.5	152.5	177.0
FP	1.340	1.340	0.996	0.996	2.064	2.064	177.9	177.9	124.0	111.0
DFP	1.341	1.341	0.996	0.996	2.061	2.063	176.7	176.8	127.4	116.0
TFP	1.324	1.324	1.014	1.014	1.976	1.974	165.4	165.5	107.2	67.0
PFP	1.323	1.323	1.017	1.017	1.946	1.951	167.3	166.0	109.2	90.0

[a] Angle between the ring planes.

Table 19. Selected computed parameters for $[2M+Cl]^-$(B), bond distances in Å, angles in degrees.

M	C_a-O_a	C_b-O_b	O_a-H_a	O_b-H_b	H_b-Cl	O_b-H_a	< (O_a-H_a-O_b)	< (O_b-H_b-Cl)	< a-b[a]
P	1.355	1.350	0.983	1.025	1.901	1.771	173.1	175.6	175
FP	1.348	1.345	0.980	1.028	1.892	1.833	176.9	177.3	162
DFP	1.349	1.347	0.980	1.029	1.884	1.822	176.4	177.2	156
TFP	1.331	1.331	0.995	1.096	1.716	1.692	162.3	175.2	95
PFP	1.326	1.329	1.002	1.142	1.637	1.636	168.6	176.6	89

[a] Angle between the ring planes.

4.3.3.2 Enthalpy levels

$\Delta_{acid}G°$s of the phenols and HCl were calculated and compared with the available experimental literature values. $\Delta_{acid}G°$s are presented in Figure 26 (a) and in Table 20 with the experimental results that are available.[94] The experimental $\Delta_{acid}G°$ values are approximately 10 to 20 kJ mol^{-1} higher than the computed values.

Both sets in Figure 26 (a) show an average increase in the acidity, i.e. the decrease in the $\Delta_{acid}G°$ enthalpy value, of approximately 20 kJ mol^{-1} for each additional fluorine substituent. The computed $\Delta_{acid}G°$ of HCl, 1378 kJ mol^{-1} (broken line in Figure 26 a), is also lower than the experimental value of 1395 kJ mol^{-1}.[94] The difference of 17 kJ mol^{-1} is about the same as for the neutral phenols. This indicates, that the computed reaction enthalpies probably deviate from experimental values approximately the same amount as the computed and experimental $\Delta_{acid}G°$s. PFP is the only phenol with a computed $\Delta_{acid}G°$ less than that of HCl, although the $\Delta_{acid}G°$ of TFP, for which there is no available experimental value, is only 8 kJ mol^{-1} larger than that of HCl.

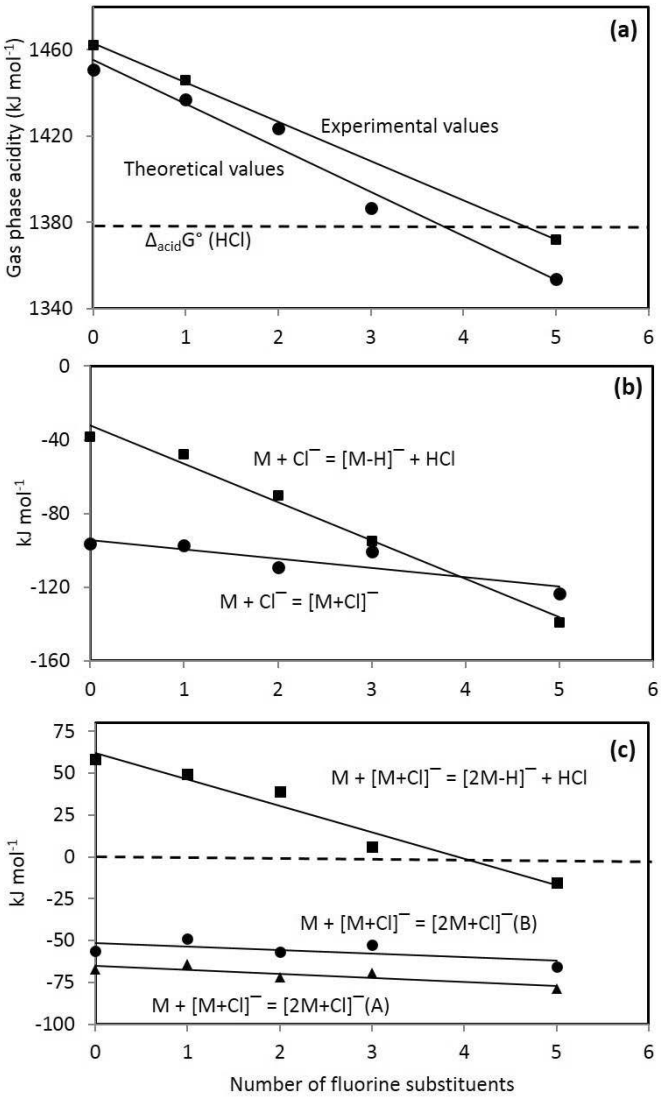

Figure 26. (a) Comparison of the computed and experimental $\Delta_{acid}G°$s and (b) and (c) the calculated enthalpies for the formation of products from the reaction of phenols with Cl^- as functions of the number of F substituents.

The reaction enthalpies for the formation of $[M+Cl]^-$, $[M-H]^-$, $[2M-H]^-$, $[2M+Cl]^-$(A), and $[2M+Cl]^-$(B) at 298 K are listed in Table 20 and plotted in Figures 26 (b) and 26 (c) as functions of the number of fluorine substituents. The reaction enthalpies for the formation of the products decrease approximately linearly with the increasing number of fluorine substituents.

Table 20. $\Delta_{acid}G°$s of studied phenols (M) and the enthalpies (kJ mol^{-1}) of the product formations in the reactions of Cl^- with phenols at 298 K.

M	$\Delta_{acid}G°$	M + Cl^- → $[M+Cl]^-$	M + Cl^- → $[M-H]^-$ + HCl	M + $[M+Cl]^-$ → $[2M+Cl]^-$(A)	M + $[M+Cl]^-$ → $[2M+Cl]^-$(B)	M + $[M+Cl]^-$ → $[2M-H]^-$ + HCl
P	1451 (1462)[a]	−97	73	−67	−56	58
FP	1437 (1446)[a]	−98	59	−64	−49	50
DFP	1424	−109	46	−72	−57	39
TFP	1387	−101	9	−70	−53	6
PFP	1354 (1372)[a]	−124	−24	−79	−66	−15

[a] The available experimental values in brackets.[94]

As shown already in Figures 22 and 23, the $[M+Cl]^-$ can be formed with all the studied phenols and the collision stabilization reaction (Equation 4) can compete with the deprotonation reaction (Equation 5). The reaction enthalpy for formation of $[M+Cl]^-$ decreases linearly from −97 kJ mol^{-1} for P to −124 kJ mol^{-1} for PFP. The decrease is approximately 5.0 kJ mol^{-1} for each additional F substituent. For $[M-H]^-$ formation, the computed enthalpy decrease for each additional fluorine substituent is much greater, ca. 17 kJ mol^{-1}. This suggests, that the $[M-H]^-$ formation depends much more on the $\Delta_{acid}G°$ than does the $[M+Cl]^-$ formation. In case of P, 2FP, and DFP, the absolute values of the reaction enthalpies of $[M-H]^-$ and $[2M-H]^-$ formation are positive, which explains why these ions are not observed in the spectra in thermal conditions. Only the $[PFP-H]^-$ and $[2PFP-H]^-$ formations are exothermic reactions. For TFP, the corresponding values are only slightly endothermic. Therefore, the observation of $[M-H]^-$ and $[2M-H]^-$ ions in the TFP and PFP mass spectra can be expected.

The enthalpies of the $[2M+Cl]^-$ formation decrease, with the increasing number of F substituents, from −64 to −79 kJ mol^{-1} and from −49 to −66 kJ mol^{-1} for the $[2M+Cl]^-$(A) and $[2M+Cl]^-$(B) respectively. The corresponding values for $[2M-H]^-$ formation are from 50 to −15 kJ mol^{-1}, which is much larger change than in the $[2M+Cl]^-$ formation. The enthalpy of $[2M+Cl]^-$ formation is strongly negative for all the phenols. Yet the $[2PFP+Cl]^-$ ion was negligible or absent in the mass spectra (Figures 23 c and 23 d). The same observation was made with TFP as well, which may be due to the dissociation of the $[2M+Cl]^-$ in the IM-MS interface.

The enthalpy changes for P and PFP constitute the extremes of the values for the different phenols. The reaction enthalpy levels, determined from the computed values presented in Table 20 for P and PFP at 298 K, are presented in Figure 27 as an example. The inset in Figure 27 shows the small transition state barrier between $[2M+Cl]^-$(A) and $[2M+Cl]^-$(B) with height of 26 kJ mol^{-1} between $[2PFP+Cl]^-$(A) and $[2PFP+Cl]^-$(B). This value was the same for all the phenols. The dissociation starts probably from $[2M+Cl]^-$(A) and goes through the transition state.

For $[2P+Cl]^-$(A), the reaction that requires the least energy, 67 kJ mol^{-1}, is the $[P+Cl]^-$ formation. The requirement for the loss of HCl is 125 kJ mol^{-1} and finally, 164 kJ mol^{-1} is needed for the Cl^- product ion formation. For $[2PFP+Cl]^-$(A), the dissociation product ion that has the lowest energy requirement, 64 kJ mol^{-1}, is $[2PFP-H]^-$. A total of 79 kJ mol^{-1} is required for $[M+Cl]^-$ formation and an additional 100 kJ mol^{-1} is required for the $[PFP-H]^-$

formation. These enthalpy levels are consistent with the sequence obtained in the CID experiments. The observed product ions with increasing collision energy are $[P+Cl]^-$ < $[2P-H]^-$ < Cl^- and $[2PFP-H]^-$ < $[PFP+Cl]^-$ < $[PFP-H]^-$ as presented in Figures 24 (a) and 24 (c) for P and PFP respectively.

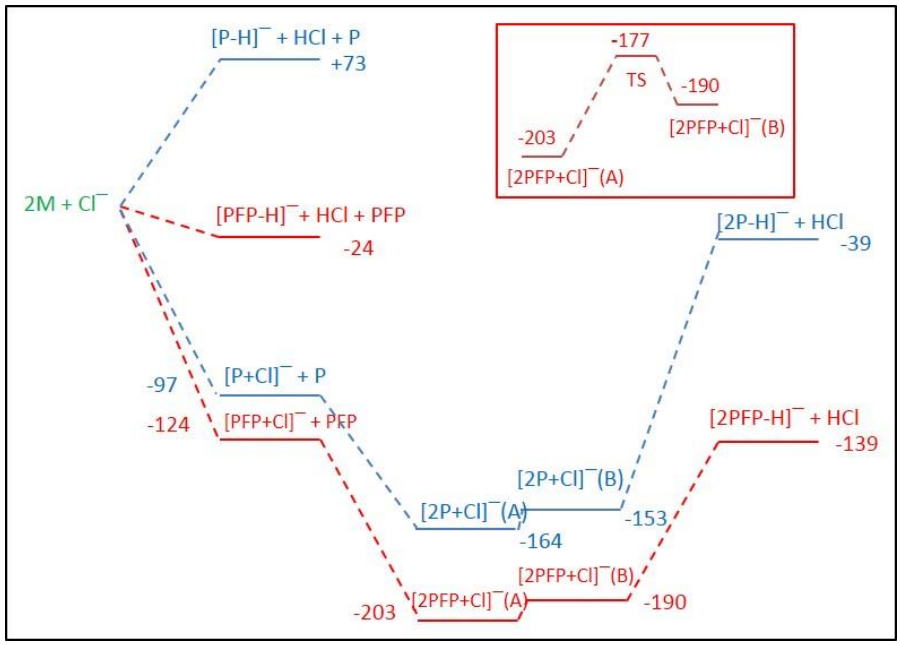

Figure 27. The relative enthalpy levels for the reactions of P and PFP with Cl^- obtained from DFT calculations using B3LYP hybrid functional and the 6-311+G(d,p) basis set. The inset illustrates the energy barrier between the two forms of the chloride dimer adduct of PFP.

In conclusion, the $\Delta_{acid}G°$ of the studied phenol has a large effect on the reaction products in the gas phase reaction between the phenol and Cl^- at ambient pressure. The $[M+Cl]^-$ formation was possible with all the studied phenols. The higher the $\Delta_{acid}G°$ of the phenol, the more likely was the competitive deprotonation reaction to happen, yielding to $[M-H]^-$ and HCl products in low sample concentrations. In high sample concentrations, the further association of M with $[M-H]^-$ or $[M+Cl]^-$ leads to formation of dimer ions $[2M-H]^-$ and $[2M+Cl]^-$. $[2PFP-H]^-$ was confirmed to be the major dimer observed in the IM spectra in both low and high temperature.

5 Summary and conclusions

The objective of the research presented in this thesis was to study the applicability of different type of IMS techniques in the direct analysis of gaseous and solid samples, and in fundamental research of gas phase ions at ambient pressure. In Publication I, it was shown that portable AIMS is a feasible technique for the dynamic monitoring of trace concentrations of the peroxide-type explosive TATP. This was proved, although the limitation of AIMS is the low resolution and the inability to identify compounds accurately. Different concentrations of gas phase TATP were generated to carrier gas flow, and TATP was screened directly from the carrier gas flow by AIMS. The instrument gave responses in less than five seconds. The measured intensities were clearly over the instrument normalized detection threshold (20 pA). AIMS responses were proportional to the measured TATP concentrations and TATP could be monitored from the gas flow in low mg m^{-3} levels. The experiments were carried out in low humidity conditions without interfering chemicals. Further studies with TATP together with interfering compounds in different humidity conditions would confirm the applicability of the technique in the real-life environment.

In Publication II, the suitability of portable AIMS in monitoring of MVOCs was investigated. Comparative studies were carried out by TD-GC-MS. The measurements were done from the headspaces of chambers containing microbe contaminated particle board samples (M). Sterile specimens in high humidity conditions in another chamber (S) were used as references. It was shown by PCA that distinct AIMS responses were measured from the chambers S and M, when the incubation of the microbes in chamber M proceeded. This indicates different chemical profiles in chambers S and M. TD-GC-MS measurements showed that only three new compounds (2-pentanone, propyl acetate and 4-methyl-2-hexanone) were identified in chamber M that were not emitted from the building material specimen, and were therefore not present in chamber S. These compounds were definitively identified as MVOCs, and 49 additional compounds were identified as MVOCs by comparing the intensity data measured from the chambers. PCA results for both AIMS and TD-GC-MS data also showed a time trend, so that when the incubation proceeded, the separation of the chemical profiles of chambers S and M, i.e. the intensities of the detected compounds, was clearly distinguished.

To use AIMS in field conditions indoors for monitoring MVOCs is challenging, as indoor concentrations are low and thus it is difficult to identify specific MVOCs reliably by AIMS. However, in method development, a dynamic continuous screening of indoor air quality could allow the development of a training set for ‘normal’ and ‘microbe contaminated’ indoor air status. This would probably require the use of multivariate data analysis with large training sets, long time monitoring of indoor air, and simultaneous measuring of at least pressure, humidity, and temperature. The good knowledge of building physics and fluid dynamics would also definitively be an advantage for obtaining reliable data.

In ambient MS analysis, interfering compounds in the sample matrix or background air can disturb the analysis, and therefore a fast separation technique like IMS before MS would be essential. In Publication III, two ambient ionization techniques, DART and DAPPI, were successfully coupled with TWIM-MS for highly selective surface analysis. It was shown

how ions generated by DAPPI and DART were totally or partly separated according to their different mobilities in the drift region of TWIMS and how the separation enhanced the spectral quality and S/N. When chloroquine was analysed from a dried blood spot sample, a higher signal intensity for the $[M+H]^+$ of chloroquine was achieved with DAPPI than with DART. The IM separation subtracted the chloroquine $[M+H]^+$ from the background interferences, and enhanced the detection of chloroquine by DART. Ambient MS can be used in fast preliminary screening of a large number of unknown samples like pharmaceutical tablets. In the DAPPI-TWIM-MS analysis of a multivitamin tablet, the IM separation enabled the detection of species with low signal intensities, e.g. thiamine and cholecalciferol. In the analysis of genuine emergency contraceptive tablets containing the synthetic hormone levonorgestrel, and falsified tablets sold as genuine, the IM separation increased the selectivity of the detection for the active ingredients in both tablets.

In addition, DAPPI and DART ionization techniques were compared for a small group of selected standards containing both polar and nonpolar compounds: BPA, B[a]P, ranitidine, cortisol, and α-tocopherol (III). Lower LODs were achieved by DAPPI than DART for all the selected compounds. The LODs were between 30−290 and 330−8200 fmol for DAPPI and DART, respectively. Also, DAPPI showed a higher signal intensity for α-tocopherol measured from the almond surface. Although the IM separation reduced the chemical noise in the mass spectrum, for DART the S/N for the α-tocopherol $M^{+\bullet}$ was 27 times higher with IM-MS than with MS alone.

Finally, in Publication IV, the reactions between Cl^- and phenol and fluorinated phenols with different acidities, were investigated under ambient pressure. The objective was to define the reaction products with different concentrations. The used methods were GC-IM-MS, CID experiments and theoretical calculations. The results showed that increasing the number of the fluorine substituents in the phenol core increases the phenol $\Delta_{acid}G°$, and that the $\Delta_{acid}G°$ has an important role in the formation of reaction products. When energetic $[M+Cl]^{-*}$ is formed in the ionization, it can be stabilized through collisions with the surrounding gas phase molecules, and form a stable $[M+Cl]^-$ adduct. This was observed with the least fluorinated phenols; P, 2FP and DFP. With highly fluorinated phenols (TFP and PFP), and therefore more acidic, the competitive reaction of the formation of deprotonated molecule $[M-H]^-$ ion was observed. Depending on the phenol, these ions formed dimers and trimers through association reactions when the sample concentration was high. For P, 2FP and DFP, which have lower $\Delta_{acid}G°$ than TFP and PFP, the Cl^- adducts $[M+Cl]^-$ and $[2M+Cl]^-$ were the major products for both low and high sample concentrations. For TFP and PFP, the $[M-H]^-$ and $[2M-H]^-$ were the main products in high concentrations. In low concentrations, the $[M-H]^-$ and $[M+Cl]^-$ were the main products. Although the intensity of $[2PFP+Cl]^-$ was low, the dissociation products of $[2PFP+Cl]^-$ were studied with more detail, because of the variety of possible product ions, and the uncertainty of the dimer identity ($[2PFP+Cl]^-$ or $[2PFP-H]^-$) in the earlier DT-IMS studies.[216] The CID results proved that the main product ion of $[2PFP+Cl]^-$ dissociation was $[2PFP-H]^-$, and altogether the results showed that the dimer that was formed in the reaction between Cl^- and PFP was $[2PFP-H]^-$, and this ion exists also in high temperature conditions in DT-IMS.

There are several types of IMS instruments for different kinds of analytical challenges. The response time and reliability are important issues when gas detection systems are

developed for *in situ* screening of hazardous chemicals. In these types of applications, the device should be light-weight, easy to maintain and use, and as specific for the target analytes as possible. On the other hand, a designated chemical pattern as a signal can be accurate enough in continuous monitoring of e.g. air quality or volatile samples from headspace.

The use of IMS as a fast separation technique in ambient MS seems a promising tool to decrease the effect of the interfering compounds in the mass spectrum without increasing the total analysis time remarkably. Also, the extra dimension in the analysis amplifies the reliability of the analysis. The combination of IMS and ambient MS can have important applications in e.g. the screening of illicit drugs, explosives or pharmaceuticals from tablets, biological matrices, environmental samples, and food products. The coupling of a compatible ion source, IMS instrument, and MS together with thorough method optimization are key elements to achieving all the benefits of the hyphenated IMS and ambient MS technique.

In the fundamental studies, both standalone and hyphenated instruments are beneficial, and often the wanted instrument qualities are obtained by manufacturing the IMS instrument in-house. It is important to understand the theory of the observed reactions in the research, validation, and routine work in analytical chemistry or instrument development, for example. In addition, the utilization of theoretical calculations is an efficient tool in the evaluation of the observed phenomenon.

Overall, IMS is a diverse analytical technique, the potential of which in research and everyday use is obvious and still increasing, e.g. in the monitoring rapidly hazardous chemicals, ambient MS, mass spectrometric imaging, and in the analysis of biological samples.

6 References

[1] G.A. Eiceman. Ion-mobility spectrometry as a fast monitor of chemical composition. *TrAC, Trends Anal. Chem.* **2002**, 21, 259. DOI: 10.1016/S0165-9936(02)00406-5.

[2] A.B. Kanu, H.H. Hill. Ion mobility spectrometry detection for gas chromatography. *J. Chromatogr. A.* **2008**, 1177, 12. DOI: 10.1016/j.chroma.2007.10.110.

[3] G.A. Eiceman, Z. Karpas, H.H. Hill. *Ion Mobility Spectrometry, 3rd ed.* CRC Press, Taylor & Francis Group, Boca Raton, **2014**.

[4] I.A. Buryakov, E.V. Krylov, E.G. Nazarov, U.K. Rasulev. A new method of separation of multi-atomic ions by mobility at atmospheric pressure using a high-frequency amplitude-asymmetric strong electric field. *Int. J. Mass Spectrom. Ion Processes.* **1993**, 128, 143. DOI: 10.1016/0168-1176(93)87062-W.

[5] K. Giles, S.D. Pringle, K.R. Worthington, D. Little, J.L. Wildgoose, R.H. Bateman. Applications of a traveling wave-based radio-frequency-only stacked ring ion guide. *Rapid Commun. Mass Spectrom.* **2004**, 18, 2401. DOI: 10.1002/rcm.1641.

[6] M. Utriainen, E. Kärpänoja, H. Paakkanen. Combining miniaturized ion mobility spectrometer and metal oxide gas sensor for the fast detection of toxic chemical vapors. *Sens. Actuators, B.* **2003**, 93, 17. DOI: 10.1016/S0925-4005(03)00337-X.

[7] R. Cumeras, E. Figueras, C.E. Davis, J.I. Baumbach, I. Gràcia. Review on ion mobility spectrometry. Part 1: current instrumentation. *Analyst (Cambridge, U. K.).* **2015**, 140, 1376. DOI: 10.1039/C4AN01100G.

[8] S. Armenta, M. Alcala, M. Blanco. A review of recent, unconventional applications of ion mobility spectrometry (IMS). *Anal. Chim. Acta.* **2011**, 703, 114. DOI: 10.1016/j.aca.2011.07.021.

[9] R. Fernández-Maestre, H.H. Hill Jr. Ion mobility spectrometry for the rapid analysis of over-the-counter drugs and beverages. *Int. J. Ion Mobility Spectrom.* **2009**, 12, 91. DOI: 10.1007/s12127-009-0025-x.

[10] R.M. O'Donnell, X. Sun, P.d.B. Harrington. Pharmaceutical applications of ion mobility spectrometry. *TrAC, Trends Anal. Chem.* **2008**, 27, 44. DOI: 10.1016/j.trac.2007.10.014.

[11] P. Dwivedi, C. Wu, L.M. Matz, B.H. Clowers, W.F. Seims, H.H. Hill Jr. Gas-phase chiral separations by ion mobility spectrometry. *Anal. Chem.* **2006**, 78, 8200. DOI: 10.1021/ac0608772.

[12] H. Li, B. Bendiak, W.F. Siems, D.R. Gang, H.H. Hill. Carbohydrate Structure Characterization by Tandem Ion Mobility Mass Spectrometry (IMMS)2. *Anal. Chem. (Washington, DC, U. S.).* **2013**, 85, 2760. DOI: 10.1021/ac303273z.

[13] R.G. Ewing, C.J. Miller. Detection of volatile vapors emitted from explosives with a handheld ion mobility spectrometer. *Field Anal. Chem. Technol.* **2001**, 5, 215. DOI: 10.1002/fact.10000.

[14] S. Zimmermann, S. Barth, W.K.M. Baether, J. Ringer. Miniaturized Low-Cost Ion Mobility Spectrometer for Fast Detection of Chemical Warfare Agents. *Anal. Chem. (Washington, DC, U. S.).* **2008**, 80, 6671. DOI: 10.1021/ac800559h.

[15] K. Tuovinen, H. Paakkanen, O. Hänninen. Determination of soman and VX degradation products by an aspiration ion mobility spectrometry. *Anal. Chim. Acta.* **2001**, 440, 151. DOI: 10.1016/S0003-2670(01)01063-7.

[16] G.A. Eiceman, S. Sowa, S. Lin, S.E. Bell. Ion mobility spectrometry for continuous on-site monitoring of nicotine vapors in air during the manufacture of transdermal systems. *J. Hazard. Mater.* **1995**, 43, 13. DOI: 10.1016/0304-3894(95)00023-N.

[17] J. Puton, J. Namiesnik. Ion mobility spectrometry: Current status and application for chemical warfare agents detection. *TrAC, Trends Anal. Chem.* **2016**, 85, 10. DOI: 10.1016/j.trac.2016.06.002.

[18] G.A. Eiceman, J.A. Stone. Ion Mobility Spectrometers in National Defense. *Anal. Chem.* **2004**, 76, 390A. DOI: 10.1021/ac041665c.

[19] M.A. Mäkinen, O.A. Anttalainen, M.E.T. Sillanpää. Ion Mobility Spectrometry and Its Applications in Detection of Chemical Warfare Agents. *Anal. Chem. (Washington, DC, U. S.).* **2010**, 82, 9594. DOI: 10.1021/ac100931n.

[20] S. Yamaguchi, R. Asada, S. Kishi, R. Sekioka, N. Kitagawa, K. Tokita, S. Yamamoto, Y. Seto. Detection performance of a portable ion mobility spectrometer with 63Ni radioactive ionization for chemical warfare agents. *Forensic Toxicol.* **2010**, 28, 84. DOI: 10.1007/s11419-010-0092-z.

[21] R.G. Ewing, D.A. Atkinson, G.A. Eiceman, G.J. Ewing. A critical review of ion mobility spectrometry for the detection of explosives and explosive related compounds. *Talanta.* **2001**, 54, 515. DOI: 10.1016/S0039-9140(00)00565-8.

[22] R.G. Ewing, M.J. Waltman, D.A. Atkinson. Characterization of Triacetone Triperoxide by Ion Mobility Spectrometry and Mass Spectrometry Following Atmospheric Pressure Chemical Ionization. *Anal. Chem. (Washington, DC, U. S.).* **2011**, 83, 4838. DOI: 10.1021/ac200466v.

[23] C. Lapthorn, F. Pullen, B.Z. Chowdhry. Ion mobility spectrometry-mass spectrometry (IMS-MS) of small molecules: Separating and assigning structures to ions. *Mass Spectrom. Rev.* **2013**, 32, 43. DOI: 10.1002/mas.21349.

[24] A.B. Kanu, P. Dwivedi, M. Tam, L. Matz, H.H. Hill Jr. Ion mobility-mass spectrometry. *J. Mass Spectrom.* **2008**, 43, 1. DOI: 10.1002/jms.1383.

[25] P. Dwivedi, G. Puzon, M. Tam, D. Langlais, S. Jackson, K. Kaplan, W.F. Siems, A.J. Schultz, L. Xun, A. Woods, H.H. Hill Jr. Metabolic profiling of Escherichia coli by ion mobility-mass spectrometry with MALDI ion source. *J. Mass Spectrom.* **2010**, 45, 1383. DOI: 10.1002/jms.1850.

[26] M.E. Monge, G.A. Harris, P. Dwivedi, F.M. Fernández. Mass Spectrometry: Recent Advances in Direct Open Air Surface Sampling/Ionization. *Chem. Rev. (Washington, DC, U. S.).* **2013**, 113, 2269. DOI: 10.1021/cr300309q.

[27] M. Haapala, J. Pól, V. Saarela, V. Arvola, T. Kotiaho, R.A. Ketola, S. Franssila, T.J. Kauppila, R. Kostiainen. Desorption atmospheric pressure photoionization. *Anal. Chem. (Washington, DC, U. S.).* **2007**, 79, 7867. DOI: 10.1021/ac071152g.

[28] Z. Takáts, J.M. Wiseman, B. Gologan, R.G. Cooks. Mass Spectrometry Sampling Under Ambient Conditions with Desorption Electrospray Ionization. *Science (Washington, DC, U. S.).* **2004**, 306, 471. DOI: 10.1126/science.1104404.

[29] R.B. Cody, J.A. Laramee, H.D. Durst. Versatile new ion source for the analysis of materials in open air under ambient conditions. *Anal. Chem.* **2005**, 77, 2297. DOI: 10.1021/ac050162j.

[30] T.J. Kauppila, A. Flink, U. Laakkonen, L. Aalberg, R.A. Ketola. Direct analysis of cannabis samples by desorption atmospheric pressure photoionization-mass spectrometry Analysis of cannabis with DAPPI-MS. *Drug Test. Anal.* **2013**, 5, 186. DOI: 10.1002/dta.1412.

[31] N.M. Suni, P. Lindfors, O. Laine, P. Östman, I. Ojanperä, T. Kotiaho, T.J. Kauppila, R. Kostiainen. Matrix effect in the analysis of drugs of abuse from urine with desorption atmospheric pressure photoionization-mass spectrometry (DAPPI-MS) and desorption electrospray ionization-mass spectrometry (DESI-MS). *Anal. Chim. Acta.* **2011**, 699, 73. DOI: 10.1016/j.aca.2011.05.004.

[32] Y. Su, H. Wang, J. Liu, P. Wei, R.G. Cooks, Z. Ouyang. Quantitative paper spray mass spectrometry analysis of drugs of abuse. *Analyst (Cambridge, U. K.).* **2013**, 138, 4443. DOI: 10.1039/c3an00934c.

[33] N. Talaty, C.C. Mulligan, D.R. Justes, A.U. Jackson, R.J. Noll, R.G. Cooks. Fabric analysis by ambient mass spectrometry for explosives and drugs. *Analyst (Cambridge, U. K.).* **2008**, 133, 1532. DOI: 10.1039/b807934j.

[34] A.H. Grange, G.W. Sovocool. Detection of illicit drugs on surfaces using direct analysis in real time (DART) time-of-flight mass spectrometry. *Rapid Commun. Mass Spectrom.* **2011**, 25, 1271. DOI: 10.1002/rcm.5009.

[35] M.E. Monge, P. Dwivedi, M. Zhou, F.M. Fernández, M. Payne, C. Harris, B. House, Y. Juggins, P. Cizmarik, D. Jenkins, P.N. Newton. A tiered analytical approach for investigating poor quality emergency contraceptives *PLoS One.* **2014**, 9, e95353.

[36] N.M. Suni, H. Aalto, T.J. Kauppila, T. Kotiaho, R. Kostiainen. Analysis of lipids with desorption atmospheric pressure photoionization-mass spectrometry (DAPPI-MS) and desorption electrospray ionization-mass spectrometry (DESI-MS). *J. Mass Spectrom.* **2012**, 47, 611. DOI: 10.1002/jms.2992.

[37] F.M. Fernández, D. Hostetler, K. Powell, H. Kaur, M.D. Green, D.C. Mildenhall, P.N. Newton. Poor quality drugs: grand challenges in high throughput detection, countrywide sampling, and forensics in developing countries. *Analyst (Cambridge, U. K.).* **2011**, 136, 3073. DOI: 10.1039/C0AN00627K.

[38] D.J. Weston, A.D. Ray, A.W.T. Bristow. Commentary: Challenging convention using ambient ionization and direct analysis mass spectrometric techniques. *Rapid Commun. Mass Spectrom.* **2011**, 25, 821. DOI: 10.1002/rcm.4925.

[39] S. Myung, J.M. Wiseman, S.J. Valentine, Z. Takáts, R.G. Cooks, D.E. Clemmer. Coupling Desorption Electrospray Ionization with Ion Mobility/Mass Spectrometry for Analysis of Protein Structure: Evidence for Desorption of Folded and Denatured States. *J. Phys. Chem. B.* **2006**, 110, 5045. DOI: 10.1021/jp052663e.

[40] D.J. Weston, R. Bateman, I.D. Wilson, T.R. Wood, C.S. Creaser. Direct analysis of pharmaceutical drug formulations using ion mobility spectrometry/quadrupole-time-of-flight mass spectrometry combined with desorption electrospray ionization. *Anal. Chem.* **2005**, 77, 7572. DOI: 10.1021/ac051277q.

[41] E.L. Harry, J.C. Reynolds, A.W.T. Bristow, I.D. Wilson, C.S. Creaser. Direct analysis of pharmaceutical formulations from non-bonded reversed-phase thin-layer chromatography plates by desorption electrospray ionisation ion mobility mass spectrometry. *Rapid Commun. Mass Spectrom.* **2009**, 23, 2597. DOI: 10.1002/rcm.4152.

[42] A.S. Galhena, G.A. Harris, M. Kwasnik, F.M. Fernández. Enhanced direct ambient analysis by differential mobility-filtered desorption electrospray ionization-mass spectrometry. *Anal. Chem. (Washington, DC, U. S.).* **2010**, 82, 9159. DOI: 10.1021/ac102340h.

[43] D. Morsa, V. Gabelica, E. De Pauw. Effective Temperature of Ions in Traveling Wave Ion Mobility Spectrometry. *Anal. Chem. (Washington, DC, U. S.).* **2011**, 83, 5775. DOI: 10.1021/ac201509p.

[44] D. Morsa, V. Gabelica, E. De Pauw. Fragmentation and Isomerization Due to Field Heating in Traveling Wave Ion Mobility Spectrometry. *J. Am. Soc. Mass Spectrom.* **2014**, 25, 1384. DOI: 10.1007/s13361-014-0909-9.

[45] S.I. Merenbloom, T.G. Flick, E.R. Williams. How hot are your ions in TWAVE ion mobility spectrometry?. *J. Am. Soc. Mass Spectrom.* **2012**, 23, 553. DOI: 10.1007/s13361-011-0313-7.

[46] R.G. Ewing, G.A. Eiceman, C.S. Harden, J.A. Stone. The kinetics of the decompositions of the proton bound dimers of 1,4-dimethylpyridine and dimethyl methylphosphonate from atmospheric pressure ion mobility spectra. *Int. J. Mass Spectrom.* **2006**, 255-256, 76. DOI: 10.1016/j.ijms.2006.04.003.

[47] M.Y. Rajapakse, P.E. Fowler, G.A. Eiceman, J.A. Stone. Dissociation Enthalpies of Chloride Adducts of Nitrate and Nitrite Explosives Determined by Ion Mobility Spectrometry. *J. Phys. Chem. A.* **2016**, 120, 690. DOI: 10.1021/acs.jpca.5b10765.

[48] R.M.M.Y. Rajapakse, J.A. Stone, G.A. Eiceman. An ion mobility and theoretical study of the thermal decomposition of the adduct formed between ethylene glycol dinitrate and chloride. *Int. J. Mass Spectrom.* **2014**, 371, 28. DOI: 10.1016/j.ijms.2014.07.039.

[49] M.Y. Rajapakse, J.A. Stone, G.A. Eiceman. Decomposition Kinetics of NitroglycerineÂ·Cl-(g) in Air at Ambient Pressure with a Tandem Ion Mobility Spectrometer. *J. Phys. Chem. A.* **2014**, 118, 2683. DOI: 10.1021/jp412444b.

[50] X. An, G.A. Eiceman, R. Rasanen, J.E. Rodriguez, J.A. Stone. Dissociation of Proton Bound Ketone Dimers in Asymmetric Electric Fields with Differential Mobility Spectrometry and in Uniform Electric Fields with Linear Ion Mobility Spectrometry. *J. Phys. Chem. A.* **2013**, 117, 6389. DOI: 10.1021/jp401640t.

[51] X. An, G.A. Eiceman, J.A. Stone. A determination of the effective temperatures for the dissociation of the proton bound dimer of dimethyl methylphosphonate in a planar differential mobility spectrometer. *Int. J. Ion Mobility Spectrom.* **2010**, 13, 25. DOI: 10.1007/s12127-010-0037-6.

[52] X. An, G.A. Eiceman, J.E. Rodriguez, J.A. Stone. Gas phase fragmentation of protonated esters in air at ambient pressure through ion heating by electric field in differential mobility spectrometry. *Int. J. Mass Spectrom.* **2011**, 303, 181. DOI: 10.1016/j.ijms.2011.01.031.

[53] K.J. Laszlo, E.B. Munger, M.F. Bush. Folding of Protein Ions in the Gas Phase after Cation-to-Anion Proton-Transfer Reactions. *J. Am. Chem. Soc.* **2016**, Ahead of Print. DOI: 10.1021/jacs.6b04282.

[54] C.J. Gray, B. Thomas, R. Upton, L.G. Migas, C.E. Eyers, P.E. Barran, S.L. Flitsch. Applications of ion mobility mass spectrometry for high throughput, high resolution glycan analysis. *Biochim. Biophys. Acta, Gen. Subj.* **2016**, 1860, 1688. DOI: 10.1016/j.bbagen.2016.02.003.

[55] B.T. Ruotolo, K. Giles, I. Campuzano, A.M. Sandercock, R.H. Bateman, C.V. Robinson. Evidence for Macromolecular Protein Rings in the Absence of Bulk Water. *Science (Washington, DC, U. S.).* **2005**, 310, 1658. DOI: 10.1126/science.1120177.

[56] M.F. Bush, Z. Hall, K. Giles, J. Hoyes, C.V. Robinson, B.T. Ruotolo. Collision Cross Sections of Proteins and Their Complexes: A Calibration Framework and Database for Gas-Phase Structural Biology. *Anal. Chem. (Washington, DC, U. S.).* **2010**, 82, 9557. DOI: 10.1021/ac1022953.

[57] E.A. Mason, H.W. Schamp Jr., J.T. Vanderslice. Interaction energy and mobility of Li+ ions in helium. *Phys. Rev.* **1958**, 112, 445. DOI: 10.1103/PhysRev.112.445.

[58] R. Fernández-Maestre, C.S. Harden, R.G. Ewing, C.L. Crawford, H.H. Hill. Chemical standards in ion mobility spectrometry. *Analyst (Cambridge, U. K.).* **2010**, 135, 1433. DOI: 10.1039/b915202d.

[59] M. Groessl, S. Graf, R. Knochenmuss. High resolution ion mobility-mass spectrometry for separation and identification of isomeric lipids. *Analyst (Cambridge, U. K.).* **2015**, 140, 6904. DOI: 10.1039/C5AN00838G.

[60] B.C. Hauck, E.J. Davis, A.E. Clark, W.F. Siems, C.S. Harden, V.M. McHugh, H.H.J. Hill. Determining the water content of a drift gas using reduced ion mobility measurements. *Int. J. Mass Spectrom.* **2014**, 368, 37. DOI: 10.1016/j.ijms.2014.05.010.

[61] A.A. Sysoev, S.S. Poteshin, D.M. Chernyshev, A.V. Karpov, Y.B. Tuzkov, V.V. Kyzmin, A.A. Sysoev. Analysis of new synthetic drugs by ion mobility time-of-flight mass spectrometry. *Eur. J. Mass Spectrom.* **2014**, 20, 185. DOI: 10.1255/ejms.1262.

[62] B.C. Hauck, W.F. Siems, C.S. Harden, V.M. McHugh, H.H. Hill. E/N effects on K0 values revealed by high precision measurements under low field conditions. *Rev. Sci. Instrum.* **2016**, 87, 075104/1. DOI: 10.1063/1.4955208.

[63] B.C. Hauck, W.F. Siems, C.S. Harden, V.M. McHugh, H.H. Hill. Determination of E/N Influence on K0 Values within the Low Field Region of Ion Mobility Spectrometry. *J. Phys. Chem. A.* **2017**, 121, 2274. DOI: 10.1021/acs.jpca.6b12331.

[64] J.A. Stone. The kinetics and thermodynamics of ion solvation applicable to ion mobility spectrometry. *Int. J. Ion Mobility Spectrom.* **2002**, 5, 19.

[65] A.A. Shvartsburg. *Differential ion mobility spectrometry: nonlinear ion transport and fundamentals of FAIMS.* CRC Press, Taylor & Francis group, Boca Raton, **2008**.

[66] R. Guevremont. High-field asymmetric waveform ion mobility spectrometry: a new tool for mass spectrometry. *J. Chromatogr. A.* **2004**, 1058, 3. DOI: 10.1016/j.chroma.2004.08.119.

[67] E.V. Krylov, S.L. Coy, E.G. Nazarov. Temperature effects in differential mobility spectrometry. *Int. J. Mass Spectrom.* **2009**, 279, 119. DOI: 10.1016/j.ijms.2008.10.025.

[68] R.A. Miller, G.A. Eiceman, E.G. Nazarov, A.T. King. A novel micromachined high-field asymmetric waveform-ion mobility spectrometer. *Sens. Actuators, B.* **2000**, 67, 300. DOI: 10.1016/S0925-4005(00)00535-9.

[69] R.A. Miller, E.G. Nazarov, G.A. Eiceman, A.T. King. A MEMS radio-frequency ion mobility spectrometer for chemical vapor detection. *Sens. Actuators, A.* **2001**, 91, 301. DOI: 10.1016/S0924-4247(01)00600-8.

[70] B.M. Kolakowski, Z. Mester. Review of applications of high-field asymmetric waveform ion mobility spectrometry (FAIMS) and differential mobility spectrometry (DMS). *Analyst (Cambridge, U. K.).* **2007**, 132, 842. DOI: 10.1039/b706039d.

[71] G.A. Eiceman, E.G. Nazarov, B. Tadjikov, R.A. Miller. Monitoring volatile organic compounds in ambient air inside and outside buildings with the use of a radio-frequency-based ion-mobility analyzer with a micromachined drift tube. *Field Anal. Chem. Technol.* **2000**, 4, 297. DOI: 10.1002/1520-6521(2000)4:63.0.CO;2-H.

[72] M.R. Menlyadiev, J.A. Stone, G.A. Eiceman. Tandem differential mobility spectrometry with chemical modification of ions. *Int. J. Ion Mobility Spectrom.* **2012**, 15, 123. DOI: 10.1007/s12127-012-0106-0.

[73] M.R. Menlyadiev, A. Tarassov, A.M. Kielnecker, G.A. Eiceman. Tandem differential mobility spectrometry with ion dissociation in air at ambient pressure and temperature. *Analyst (Cambridge, U. K.).* **2015**, 140, 2995. DOI: 10.1039/C4AN02159B.

[74] T. Kotiaho, F.R. Lauritsen, H. Degn, H. Paakkanen. Membrane inlet ion mobility spectrometry for online measurement of ethanol in beer and in yeast fermentation. *Anal. Chim. Acta.* **1995**, 309, 317. DOI: 10.1016/0003-2670(95)00086-F.

[75] K. Tuovinen, H. Paakkanen, O. Hänninen. Detection of pesticides from liquid matrices by ion mobility spectrometry. *Anal. Chim. Acta.* **2000**, 404, 7. DOI: 10.1016/S0003-2670(99)00697-2.

[76] M. Nousiainen, K. Peräkorpi, M. Sillanpää. Determination of gas-phase produced ethyl parathion and toluene 2,4-diisocyanate by ion mobility spectrometry, gas chromatography and liquid chromatography. *Talanta.* **2007**, 72, 984. DOI: 10.1016/j.talanta.2006.12.022.

[77] P. Mochalski, J. Rudnicka, A. Agapiou, M. Statheropoulos, A. Amann, B. Buszewski. Near real-time VOCs analysis using an aspiration ion mobility spectrometer. *J. Breath Res.* **2013**, 7, 026002, 11. DOI: 10.1088/1752-7155/7/2/026002.

[78] O. Raatikainen, V. Reinikainen, P. Minkkinen, T. Ritvanen, P. Muje, J. Pursiainen, T. Hiltunen, P. Hyvönen, A. von Wright, S. Reinikainen. Multivariate modelling of fish freshness index based on ion mobility spectrometry measurements. *Anal. Chim. Acta.* **2005**, 544, 128. DOI: 10.1016/j.aca.2005.02.029.

[79] M. Kolehmainen, P. Rönkkö, O. Raatikainen. Monitoring of yeast fermentation by ion mobility spectrometry measurement and data visualisation with Self-Organizing Maps. *Anal. Chim. Acta.* **2003**, 484, 93. DOI: 10.1016/S0003-2670(03)00307-6.

[80] A.A. Shvartsburg, R.D. Smith. Fundamentals of Traveling Wave Ion Mobility Spectrometry. *Anal. Chem. (Washington, DC, U. S.).* **2008**, 80, 9689. DOI: 10.1021/ac8016295.

[81] K. Giles, J.P. Williams, I. Campuzano. Enhancements in travelling wave ion mobility resolution. *Rapid Commun. Mass Spectrom.* **2011**, 25, 1559. DOI: 10.1002/rcm.5013.

[82] S.D. Pringle, K. Giles, J.L. Wildgoose, J.P. Williams, S.E. Slade, K. Thalassinos, R.H. Bateman, M.T. Bowers, J.H. Scrivens. An investigation of the mobility separation of some peptide and protein ions using a new hybrid quadrupole/travelling wave IMS/oa-ToF instrument. *Int. J. Mass Spectrom.* **2007**, 261, 1. DOI: 10.1016/j.ijms.2006.07.021.

[83] K. Giles, J.L. Wildgoose, D.J. Langridge, I. Campuzano. A method for direct measurement of ion mobilities using a travelling wave ion guide. *Int. J. Mass Spectrom.* **2010**, 298, 10. DOI: 10.1016/j.ijms.2009.10.008.

[84] S. Hyung, B.T. Ruotolo. Integrating mass spectrometry of intact protein complexes into structural proteomics. *Proteomics.* **2012**, 12, 1547. DOI: 10.1002/pmic.201100520.

[85] B.T. Ruotolo, J.L.P. Benesch, A.M. Sandercock, S. Hyung, C.V. Robinson. Ion mobility-mass spectrometry analysis of large protein complexes. *Nat. Protoc.* **2008**, 3, 1139. DOI: 10.1038/nprot.2008.78.

[86] H. Li, K. Giles, B. Bendiak, K. Kaplan, W.F. Siems, H.H. Hill. Resolving Structural Isomers of Monosaccharide Methyl Glycosides Using Drift Tube and Traveling Wave Ion Mobility Mass Spectrometry. *Anal. Chem. (Washington, DC, U. S.).* **2012**, 84, 3231. DOI: 10.1021/ac203116a.

[87] H. Li, B. Bendiak, W.F. Siems, D.R. Gang, H.H. Hill. Carbohydrate Structure Characterization by Tandem Ion Mobility Mass Spectrometry (IMMS)2. *Anal. Chem. (Washington, DC, U. S.).* **2013**, 85, 2760. DOI: 10.1021/ac303273z.

[88] L. Dong, H. Shion, R.G. Davis, B. Terry-Penak, J. Castro-Perez, R.B. van Breemen. Collision Cross-Section Determination and Tandem Mass Spectrometric Analysis of Isomeric Carotenoids Using Electrospray Ion Mobility Time-of-Flight Mass Spectrometry. *Anal. Chem. (Washington, DC, U. S.).* **2010**, 82, 9014. DOI: 10.1021/ac101974g.

[89] H. Borsdorf, G.A. Eiceman. Ion mobility spectrometry: principles and applications. *Appl. Spectrosc. Rev.* **2006**, 41, 323. DOI: 10.1080/05704920600663469.

[90] A. Good, D.A. Durden, P. Kebarle. Ion-molecule reactions in pure nitrogen and nitrogen containing traces of water at total pressures 0.5-4 torr. kinetics of clustering reactions forming H+(H2O)n. *J. Chem. Phys.* **1970**, 52, 212. DOI: 10.1063/1.1672667.

[91] U. Gaik, M. Sillanpää, Z. Witkiewicz, J. Puton. Nitrogen oxides as dopants for the detection of aromatic compounds with ion mobility spectrometry. *Anal. Bioanal. Chem.* **2017**, Ahead of Print. DOI: 10.1007/s00216-017-0265-2.

[92] E. Waraksa, U. Perycz, J. Namiesnik, M. Sillanpää, T. Dymerski, M. Wójtowicz, J. Puton. Dopants and gas modifiers in ion mobility spectrometry. *TrAC, Trends Anal. Chem.* **2016**, 82, 237. DOI: 10.1016/j.trac.2016.06.009.

[93] J. Puton, M. Nousiainen, M. Sillanpää. Ion mobility spectrometers with doped gases. *Talanta.* **2008**, 76, 978. DOI: 10.1016/j.talanta.2008.05.031.

[94] NIST Chemistry webbook, http://webbook.nist.gov/chemistry/.

[95] J.A.D. Stockdale, L.G. Christophorou, G.S. Hurst. Capture of thermal electrons by oxygen. *J. Chem. Phys.* **1967**, 47, 3267. DOI: 10.1063/1.1712388.

[96] K.A. Daum, D.A. Atkinson, R.G. Ewing. Formation of halide reactant ions and effects of excess reagent chemical on the ionization of TNT in ion mobility spectrometry. *Talanta.* **2001**, 55, 491. DOI: 10.1016/S0039-9140(01)00453-2.

[97] K.A. Daum, D.A. Atkinson, R.G. Ewing, W.B. Knighton, E.P. Grimsrud. Resolving interferences in negative mode ion mobility spectrometry using selective reactant ion chemistry. *Talanta.* **2001**, 54, 299. DOI: 10.1016/S0039-9140(00)00656-1.

[98] G.A. Eiceman, E.V. Krylov, N.S. Krylova, E.G. Nazarov, R.A. Miller. Separation of Ions from Explosives in Differential Mobility Spectrometry by Vapor-Modified Drift Gas. *Anal. Chem.* **2004**, 76, 4937. DOI: 10.1021/ac035502k.

[99] A.H. Lawrence, P. Neudorfl. Detection of ethylene glycol dinitrate vapors by ion mobility spectrometry using chloride reagent ions. *Anal. Chem.* **1988**, 60, 104. DOI: 10.1021/ac00153a002.

[100] J.W. Leonhardt. New detectors in environmental monitoring using tritium sources. *J. Radioanal. Nucl. Chem.* **1996**, 206, 333. DOI: 10.1007/BF02039661.

[101] T. Keller, A. Miki, P. Regenscheit, R. Dirnhofer, A. Schneider, H. Tsuchihashi. Detection of designer drugs in human hair by ion mobility spectrometry (IMS). *Forensic Sci. Int.* **1998**, 94, 55. DOI: 10.1016/S0379-0738(98)00051-6.

[102] A.H. Lawrence. Detection of drug residues on the hands of subjects by surface sampling and ion mobility spectrometry. *Forensic Sci. Int.* **1987**, 34, 73. DOI: 10.1016/0379-0738(87)90086-7.

[103] R.B. Turner, J.L. Brokenshire. Hand-held ion mobility spectrometers. *Trends Anal. Chem.* **1994**, 13, 275. DOI: 10.1016/0165-9936(94)87064-0.

[104] S. Cai, J. Stevens, J.A. Syage. Ultra high performance liquid chromatography-atmospheric pressure photoionization-mass spectrometry for high-sensitivity analysis of US Environmental Protection Agency sixteen priority pollutant polynuclear aromatic hydrocarbons in oysters. *J. Chromatogr. A.* **2012**, 1227, 138. DOI: 10.1016/j.chroma.2011.12.111.

[105] K.S. Hakala, L. Laitinen, A.M. Kaukonen, J. Hirvonen, R. Kostiainen, T. Kotiaho. Development of LC/MS/MS Methods for Cocktail Dosed Caco-2 Samples Using Atmospheric Pressure Photoionization and Electrospray Ionization. *Anal. Chem.* **2003**, 75, 5969. DOI: 10.1021/ac034679b.

[106] K.A. Hanold, S.M. Fischer, P.H. Cormia, C.E. Miller, J.A. Syage. Atmospheric Pressure Photoionization. 1. General Properties for LC/MS. *Anal. Chem.* **2004**, 76, 2842. DOI: 10.1021/ac035442i.

[107] D.B. Robb, M.W. Blades. State-of-the-art in atmospheric pressure photoionization for LC/MS. *Anal. Chim. Acta.* **2008**, 627, 34. DOI: 10.1016/j.aca.2008.05.077.

[108] R.D. McCulloch, D.B. Robb. Field-Free Atmospheric Pressure Photoionization-Liquid Chromatography-Mass Spectrometry for the Analysis of Steroids within Complex Biological Matrices. *Anal. Chem. (Washington, DC, U. S.).* **2017**, 89, 4169. DOI: 10.1021/acs.analchem.7b00157.

[109] D.B. Robb, T.R. Covey, A.P. Bruins. Atmospheric pressure photoionization: an ionization method for liquid chromatography-mass spectrometry. *Anal. Chem.* **2000**, 72, 3653. DOI: 10.1021/ac0001636.

[110] D.B. Robb, M.W. Blades. Effects of solvent flow, dopant flow, and lamp current on dopant-assisted atmospheric pressure photoionization (DA-APPI) for LC-MS. Ionization via proton transfer. *J. Am. Soc. Mass Spectrom.* **2005**, 16, 1275. DOI: 10.1016/j.jasms.2005.03.017.

[111] J.I. Baumbach, S. Sielemann, Z. Xie, H. Schmidt. Detection of the Gasoline Components Methyl tert-Butyl Ether, Benzene, Toluene, and m-Xylene Using Ion Mobility Spectrometers with a Radioactive and UV Ionization Source. *Anal. Chem.* **2003**, 75, 1483. DOI: 10.1021/ac020342i.

[112] H. Borsdorf, K. Neitsch, G.A. Eiceman, J.A. Stone. A comparison of the ion chemistry for mono-substituted toluenes and anilines by three methods of atmospheric pressure ionization with ion mobility spectrometry. *Talanta.* **2009**, 78, 1464. DOI: 10.1016/j.talanta.2009.02.043.

[113] G.A. Eiceman, V.J. Vandiver. Charge-exchange in binary mixtures of polycyclic aromatic hydrocarbons using photoionization-ion mobility spectrometry. *Anal. Chem.* **1986**, 58, 2331. DOI: 10.1021/ac00124a046.

[114] J. Laakia, A. Adamov, M. Jussila, C.S. Pedersen, A.A. Sysoev, T. Kotiaho. Separation of different ion structures in atmospheric pressure photoionization-ion mobility spectrometry-mass spectrometry (APPI-IMS-MS). *J. Am. Soc. Mass Spectrom.* **2010**, 21, 1565. DOI: 10.1016/j.jasms.2010.04.018.

[115] L. Ahonen, M. Fasciotti, G.B.a. Gennäs, T. Kotiaho, R.J. Daroda, M. Eberlin, R. Kostiainen. Separation of steroid isomers by ion mobility mass spectrometry. *J. Chromatogr. A.* **2013**, 1310, 133. DOI: 10.1016/j.chroma.2013.08.056.

[116] H. Borsdorf, E.G. Nazarov, R.A. Miller. Atmospheric-pressure ionization studies and field dependence of ion mobilities of isomeric hydrocarbons using a miniature differential mobility spectrometer. *Anal. Chim. Acta.* **2006**, 575, 76. DOI: 10.1016/j.aca.2006.05.066.

[117] H. Borsdorf, E.G. Nazarov, R.A. Miller. Time-of-flight ion mobility spectrometry and differential mobility spectrometry: A comparative study of their efficiency in the analysis of halogenated compounds. *Talanta.* **2007**, 71, 1804. DOI: 10.1016/j.talanta.2006.08.017.

[118] S. Roetering, E.G. Nazarov, H. Borsdorf, C. Weickhardt. Effect of dopants on the analysis of pesticides by means of differential mobility spectrometry with atmospheric pressure photoionization. *Int. J. Ion Mobility Spectrom.* **2010**, 13, 47. DOI: 10.1007/s12127-010-0043-8.

[119] L. Hintikka, M. Haapala, T. Kuuranne, A. Leinonen, R. Kostiainen. Analysis of anabolic steroids in urine by gas chromatography-microchip atmospheric pressure photoionization-mass spectrometry with chlorobenzene as dopant. *J. Chromatogr. A.* **2013**, 1312, 111. DOI: 10.1016/j.chroma.2013.08.098.

[120] L.L. Ahonen, M. Haapala, V. Saarela, S. Franssila, T. Kotiaho, R. Kostiainen. Feasibility of capillary liquid chromatography/microchip atmospheric pressure photoionization mass spectrometry in analyzing anabolic steroids in urine samples. *Rapid Commun. Mass Spectrom.* **2010**, 24, 958. DOI: 10.1002/rcm.4468.

[121] T.J. Kauppila, H. Kersten, T. Benter. Ionization of EPA Contaminants in Direct and Dopant-Assisted Atmospheric Pressure Photoionization and Atmospheric Pressure Laser Ionization. *J. Am. Soc. Mass Spectrom.* **2015**, 26, 1036. DOI: 10.1007/s13361-015-1092-3.

[122] T.J. Kauppila, T. Kuuranne, E.C. Meurer, M.N. Eberlin, T. Kotiaho, R. Kostiainen. Atmospheric Pressure Photoionization Mass Spectrometry. Ionization Mechanism and the Effect of Solvent on the Ionization of Naphthalenes. *Anal. Chem.* **2002**, 74, 5470. DOI: 10.1021/ac025659x.

[123] T.J. Kauppila, H. Kersten, T. Benter. The Ionization Mechanisms in Direct and Dopant-Assisted Atmospheric Pressure Photoionization and Atmospheric Pressure Laser Ionization. *J. Am. Soc. Mass Spectrom.* **2014**, 25, 1870. DOI: 10.1007/s13361-014-0988-7.

[124] D.B. Robb, D.R. Smith, M.W. Blades. Investigation of Substituted-Benzene Dopants for Charge Exchange Ionization of Nonpolar Compounds by Atmospheric Pressure Photoionization. *J. Am. Soc. Mass Spectrom.* **2008**, 19, 955. DOI: 10.1016/j.jasms.2008.03.013.

[125] T.J. Kauppila, R. Kostiainen, A.P. Bruins. Anisole, a new dopant for atmospheric pressure photoionization mass spectrometry of low proton affinity, low ionization energy compounds. *Rapid Commun. Mass Spectrom.* **2004**, 18, 808. DOI: 10.1002/rcm.1408.

[126] W.B. Tzeng, S. Wei, A.W. Castleman Jr. Multiphoton ionization of acetone clusters: metastable unimolecular decomposition of acetone cluster ions and the influence of solvation on intracluster ion-molecule reactions. *J. Am. Chem. Soc.* **1989**, 111, 6035. DOI: 10.1021/ja00198a010.

[127] T.J. Kauppila, T. Kotiaho, R. Kostiainen, A.P. Bruins. Negative ion-atmospheric pressure photoionization-mass spectrometry. *J. Am. Soc. Mass Spectrom.* **2004**, 15, 203. DOI: 10.1016/j.jasms.2003.10.012.

[128] L. Song, A.D. Wellman, H. Yao, J. Adcock. Electron capture atmospheric pressure photoionization mass spectrometry: analysis of fullerenes, perfluorinated compounds, and pentafluorobenzyl derivatives. *Rapid Commun. Mass Spectrom.* **2007**, 21, 1343. DOI: 10.1002/rcm.2963.

[129] S. Klee, S. Albrecht, V. Derpmann, H. Kersten, T. Benter. Generation of ion-bound solvent clusters as reactant ions in dopant-assisted APPI and APLI. *Anal. Bioanal. Chem.* **2013**, 405, 6933. DOI: 10.1007/s00216-013-7114-8.

[130] E. Basso, E. Marotta, R. Seraglia, M. Tubaro, P. Traldi. On the formation of negative ions in atmospheric pressure photoionization conditions. *J. Mass Spectrom.* **2003**, 38, 1113. DOI: 10.1002/jms.528.

[131] L. Luosujärvi, V. Arvola, M. Haapala, J. Pól, V. Saarela, S. Franssila, T. Kotiaho, R. Kostiainen, T.J. Kauppila. Desorption and Ionization Mechanisms in Desorption Atmospheric Pressure Photoionization. *Anal. Chem. (Washington, DC, U. S.).* **2008**, 80, 7460. DOI: 10.1021/ac801186x.

[132] T.J. Kauppila, A. Flink, M. Haapala, U. Laakkonen, L. Aalberg, R.A. Ketola, R. Kostiainen. Desorption atmospheric pressure photoionization-mass spectrometry in routine analysis of confiscated drugs. *Forensic Sci. Int.* **2011**, 210, 206. DOI: 10.1016/j.forsciint.2011.03.018.

[133] T.J. Kauppila, V. Arvola, M. Haapala, J. Pól, L. Aalberg, V. Saarela, S. Franssila, T. Kotiaho, R. Kostiainen. Direct analysis of illicit drugs by desorption atmospheric pressure photoionization. *Rapid Commun. Mass Spectrom.* **2008**, 22, 979. DOI: 10.1002/rcm.3461.

[134] L. Luosujärvi, S. Kanerva, V. Saarela, S. Franssila, R. Kostiainen, T. Kotiaho, T.J. Kauppila. Environmental and food analysis by desorption atmospheric pressure photoionization-mass spectrometry *Rapid Commun Mass Spectrom.* **2010**, 24, 1343.

[135] T.J. Kauppila, A. Flink, J. Pukkila, R.A. Ketola. Analysis of nitrogen-based explosives with desorption atmospheric pressure photoionization mass spectrometry. *Rapid Commun. Mass Spectrom.* **2016**, 30, 467. DOI: 10.1002/rcm.7469.

[136] D.C. Podgorski, R. Hamdan, A.M. McKenna, L. Nyadong, R.P. Rodgers, A.G. Marshall, W.T. Cooper. Characterization of Pyrogenic Black Carbon by Desorption Atmospheric Pressure Photoionization Fourier Transform Ion Cyclotron Resonance Mass Spectrometry. *Anal. Chem. (Washington, DC, U. S.).* **2012**, 84, 1281. DOI: 10.1021/ac202166x.

[137] J. Rejsek, V. Vrkoslav, A. Vaikkinen, M. Haapala, T.J. Kauppila, R. Kostiainen, J. Cvacka. Thin-Layer Chromatography/Desorption Atmospheric Pressure Photoionization Orbitrap Mass Spectrometry of Lipids. *Anal. Chem. (Washington, DC, U. S.).* **2016**, 88, 12279. DOI: 10.1021/acs.analchem.6b03465.

[138] R.B. Cody. Observation of molecular ions and analysis of nonpolar compounds with the direct analysis in real time ion source. *Anal. Chem. (Washington, DC, U. S.).* **2009**, 81, 1101. DOI: 10.1021/ac8022108.

[139] L. Song, S.C. Gibson, D. Bhandari, K.D. Cook, J.E. Bartmess. Ionization Mechanism of Positive-Ion Direct Analysis in Real Time: A Transient Microenvironment Concept. *Anal. Chem. (Washington, DC, U. S.).* **2009**, 81, 10080. DOI: 10.1021/ac901122b.

[140] R.A. Musah, M.A. Domin, M.A. Walling, J.R.E. Shepard. Rapid identification of synthetic cannabinoids in herbal samples via direct analysis in real time mass spectrometry. *Rapid Commun. Mass Spectrom.* **2012**, 26, 1109. DOI: 10.1002/rcm.6205.

[141] S. Gwak, J.R. Almirall. Rapid screening of 35 new psychoactive substances by ion mobility spectrometry (IMS) and direct analysis in real time (DART) coupled to quadrupole time-of-flight mass spectrometry (QTOF-MS). *Drug Test. Anal.* **2015**, 7, 884. DOI: 10.1002/dta.1783.

[142] J.M. Nilles, T.R. Connell, H.D. Durst. Quantitation of Chemical Warfare Agents Using the Direct Analysis in Real Time (DART) Technique. *Anal. Chem. (Washington, DC, U. S.).* **2009**, 81, 6744. DOI: 10.1021/ac900682f.

[143] F. Rowell, J. Seviour, A.Y. Lim, C.G. Elumbaring-Salazar, J. Loke, J. Ma. Detection of nitro-organic and peroxide explosives in latent fingermarks by DART- and SALDI-TOF-mass spectrometry. *Forensic Sci. Int.* **2012**, 221, 84. DOI: 10.1016/j.forsciint.2012.04.007.

[144] M. Busman, J.R. Bobell, C.M. Maragos. Determination of the aflatoxin M1 (AFM1) from milk by direct analysis in real time - mass spectrometry (DART-MS). *Food Control.* **2015**, 47, 592. DOI: 10.1016/j.foodcont.2014.08.003.

[145] L. Vaclavik, M. Zachariasova, V. Hrbek, J. Hajslova. Analysis of multiple mycotoxins in cereals under ambient conditions using direct analysis in real time (DART) ionization coupled to high resolution mass spectrometry. *Talanta.* **2010**, 82, 1950. DOI: 10.1016/j.talanta.2010.08.029.

[146] M. Dole, L.L. Mack, R.L. Hines, R.C. Mobley, L.D. Ferguson, M.B. Alice. Molecular beams of macroions. *J. Chem. Phys.* **1968**, 49, 2240. DOI: 10.1063/1.1670391.

[147] J.V. Iribarne, B.A. Thomson. On the evaporation of small ions from charged droplets. *J. Chem. Phys.* **1976**, 64, 2287. DOI: 10.1063/1.432536.

[148] B.A. Thomson, J.V. Iribarne. Field-induced ion evaporation from liquid surfaces at atmospheric pressure. *J. Chem. Phys.* **1979**, 71, 4451. DOI: 10.1063/1.438198.

[149] A.B. Costa, R.G. Cooks. Simulation of atmospheric transport and droplet-thin film collisions in desorption electrospray ionization. *Chem. Commun. (Cambridge, U. K.).* **2007**, 3915. DOI: 10.1039/b710511h.

[150] A. Venter, P.E. Sojka, R.G. Cooks. Droplet Dynamics and Ionization Mechanisms in Desorption Electrospray Ionization Mass Spectrometry. *Anal. Chem.* **2006**, 78, 8549. DOI: 10.1021/ac0615807.

[151] Z. Takáts, J.M. Wiseman, R.G. Cooks. Ambient mass spectrometry using desorption electrospray ionization (DESI): Instrumentation, mechanisms and applications in forensics, chemistry, and biology. *J. Mass Spectrom.* **2005**, 40, 1261. DOI: 10.1002/jms.922.

[152] R. Cumeras, E. Figueras, C.E. Davis, J.I. Baumbach, I. Gracia. Review on Ion Mobility Spectrometry. Part 2: hyphenated methods and effects of experimental parameters. *Analyst (Cambridge, U. K.).* **2015**, 140, 1391. DOI: 10.1039/C4AN01101E.

[153] L.M. Matz, P.S. Tornatore, H.H. Hill. Evaluation of suspected interferents for TNT detection by ion mobility spectrometry. *Talanta.* **2001**, 54, 171. DOI: 10.1016/S0039-9140(00)00663-9.

[154] A.H. Lawrence. Ion mobility spectrometry/mass spectrometry of some prescription and illicit drugs. *Anal. Chem.* **1986**, 58, 1269. DOI: 10.1021/ac00297a069.

[155] P. Rearden, P.B. Harrington. Rapid screening of precursor and degradation products of chemical warfare agents in soil by solid-phase microextraction ion mobility spectrometry (SPME-IMS). *Anal. Chim. Acta.* **2005**, 545, 13. DOI: 10.1016/j.aca.2005.04.035.

[156] Q. Meng, Z. Karpas, G.A. Eiceman. Monitoring indoor ambient atmospheres for volatile organic compounds using an ion mobility analyzer array with selective chemical ionization. *Int. J. Environ. Anal. Chem.* **1995**, 61, 81. DOI: 10.1080/03067319508026239.

[157] M.A. McCooeye, B. Ells, D.A. Barnett, R.W. Purves, R. Guevremont. Quantitation of morphine and codeine in human urine using high-field asymmetric waveform ion mobility spectrometry (FAIMS) with mass spectrometric detection. *J. Anal. Toxicol.* **2001**, 25, 81. DOI: 10.1093/jat/25.2.81.

[158] V. Domalain, M. Hubert-Roux, V. Tognetti, L. Joubert, C.M. Lange, J. Rouden, C. Afonso. Enantiomeric differentiation of aromatic amino acids using traveling wave ion mobility-mass spectrometry. *Chem. Sci.* **2014**, 5, 3234. DOI: 10.1039/c4sc00443d.

[159] P.M. Lalli, Y.E. Corilo, M. Fasciotti, M.F. Riccio, G.F. Sa, R.J. Daroda, G.H.M.F. Souza, M. McCullagh, M.D. Bartberger, M.N. Eberlin, I.D.G. Campuzano. Baseline resolution of isomers by traveling wave ion mobility mass spectrometry: investigating the effects of polarizable drift gases and ionic charge distribution. *J. Mass Spectrom.* **2013**, 48, 989. DOI: 10.1002/jms.3245.

[160] P. Benigni, R. Marin, J.C. Molano-Arevalo, A. Garabedian, J.J. Wolff, M.E. Ridgeway, M.A. Park, F. Fernández-Lima. Towards the analysis of high molecular weight proteins and protein complexes using TIMS-MS. *Int. J. Ion Mobility Spectrom.* **2016**, 19, 95. DOI: 10.1007/s12127-016-0201-8.

[161] E. Jurneczko, J. Kalapothakis, I.D.G. Campuzano, M. Morris, P.E. Barran. Effects of Drift Gas on Collision Cross Sections of a Protein Standard in Linear Drift Tube and Traveling Wave Ion Mobility Mass Spectrometry. *Anal. Chem. (Washington, DC, U. S.).* **2012**, 84, 8524. DOI: 10.1021/ac301260d.

[162] W.B. Ridenour, M. Kliman, J.A. McLean, R.M. Caprioli. Structural Characterization of Phospholipids and Peptides Directly from Tissue Sections by MALDI Traveling-Wave Ion Mobility-Mass Spectrometry. *Anal. Chem. (Washington, DC, U. S.).* **2010**, 82, 1881. DOI: 10.1021/ac9026115.

[163] J. Ujma, K. Giles, M. Morris, P.E. Barran. New High Resolution Ion Mobility Mass Spectrometer Capable of Measurements of Collision Cross Sections from 150 to 520 K. *Anal. Chem. (Washington, DC, U. S.).* **2016**, 88, 9469. DOI: 10.1021/acs.analchem.6b01812.

[164] P. Dwivedi, A.J. Schultz, H.H. Hill Jr. Metabolic5 profiling of human blood by high-resolution ion mobility mass spectrometry (IM-MS). *Int. J. Mass Spectrom.* **2010**, 298, 78. DOI: 10.1016/j.ijms.2010.02.007.

[165] J. Gallegos, C. Arce, R. Jordano, L. Arce, L.M. Medina. Target identification of volatile metabolites to allow the differentiation of lactic acid bacteria by gas chromatography-ion mobility spectrometry. *Food Chem.* **2017**, 220, 362. DOI: 10.1016/j.foodchem.2016.10.022.

[166] T.P.I. Lintonen, P.R.S. Baker, M. Suoniemi, B.K. Ubhi, K.M. Koistinen, E. Duchoslav, J.L. Campbell, K. Ekroos. Differential Mobility Spectrometry-Driven Shotgun Lipidomics. *Anal. Chem. (Washington, DC, U. S.).* **2014**, 86, 9662. DOI: 10.1021/ac5021744.

[167] S.J. Allen, A.M. Schwartz, M.F. Bush. Effects of Polarity on the Structures and Charge States of Native-Like Proteins and Protein Complexes in the Gas Phase. *Anal. Chem. (Washington, DC, U. S.).* **2013**, 85, 12055. DOI: 10.1021/ac403139d.

[168] A.A. Shvartsburg, R.D. Smith. High-Resolution Differential Ion Mobility Spectrometry of a Protein. *Anal. Chem. (Washington, DC, U. S.).* **2013**, 85, 10. DOI: 10.1021/ac3029129.

[169] D.P. Smith, T.W. Knapman, I. Campuzano, R.W. Malham, J.T. Berryman, S.E. Radford, A.E. Ashcroft. Deciphering drift time measurements from travelling wave ion mobility spectrometry-mass spectrometry studies. *Eur. J. Mass Spectrom.* **2009**, 15, 113. DOI: 10.1255/ejms.947.

[170] H. Li, B.K. Smith, L. Mark, P. Nemes, J. Nazarian, A. Vertes. Ambient molecular imaging by laser ablation electrospray ionization mass spectrometry with ion mobility separation. *Int. J. Mass Spectrom.* **2015**, 377, 681. DOI: 10.1016/j.ijms.2014.06.025.

[171] K. Skraskova, E. Claude, E.A. Jones, M. Towers, S.R. Ellis, R.M.A. Heeren. Enhanced capabilities for imaging gangliosides in murine brain with matrix-assisted laser desorption/ionization and desorption electrospray ionization mass spectrometry coupled to ion mobility separation. *Methods (Amsterdam, Neth.).* **2016**, 104, 69. DOI: 10.1016/j.ymeth.2016.02.014.

[172] R.V. Bennett, C.M. Gamage, A.S. Galhena, F.M. Fernández. Contrast-Enhanced Differential Mobility-Desorption Electrospray Ionization-Mass Spectrometry Imaging of Biological Tissues. *Anal. Chem. (Washington, DC, U. S.).* **2014**, 86, 3756. DOI: 10.1021/ac5007816.

[173] G.A. Buttigieg, A.K. Knight, S. Denson, C. Pommier, M. Bonner Denton. Characterization of the explosive triacetone triperoxide and detection by ion mobility spectrometry. *Forensic Sci. Int.* **2003**, 135, 53. DOI: 10.1016/S0379-0738(03)00175-0.

[174] W. Fan, M. Young, J. Canino, J. Smith, J. Oxley, J.R. Almirall. Fast detection of triacetone triperoxide (TATP) from headspace using planar solid-phase microextraction (PSPME) coupled to an IMS detector. *Anal. Bioanal. Chem.* **2012**, 403, 401. DOI: 10.1007/s00216-012-5878-x.

[175] C.K. Hilton, C.A. Krueger, A.J. Midey, M. Osgood, J. Wu, C. Wu. Improved analysis of explosives samples with electrospray ionization-high resolution ion mobility spectrometry (ESI-HRIMS). *Int. J. Mass Spectrom.* **2010**, 298, 64. DOI: 10.1016/j.ijms.2010.08.011.

[176] D. Jiang, L. Peng, M. Wen, Q. Zhou, C. Chen, X. Wang, W. Chen, H. Li. Dopant-Assisted Positive Photoionization Ion Mobility Spectrometry Coupled with Time-Resolved Thermal Desorption for On-Site Detection of Triacetone Triperoxide and Hexamethylene Trioxide Diamine in Complex Matrices. *Anal. Chem. (Washington, DC, U. S.).* **2016**, 88, 4391. DOI: 10.1021/acs.analchem.5b04830.

[177] J. Kozole, J. Tomlinson-Phillips, J.R. Stairs, J.D. Harper, S.R. Lukow, R.T. Lareau, H. Boudries, H. Lai, C.S. Brauer. Characterizing the gas phase ion chemistry of an ion trap mobility spectrometry based explosive trace detector using a tandem mass spectrometer. *Talanta.* **2012**, 99, 799. DOI: 10.1016/j.talanta.2012.07.030.

[178] J. Kozole, L.A. Levine, J. Tomlinson-Phillips, J.R. Stairs. Gas phase ion chemistry of an ion mobility spectrometry based explosive trace detector elucidated by tandem mass spectrometry. *Talanta.* **2015**, 140, 10. DOI: 10.1016/j.talanta.2015.03.001.

[179] J.C. Oxley, J.L. Smith, L.J. Kirschenbaum, S. Marimganti, S. Vadlamannati. Detection of explosives in hair using ion mobility spectrometry. *J. Forensic Sci.* **2008**, 53, 690. DOI: 10.1111/j.1556-4029.2008.00719.x.

[180] J. Tomlinson-Phillips, A. Wooten, J. Kozole, J. Deline, P. Beresford, J. Stairs. Characterization of TATP gas phase product ion chemistry via isotope labeling experiments using ion mobility spectrometry interfaced with a triple quadrupole mass spectrometer. *Talanta.* **2014**, 127, 152. DOI: 10.1016/j.talanta.2014.03.044.

[181] G.W. Cook, P.T. LaPuma, G.L. Hook, B.A. Eckenrode. Using gas chromatography with ion mobility spectrometry to resolve explosive compounds in the presence of interferents. *J. Forensic Sci.* **2010**, 55, 1582. DOI: 10.1111/j.1556-4029.2010.01522.x.

[182] A.R. Hill, M. Edgar, M. Chatzigeorgiou, J.C. Reynolds, P.F. Kelly, C.S. Creaser. Analysis of triacetone triperoxide complexes with alkali metal ions by electrospray and extractive electrospray ionisation combined with ion mobility spectrometry and mass spectrometry. *Eur. J. Mass Spectrom.* **2015**, 21, 265. DOI: 10.1255/ejms.1348.

[183] V. Ruzsanyi, S. Sielemann, J.I. Baumbach. Determination of microbial volatile organic compounds (MVOC) using IMS with different ionization sources. *Int. J. Ion Mobility Spectrom.* **2002**, 5, 138.

[184] V. Ruzsanyi, J.I. Baumbach, G.A. Eiceman. Detection of th mold markers using ion mobility spectrometry. *Int. J. Ion Mobility Spectrom.* **2003**, 6, 53.

[185] C. Tiebe, H. Miessner, B. Koch, T. Huebert. Detection of microbial volatile organic compounds (MVOCs) by ion-mobility spectrometry. *Anal. Bioanal. Chem.* **2009**, 395, 2313. DOI: 10.1007/s00216-009-3147-4.

[186] C. Tiebe, T. Huebert, B. Koch, U. Ritter, I. Stephan. Investigation of gaseous metabolites from moulds by Ion Mobility Spectrometry (IMS) and Gas Chromatography-Mass Spectrometry (GC-MS). *Int. J. Ion Mobility Spectrom.* **2010**, 13, 17. DOI: 10.1007/s12127-009-0035-8.

[187] T. Huebert, C. Tiebe, I. Stephan. Detection of fungal infestations of wood by ion mobility spectrometry. *Int. Biodeterior. Biodegrad.* **2011**, 65, 675. DOI: 10.1016/j.ibiod.2011.03.008.

[188] Y. Arnanthigo, O. Anttalainen, Z. Safaei, M. Sillanpää. Sniff-testing for indoor air contaminants from new buildings environment detecting by aspiration-type ion mobility spectrometry. *Int. J. Ion Mobility Spectrom.* **2016**, 19, 15. DOI: 10.1007/s12127-016-0189-0.

[189] D. Gallart-Mateu, S. Armenta, M. de la Guardia. Indoor and outdoor determination of pesticides in air by ion mobility spectrometry. *Talanta.* **2016**, 161, 632. DOI: 10.1016/j.talanta.2016.09.020.

[190] S. Li, J. Jia, X. Gao, X. He, J. Li. Detection of Toluene, Methanol and Formaldehyde Using Corona Discharge Ion Mobility Spectrometry. *Anal. Lett.* **2012**, 45, 841. DOI: 10.1080/00032719.2012.655680.

[191] W. Vautz, S. Sielemann, E. Uhde, J.I. Baumbach. Detection of emission from material surfaces using ion mobility spectrometry. *Int. J. Ion Mobility Spectrom.* **2004**, 7, 25.

[192] W. Vautz, S. Sielemann, J.I. Baumbach. Qualitative detection of odours using ion mobility spectrometry. *Int. J. Ion Mobility Spectrom.* **2005**, 8, 8.

[193] W. Vautz, S. Sielemann, J.I. Baumbach. Determination of terpenes in humid ambient air using ultraviolet ion mobility spectrometry. *Anal. Chim. Acta.* **2004**, 513, 393. DOI: 10.1016/j.aca.2004.03.016.

[194] W. Vautz, J.I. Baumbach, E. Uhde. Detection of emissions from surfaces using ion mobility spectrometry. *Anal. Bioanal. Chem.* **2006**, 384, 980. DOI: 10.1007/s00216-005-0240-1.

[195] S. Armenta, M. Blanco. Ion Mobility Spectrometry: A Comprehensive and Versatile Tool for Occupational Pharmaceutical Exposure Assessment. *Anal. Chem. (Washington, DC, U. S.).* **2012**, 84, 4560. DOI: 10.1021/ac300655t.

[196] T.F. Limero, E.G. Nazarov, M. Menlyadiev, G.A. Eiceman. Characterization of ion processes in a GC/DMS air quality monitor by integration of the instrument to a mass spectrometer. *Analyst (Cambridge, U. K.).* **2015**, 140, 922. DOI: 10.1039/C4AN01800A.

[197] M. Bouza, J. Orejas, S. López-Vidal, J. Pisonero, N. Bordel, R. Pereiro, A. Sanz-Medel. A flowing atmospheric pressure afterglow as an ion source coupled to a differential mobility analyzer for volatile organic compound detection. *Analyst (Cambridge, U. K.).* **2016**, 141, 3437. DOI: 10.1039/C5AN01938A.

[198] G.A. Eiceman, G.K. Anderson, W.C. Danen, M.J. Ferris, J.J. Tiee. Laser desorption and ionization of solid polycyclic aromatic hydrocarbons in air with analysis by ion mobility spectrometry. *Anal. Lett.* **1988**, 21, 539.

[199] G.A. Eiceman, D. Young, H. Schmidt, J.E. Rodriguez, J.I. Baumbach, W. Vautz, D.A. Lake, M.V. Johnston. Ion mobility spectrometry of gas-phase ions from laser ablation of solids in air at ambient pressure. *Appl. Spectrosc.* **2007**, 61, 1076. DOI: 10.1366/000370207782217671.

[200] G.A. Harris, M. Kwasnik, F.M. Fernández. Direct Analysis in Real Time Coupled to Multiplexed Drift Tube Ion Mobility Spectrometry for Detecting Toxic Chemicals. *Anal. Chem. (Washington, DC, U. S.).* **2011**, 83, 1908. DOI: 10.1021/ac102246h.

[201] G.A. Harris, S. Graf, R. Knochenmuss, F.M. Fernández. Coupling laser ablation/desorption electrospray ionization to atmospheric pressure drift tube ion mobility spectrometry for the screening of antimalarial drug quality. *Analyst (Cambridge, U. K.).* **2012**, 137, 3039. DOI: 10.1039/c2an35431d.

[202] J.D. Keelor, P. Dwivedi, F.M. Fernández. An Effective Approach for Coupling Direct Analysis in Real Time with Atmospheric Pressure Drift Tube Ion Mobility Spectrometry. *J. Am. Soc. Mass Spectrom.* **2014**, 25, 1538. DOI: 10.1007/s13361-014-0926-8.

[203] K.M. Roscioli, J.A. Tufariello, X. Zhang, S.X. Li, G.H. Goetz, G. Cheng, W.F. Siems, H.H. Hill. Desorption electrospray ionization (DESI) with atmospheric pressure ion mobility spectrometry for drug detection. *Analyst (Cambridge, U. K.).* **2014**, 139, 1740. DOI: 10.1039/c3an02113k.

[204] P.A. D'Agostino, C.L. Chenier. Desorption electrospray ionization mass spectrometric analysis of organophosphorus chemical warfare agents using ion mobility and tandem mass spectrometry. *Rapid Commun. Mass Spectrom.* **2010**, 24, 1617. DOI: 10.1002/rcm.4547.

[205] N.A. Devenport, D.J. Blenkhorn, D.J. Weston, J.C. Reynolds, C.S. Creaser. Direct Determination of Urinary Creatinine by Reactive-Thermal Desorption-Extractive Electrospray-Ion Mobility-Tandem Mass Spectrometry. *Anal. Chem. (Washington, DC, U. S.).* **2014**, 86, 357. DOI: 10.1021/ac403133t.

[206] W.F. Duvivier, T.A. van Beek, M.W.F. Nielen. Critical comparison of mass analyzers for forensic hair analysis by ambient ionization mass spectrometry. *Rapid Commun. Mass Spectrom.* **2016**, 30, 2331. DOI: 10.1002/rcm.7722.

[207] C.L. Feider, N. Elizondo, L.S. Eberlin. Ambient Ionization and FAIMS Mass Spectrometry for Enhanced Imaging of Multiply Charged Molecular Ions in Biological Tissues. *Anal. Chem. (Washington, DC, U. S.).* **2016**, 88, 11533. DOI: 10.1021/acs.analchem.6b02798.

[208] G. Kaur-Atwal, D.J. Weston, P.S. Green, S. Crosland, P.L.R. Bonner, C.S. Creaser. Analysis of tryptic peptides using desorption electrospray ionisation combined with ion mobility spectrometry/mass spectrometry. *Rapid Commun. Mass Spectrom.* **2007**, 21, 1131. DOI: 10.1002/rcm.2941.

[209] H. Li, P. Balan, A. Vertes. Molecular Imaging of Growth, Metabolism, and Antibiotic Inhibition in Bacterial Colonies by Laser Ablation Electrospray Ionization Mass Spectrometry. *Angew. Chem., Int. Ed.* **2016**, 55, 15035. DOI: 10.1002/anie.201607751.

[210] N.E. Manicke, M. Belford. Separation of Opiate Isomers Using Electrospray Ionization and Paper Spray Coupled to High-Field Asymmetric Waveform Ion Mobility Spectrometry. *J. Am. Soc. Mass Spectrom.* **2015**, 26, 701. DOI: 10.1007/s13361-015-1096-z.

[211] S.A. Stopka, A. Vertes, B.J. Agtuca, G. Stacey, D.W. Koppenaal, L. Pasa-Tolic, C.R. Anderton. Laser Ablation Electrospray Ionization Mass Spectrometry with Ion Mobility Separation Reveals Metabolites in the Symbiotic Interactions of Soybean Roots and Rhizobia *Plant J.* **2017**.

[212] J.P. Williams, J.H. Scrivens. Coupling desorption electrospray ionization and neutral desorption/extractive electrospray ionization with a travelling-wave based ion mobility mass spectrometer for the analysis of drugs. *Rapid Commun. Mass Spectrom.* **2008**, 22, 187. DOI: 10.1002/rcm.3346.

[213] X. Zang, J.J. Pérez, C.M. Jones, M.E. Monge, N.A. McCarty, A.A. Stecenko, F.M. Fernández. Comparison of Ambient and Atmospheric Pressure Ion Sources for Cystic Fibrosis Exhaled Breath Condensate Ion Mobility-Mass Spectrometry Metabolomics. *J. Am. Soc. Mass Spectrom.* **2017**, Ahead of Print. DOI: 10.1007/s13361-017-1660-9.

[214] F.A.M.G. van Geenen, M.C.R. Franssen, A.H.M. Schotman, H. Zuilhof, M.W.F. Nielen. Ambient Characterization of Synthetic Fibers by Laser Ablation Electrospray Ionization Mass Spectrometry. *Anal. Chem. (Washington, DC, U. S.).* **2017**, 89, 4031. DOI: 10.1021/acs.analchem.6b04641.

[215] A.H. Lawrence, P. Neudorfl, J.A. Stone. The formation of chloride adducts in the detection of dinitro-compounds by ion mobility spectrometry. *Int. J. Mass Spectrom.* **2001**, 209, 185. DOI: 10.1016/S1387-3806(01)00497-3.

[216] G.A. Eiceman, J.F. Bergloff, J.E. Rodriguez, W. Munro, Z. Karpas. Atmospheric pressure chemical ionization of fluorinated phenols in atmospheric pressure chemical ionization mass spectrometry, tandem mass spectrometry, and ion mobility spectrometry. *J. Am. Soc. Mass Spectrom.* **1999**, 10, 1157. DOI: 10.1016/S1044-0305(99)00082-3.

[217] V. Saarela, M. Haapala, R. Kostiainen, T. Kotiaho, S. Franssila. Glass microfabricated nebulizer chip for mass spectrometry. *Lab Chip.* **2007**, 7, 644. DOI: 10.1039/b700101k.

[218] T.J. Kauppila, P. Östman, S. Marttila, R.A. Ketola, T. Kotiaho, S. Franssila, R. Kostiainen. Atmospheric Pressure Photoionization-Mass Spectrometry with a Microchip Heated Nebulizer. *Anal. Chem.* **2004**, 76, 6797. DOI: 10.1021/ac049058c.

[219] B.D. Musselman. Sampling system for use with surface ionization spectroscopy *U.S. Patent US 8217341.* **2012**.

[220] J.C. Oxley, J.L. Smith, K. Shinde, J. Moran. Determination of the vapor density of triacetone triperoxide (TATP) using a gas chromatography headspace technique. *Propellants, Explos., Pyrotech.* **2005**, 30, 127. DOI: 10.1002/prep.200400094.

[221] A. Stambouli, A. El Bouri, T. Bouayoun, M.A. Bellimam. Headspace-GC/MS detection of TATP traces in post-explosion debris. *Forensic Sci. Int.* **2004**, 146, S191. DOI: 10.1016/j.forsciint.2004.09.060.

[222] C. Mullen, D. Huestis, M. Coggiola, H. Oser. Laser photoionization of triacetone triperoxide (TATP) by femtosecond and nanosecond laser pulses. *Int. J. Mass Spectrom.* **2006**, 252, 69. DOI: 10.1016/j.ijms.2006.01.018.

[223] M.E. Sigman, C.D. Clark, R. Fidler, C.L. Geiger, C.A. Clausen. Analysis of triacetone triperoxide by gas chromatography/mass spectrometry and gas chromatography/tandem mass spectrometry by electron and chemical ionization. *Rapid Commun. Mass Spectrom.* **2006**, 20, 2851. DOI: 10.1002/rcm.2678.

[224] A. Claeson, J. Levin, G. Blomquist, A. Sunesson. Volatile metabolites from microorganisms grown on humid building materials and synthetic media. *J. Environ. Monit.* **2002**, 4, 667. DOI: 10.1039/B202571J.

[225] S. Wold, K. Esbensen, P. Geladi. Principal component analysis. *Chemom. Intell. Lab. Syst.* **1987**, 2, 37. DOI: 10.1016/0169-7439(87)80084-9.

[226] P. Pasanen, A. Korpi, P. Kalliokoski, A. Pasanen. Growth and volatile metabolite production of Aspergillus versicolor in house dust. *Environ. Int.* **1997**, 23, 425. DOI: 10.1016/S0160-4120(97)00027-5.

[227] K. Peltonen, A. Zitting, H. Koskinen, A. Itkonen. Free radicals from photodecomposition of bisphenol-A. *Photochem. Photobiol.* **1986**, 43, 481. DOI: 10.1111/j.1751-1097.1986.tb09523.x.

[228] M.D. Jones, R.S. Plumb. The application of sub-2-Î¼m particle liquid chromatography-operated high mobile linear velocities coupled to orthogonal accelerated time-of-flight mass spectrometry for the analysis of ranitidine and its impurities. *J. Sep. Sci.* **2006**, 29, 2409. DOI: 10.1002/jssc.200600118.

[229] J. Van der Greef, N.M.M. Nibbering. Detection of unimolecular gas phase decompositions of ions, generated upon field desorption, in the time range of 10-11-10-9s. *Int. J. Mass Spectrom. Ion Phys.* **1977**, 25, 357. DOI: 10.1016/0020-7381(77)80062-4.

[230] M.J. Culzoni, P. Dwivedi, M.D. Green, P.N. Newton, F.M. Fernández. Ambient mass spectrometry technologies for the detection of falsified drugs. *MedChemComm.* **2014**, 5, 9. DOI: 10.1039/c3md00235g.

[231] M. J. Frisch, G. W. Trucks, H. B. Schlegel, G. E. Scuseria, M. A. Robb, J. R. Cheeseman, J. A. Montgomery, Jr., T. Vreven, K. N. Kudin, J. C. Burant, J. M. Millam, S. S. Iyengar, J. Tomasi, V. Barone, B. Mennucci, M. Cossi, G. Scalmani, N. Rega, G. A. Petersson, H. Nakatsuji, M. Hada, M. Ehara, K. Toyota, R. Fukuda, J. Hasegawa, M. Ishida, T. Nakajima, Y. Honda, O. Kitao, H. Nakai, M. Klene, X. Li, J. E. Knox, H. P. Hratchian, J. B. Cross, V. Bakken, C. Adamo, J. Jaramillo, R. Gomperts, R. E. Stratmann, O. Yazyev, A. J. Austin, R. Cammi, C. Pomelli, J. W. Ochterski, P. Y. Ayala, K. Morokuma, G. A. Voth, P. Salvador, J. J. Dannenberg, V. G. Zakrzewski, S. Dapprich, A. D. Daniels, M. C. Strain, O. Farkas, D. K. Malick, A. D. Rabuck, K. Raghavachari, J. B. Foresman, J. V. Ortiz, Q. Cui, A. G. Baboul, S. Clifford, J. Cioslowski, B. B. Stefanov, G. Liu, A. Liashenko, P. Piskorz, I. Komaromi, R. L. Martin, D. J. Fox, T. Keith, M. A. Al-Laham, C. Y. Peng, A. Nanayakkara, M. Challacombe, P. M. W. Gill, B. Johnson, W. Chen, M. W. Wong, C. Gonzalez, J. A. Pople. Gaussian 03, Revision C.02 *Gaussian, Inc., Wallingford CT.* **2004**.

[232] G. Bouchoux. Gas-phase basicities of polyfunctional molecules. Part 1: theory and methods. *Mass Spectrom. Rev.* **2007**, 26, 775. DOI: 10.1002/mas.20151.